

**Experimental and Theoretical
investigations into the switching of Liquid
Crystal Devices**

James Hind

A thesis submitted in partial fulfilment of the
requirements of The Nottingham Trent University
for the degree of Doctor of Philosophy

July 2007

Contents

	Page
Acknowledgments	5
Abstract	6
Chapter 1. Introduction	
1.1	Liquid crystal phases 11
1.2	Anisotropy and permittivity 12
1.3	Ferroelectricity 13
1.4	Elastic constants and the Freedericksz effect 15
1.5	Liquid crystal devices 17
1.6	Modelling of liquid crystals 22
1.7	Flexoelectricity 23
1.8	Summary 24
Chapter 2. Experimental Methods	
2.1	Capacitance cell test 25
2.2	The Freedericksz measurement 28
2.3	Transient technique and theory 30
2.4	Waveforms used 36
2.5	Validity of technique 39

Chapter 3. Transient Capacitance Study

3.1	Introduction	42
3.2	Theory	43
3.3	Static permittivity measurements	45
3.4	Transient permittivity technique	49
3.5	Transient permittivity results	51
3.6	Conclusions	61

Chapter 4. Transitive Capacitance Study of Dual Frequency Liquid Crystals

4.1	Introduction	62
4.2	Theory	63
4.3	Amplitude modulation	67
4.4	Frequency modulation	69
4.5	Homeotropic defects	73
4.6	Pulsed addressing	76
4.7	Discussion	79

Chapter 5. Transient Capacitance of Flexoelectric and Ionic Liquid Crystals

5.1	Introduction	80
5.2	Theory	81

5.3	Experimental method	84
5.4	Behaviour of ions	99
5.5	Discussion	101
Chapter 6. Double Minima in the Surface Stabilised Ferroelectric Liquid Crystal Switching Response		
6.1	Introduction	102
6.2	Theory	103
6.3	Method	108
6.4	Conclusion	112
6.5	Summary	121
Chapter 7. Conclusions and Further Work		122
References		123
Publications & Conferences		130

Acknowledgements

This work is dedicated to my family for their love, support and tolerance during its construction. I am, of course, grateful to Nottingham Trent University, in particular the staff of the physics department. Special thanks are due to Carl and Mike for their patience and expert supervision. I would also like to thank my friends; Minty et al for keeping me just this side of sane throughout.

Abstract

This work addresses the dynamic switching of liquid crystal cells. While static measurements of the permittivity liquid crystal cells are well established, here a novel transient permittivity technique is developed and applied to several liquid crystalline substances in a variety of geometries. This technique utilises A.C. waveforms to measure the permittivity of a cell during the dynamic processes of switching and relaxing, allowing a detailed picture of the switching process to be constructed on small time scales. The results for several materials are presented and compared to theoretical predictions stemming from standard liquid crystal continuum theory. The technique is expanded to utilise frequency modulation when applied to dual frequency materials and is adapted to D.C. fields. Novel experimental results concerning surface stabilised ferroelectric liquid crystals have recently shown an unexpected second minimum in the τ -V response curve. The origin of this phenomenon is explored via a numerical simulation program and a qualitative explanation found regarding the torque generated by the surface alignment that is consistent with established theory.

Chapter 1: Introduction to Liquid Crystals

1.1 Liquid crystal phases

Liquid crystals were discovered in 1888 by Friedrich Reinitzer [Lehmann 1889]. They are defined as substances that can exist stably part-way between the liquid and solid states with their molecules (mesogens) partly ordered (exhibiting elements of positional or orientational order). Such substances tend to permit several stable mesophases between the solid and liquid states. The determination of which phase is present is usually a function of temperature (thermotropic), although some lyotropic liquid crystals change state with concentration and some amphotropic depend on both temperature and concentration. Individual liquid crystal substances may exhibit some or all of the following phases

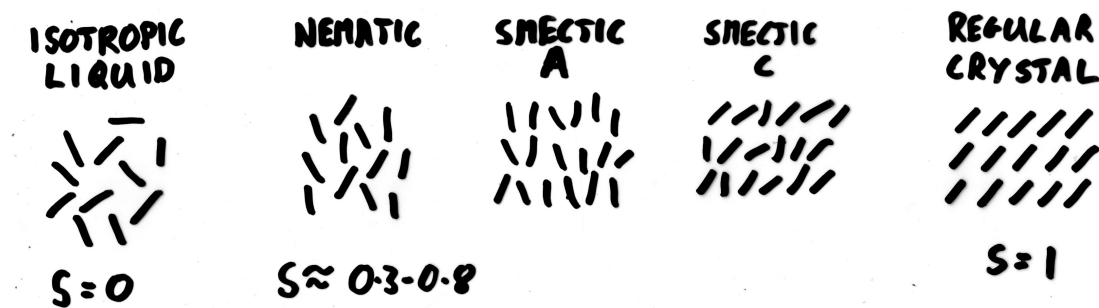


Figure 1.1 : Depiction of different liquid crystal phases formed by calamitic liquid crystals.

Figure (1.1) shows diagrammatically a typical progression of state with lowering of temperature. For each state the approximate order parameter S is shown. An initially isotropic liquid undergoes a phase transition to a slightly more ordered state where the molecules central axis (director) adopts a discernable average direction; the nematic phase. Further cooling produces a yet more ordered state with the formation of an internal layer structure; the smectic A phase. Mesogens are free to move within their layer and layers are free to slide over one another. At lower energies still we see the smectic C state where the Mesogens align their directors at an angle θ to the layer normal. Lastly we see a fully solid crystalline arrangement. Liquid crystals may exhibit other phases such as columnar and blue phases which will not be dealt with here [Chandresakhar 1992, DeGennes 1993].

Nematics possess orientational order only; they tend to be calamitic (rod-like) molecules and so align their long molecular axis along a common axis termed the director. Note that for many purposes the director is bi-directional (whether the arrow on the axis points 'up' or 'down' is immaterial), giving a preferred axis for alignment which allows for a two-fold degeneracy in direction (A vertically aligned director will likely have equal proportions of 'up' and 'down' pointing mesogens).

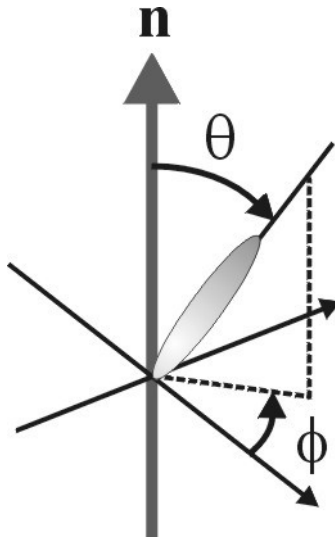


Figure 1.2 : Depiction of mesogens alignment with director (n)

The degree of alignment within a nematic sample is determined by an order parameter S defined in equation (1) [Tsvetkov 1942].

$$S = \frac{1}{2} \langle 3 \cos^2 \theta - 1 \rangle \quad (1)$$

where unity denotes perfect ordering and zero denotes an isotropic liquid. Theta in this case is simply the average angle made between the director (optical axis) and the individual mesogen molecules Figure (1.2). The order parameter for nematics usually lies in the range 0.3 and 0.9

Smectics possess some degree of positional (translational) order also. They organise into layered structures which still allow for the movement of individual molecules within the layers. The director may tilt with respect to the layer normal (Smectic C) . The angle of this tilt, termed theta, is usually around 20 – 25 degrees. If the mesogens are chiral the direction of tilt may vary linearly with progression through the layers, giving rise to a chiral smectic phase - Figure (1.3). Chiral smectics which exhibit a cyclic variation in tilt direction with progression through the layers form a helical structure with a constant pitch. Chiral smectics possessing a permanent dipole form a ferroelectric phase. Although macroscopically these dipoles cancel out, interesting effects can occur on small scales. When the pitch of the layer tilt rotation is unwound there is enough internal alignment to produce a field. [De Gennes 1993] When trapped between the curved face of a hemispheric lens and a plane disclinations may be seen at regular intervals corresponding to the half integer wavelengths able to fit between the plate and the lens. These disclinations are termed Cano rings.

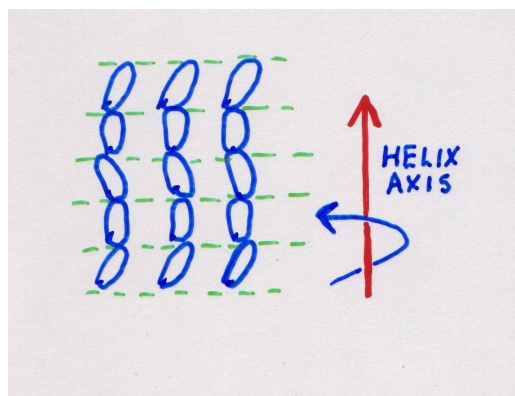


Figure 1.3 : Chiral Smectic layer structure

1.2 Anisotropy and permittivity

One common aspect of the different liquid crystal phases is molecular anisotropy. Liquid crystal mesogens experience polarisability anisotropy (a difference in the induced dipole moment per unit field) possessed as they are of two components to their refractive index. There is the extraordinary refractive index n_e (along the long molecular axis) and the ordinary refractive index n_o (along the short molecular axis). This leads to birefringence; the refractive index of the material, as experienced by incident light, varies with the angle of polarisation of the light. Treating light as a transverse electromagnetic wave it may be resolved into 2 orthogonal components each at 45 degrees to the original plane of polarisation. As the speed of light through a medium depends on the refractive index of the medium and that refractive index is experienced differently for each component of the light wave; each component will travel with a different velocity. This phenomenon tends to induce a circular (or elliptic) polarisation of straight polarised light since it introduces an arbitrary phase difference between the two components which no longer sum to give the same linear polarisation. [Collings, 1990]

There is also anisotropy in terms of the electric permittivity (and magnetic susceptibility) of the molecules (dielectric anisotropy). This is because the refractive index of a substance is the square root of the product of the substance's relative permittivity and permeability. Considering the classic calamitic molecule it is easy to see that electron transfer (and therefore permittivity) will vary with the direction of an

applied field. This permits the orientation of the molecules to be manipulated with the application of an electric or magnetic field. The magnitude of this effect depends on the strength of any dipole naturally exhibited by the mesogens or induced by the field, the strength of the applied field and the degree of orientational freedom enjoyed by the mesogens (This last being chiefly determined by the viscosity of the sample though surface anchoring also has an effect [Blinov 1983]. Moreover any permanent dipole expressed by the molecules contributes at low frequencies (up to 1MHz). The refractive index is measured at high frequencies (10^{14} Hz). This tends to give a permittivity which is high at low frequencies and low at optical frequencies due to a Debye style relaxation of the orientational contribution to the polarisation.[Stewart, 2004]

1.3 Ferroelectricity

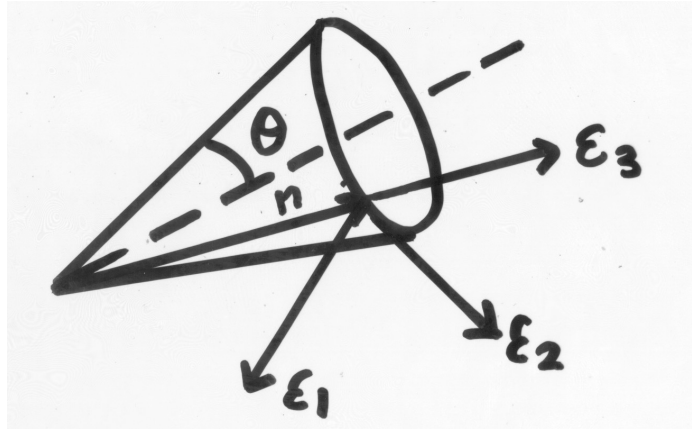


Figure (1.4). Dielectric permittivities of Smectic C phase

In figure (1.4) the dashed line represents the layer normal, θ the smectic cone angle and n the director. Shown are the three dielectric permittivities. Dielectric biaxiality is defined as $\partial\epsilon = \epsilon_2 - \epsilon_1$, Uniaxial anisotropy as $\Delta\epsilon = \epsilon_3 - \epsilon_1$ [Brown, 1999; De Gennes 1993].

Liquid crystals with mesogens which possess permanent dipoles may also demonstrate ferroelectric properties (usually when they are composed of chiral Mesogens) [Collings 1997]. In the nematic case this is seen in the splay defect of the HAN (hybrid aligned nematic) geometry where one surface is planar aligned and the other homeotropic. Just as the domain structure of iron usually sums to give no net field macroscopically as a low energy configuration; such is the case with liquid crystals. The chiral nature of ferroelectric liquid crystals introduces a pitch in layer tilting which, viewed macroscopically, gives no net internal or external field. Should the pitch be unwound on a small scale (such as by the boundary conditions imposed

by surface stabilisation – see below) then the spontaneous polarisation of the Mesogens may couple usefully with an applied electric or magnetic field.[Meyer, 1975]

1.4 Elastic constants and the Freedericksz effect

The internal stresses of liquid crystals may be described using the three Frank elastic constants; bend (k_{33}), twist (k_{22}) and splay (k_{11}) which are shown in figure(1.5). Typically $k_{11} > k_{22} > k_{33}$ and usual values are in the area of 10pN. It is competition between these forces as well as packing considerations that helps to determine the inter-molecular structure of a particular substance. Once the liquid crystal has adopted a stable state these internal elastic forces act to resist deformation and must be overcome in order to switch the state of a cell [Meyer,1969].

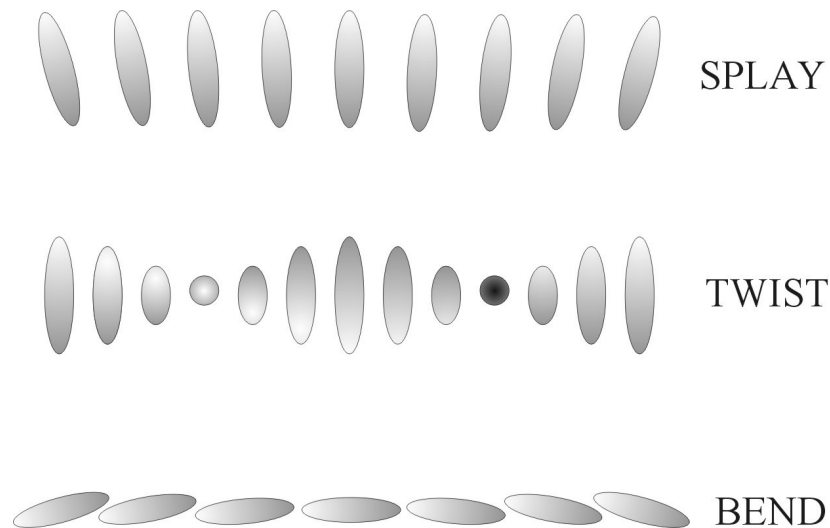


Figure (1.5). The three Frank elastic constants

Weak fields applied at right angles to the director are unable to overcome the internal elastic forces of the liquid crystal, largely because of the degenerate nature of the

director. The point at which the applied field is strong enough to overcome these forces is known as a Fredericksz transition and provides a threshold voltage for perturbation. The capacitance of a dielectric material is explicitly dependant on its electric permittivity and so the capacitance of a liquid crystal varies with director orientation, which in turn varies with the magnitude of an applied potential difference across the cell. Figure (1.6) shows the change in director profile (and so permittivity) during a Fredericksz transition [Fredericksz 1933, 1934]. The Fredericksz transition threshold voltage may be predicted from equation (2) where K denotes the average elastic constant. This will be one of k_{11} (planar), k_{22} (homeotropic), or k_{33} (twist), depending on the geometry and $\Delta \epsilon$ is $\epsilon_{\parallel} - \epsilon_{\perp}$.

$$V_0 = \sqrt{\frac{\pi^2 K}{\epsilon_0 \Delta \epsilon}} \quad (2)$$

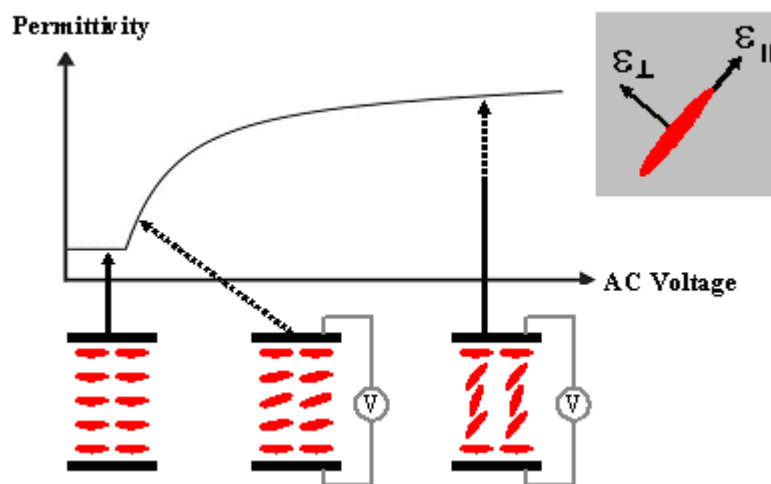


Figure (1.6) . The Fredericksz transition and its effect on cell permittivity.

[Brown 2003]

The three figures at the bottom of Figure (1.6) show the position of the mesogens in the sample. Initially they are depicted parallel to the cell walls; in a planar configuration. Provided the applied field is below that required for the Freedericksz transition such a state is stable. Once the field exceeds the Freedericksz threshold the molecules begin to reorient in line with the field. At high fields the bulk of the material has adopted a homeotropic alignment giving rise to a splay deformation across the cell. The threshold can be reduced by utilising a weak anchoring to the substrate; this also has the effect of reducing the field strength required to achieve a given degree of deformation. The director orientation in the centre of the cell is highly dependant on the elastic constants: k_{11} , k_{33} and the permittivity anisotropy; that is the ratios $\Delta k/k_{11}$ and $\Delta \varepsilon / \varepsilon_{perp}$. If the elastic ratio is positive then for a given applied field the maximum director deviation is reduced. If the permittivity ratio is positive then the maximum deviation is increased. As a result of this dependency the elastic constants and the permittivities may be estimated by fitting the shape of a Freedericksz transition curve [Blinov, 1983] the permittivities being deducible from the undisturbed planar and homeotropic alignments.

1.5 Liquid crystal devices

Liquid crystals have become an integral part of modern life. Their applications are wide ranging and include: display devices such as flat panel computer screens, paint which changes colour in response to temperature variations, phase gratings for telecommunications, cleansing agents such as soap, windows that can change between clear and opaque states, etc. [Clark 2000, Warr 1995] Most liquid crystal display devices make use of both dielectric anisotropy and birefringence. Consider light incident on a polarizer; only light with the correct plane of vibration will be able to pass through. Should this light then encounter an identical polarizer at ninety degrees to the previous one, the remainder of the light will be blocked. If we were to interpose a slab of birefringent material between the two polarizers then some of the now plane polarized light will have its axis of vibration rotated and so be able to pass through the second polarizer also. The degree to which this effect is manifest is dependant on the contact angle between the light and the mesogens, which may in turn be controlled by the application of an electric field to align the molecules as desired. This technique is usually exploited by either placing a mirror behind the cell to reflect incident light or not as required (passive display, e.g. calculator screen), or by placing a light source behind the cell which then acts as a high speed shutter (active display, e.g. laptop screen). This process, in one form or another, is the basis of most liquid crystal optical displays.

The liquid crystal tends to be confined to a thin cell sandwiched by transparent electrodes (e.g. indium tin oxide). The initial alignment of the director may be set by

coating the inside of the cell walls with a polymer which is then rubbed in a preferred direction. The mesogens in contact with this surface tend to align with the rubbing direction, elastic forces then spread this preference throughout the sample. This technique gives rise to a planar orientation. The prior deposition of micro structures normal to the cell wall gives rise to a homeotropic orientation through a similar process. Note that although anchored at the surfaces the bulk of the liquid crystal is free (to a degree dependant on viscosity and cell width) to adopt a contrary alignment if encouraged to do so by the application of an external electric or magnetic field. This is exemplified by the hybrid aligned nematic (HAN) cell. In addition to the strong anchoring to the planar and homeotropic states weak anchoring is sometimes used. In these cases the energy required to break alignment varies greatly and this can be used to influence the behaviour of a cell undergoing a Fredericksz transition. [Blinov, 1983]

Surface stabilised ferroelectric liquid crystals (SSFLC) are aligned at the cell walls as described above but tend to adopt an internal chevron formation such that the director rotates around the surface of a cone normal to the layer as a function of distance through each half of the cell. The degree and direction of this rotation may be manipulated by altering the surface boundary conditions. The permanent dipole of the mesogens means that they react strongly to an applied field and tend to switch quickly. The nature of the chevron interface allows for two stable positions for the central mesogens to occupy. Note that if the director were resolved into horizontal and vertical components at each point, the horizontal components would cancel and the vertical components would sum. In the example shown in Figure (1.7) that would leave the director pointing 'up'. If the alternative central position were adopted then the director would point 'down'. That is what happens when the cell is switched by an

applied field. These two states result in the on and off positions required of an electro-optic device. In addition these two states are stable. This is an important quality for devices because it allows for the status of the cell (on or off) to be preserved without an applied field. This reduces the energy cost of storing an image dramatically. An applied field is still required to switch between states. [Jones, 1993, Brown 1999]

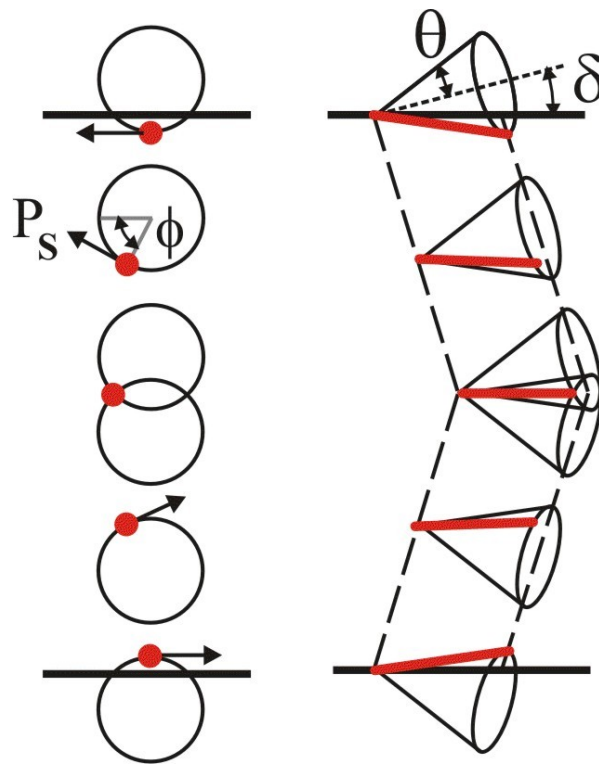


Figure (1.7). The chevron geometry of a SSFLC cell

Figure (1.7) shows the chevron formation of a SSFLC. Theta represents the fictional smectic cone angle (the degree of tilt of the mesogens relative to the layer normal); Phi the azimuthal angle occupied by the director on the fictional smectic cone and

delta the layer tilt angle relative to the cell surfaces. The spontaneous polarisation (P_s) vector is denoted with the black arrows at several points.

1.6 Modelling of liquid crystals

Over the years several attempts have been made to model the macroscopic behaviour of liquid crystals, whether the area of interest was the electromagnetic properties or the phase transitions. One of the more common techniques utilised is the Maier-Saupe theory, though it is generally preferred by experimentalists than theorists. Aside from the generalisations inherent in any mean field theory the Maier-Saupe theory neglects short range repulsive forces (e.g. steric). Nevertheless it is capable of accurately predicting first order phase transitions. Advances in computing power have allowed increasingly large numbers of molecules to be studied in ‘real time’ simulations; the results are then extrapolated to real world macro scale systems. In most of these models the motion of the particles is solved iteratively which makes the end result vulnerable to error from large step sizes and vulnerable to the limits of processing power from small step sizes. In general these models utilise the equations of liquid crystal continuum theory to predict the forces (visco elastic, external electric or magnetic, internal dipole/dipole interaction, etc.) impinging on a mesogen and alter its position/orientation/ energy etc as required. The model then moves on a short amount of time and repeats this process. Of course when the interactions between many molecules are considered this quickly becomes computationally expensive.

1.7 Flexoelectricity

Flexoelectricity is the liquid crystal analogue of piezoelectricity in solid polar crystal lattices. In the case of solid crystals this extra surface polarisation arises from either a compression or expansion along one of the axes normal to a face of the cubic cell. The resultant spatial imbalance of charge constitutes an electromagnetic field. The procedure is reversible in as much as an applied field can cause a corresponding deformation. In the case of liquid crystals however neither compression nor extension is required, instead either a splay or bend deformation is needed, along with one of a few particular mesogenic anisotropies. It has been found that for 'pear shaped' molecules an applied field can cause them to align with the field. In the case of these molecules however their anisotropy along the long molecular axis leads to a splay deformation. As with piezoelectricity the process may be reversed in that a splay deformation gives rise to an equivalent polarisation. The same has also been shown to occur for 'banana' shaped mesogens; in this case it is a bend deformation that drives the process. [Billeter, 2000] An important manifestation of flexoelectricity in traditional calamitic liquid crystals is evident when they are confined to the Hybrid aligned nematic geometry. In this alignment; with one planar and one homeotropic substrate the director experiences a splay deformation along the axis normal to the cell surface. The strength of the resultant polarisation depends on the strength of the field, the degree of splay in evidence and the dielectric anisotropy.

1.9 summary

Many of the commercial and academic uses of liquid crystals involve precise knowledge and manipulation of the Freedericksze threshold. This allows for the fast switching and sharp definition between alignments which is required for the manufacture of clear and fast reacting displays. The factors which affect this have been discussed and explained. Given the wide variety of display applications in which liquid crystals are employed it is of great interest to have as wide a variety as possible of techniques to analyse these transitions. It is also very useful to have cheap, fast, reliable techniques both to explore the transition in real time and to easily characterise the physical properties (such as permittivities and elastic constants) of new materials as they are developed. In the following chapters a novel technique for the exploration of the switching and relaxing of liquid crystal cells is developed and employed across a range of materials. The technique is shown to be robust and adaptable to different alignments as well as being consistent and accurate. Theoretical investigations into the physical response of liquid crystal cells to their surface alignment geometries are also undertaken. A link between particular alignments and the resulting variations in applied field response time is proposed and explained in terms of the torque exerted on the director by the field.

Chapter 2: Experimental techniques

2.1 Capacitance test cell

In order to study the behaviour of liquid crystal samples small amounts were placed in cells. A cell is constructed from two overlapping parallel glass substrates; each coated with a circle of Indium Tin Oxide in the centre and along a thin channel to the edges of the internal surfaces; this is used as transparent electrodes. The distance between the plates (cell thickness) was either 5 or $22\ \mu m$ for the cells used. Severe deviation from this width may be spotted by looking for birefringent rings apparent on the surface of the cells. A third electrode may be employed on one surface circling the central electrode at a short distance (around $5\ \mu m$) to act as a guard ring. This electrode is held at earth and acts to displace fringing of the applied field away from the central active area being studied. Since the distance between the guard ring and the central electrode must not exceed (or, for preference, even approach) the thickness of the cell this technique was only employable on the $22\ \mu m$ cells.

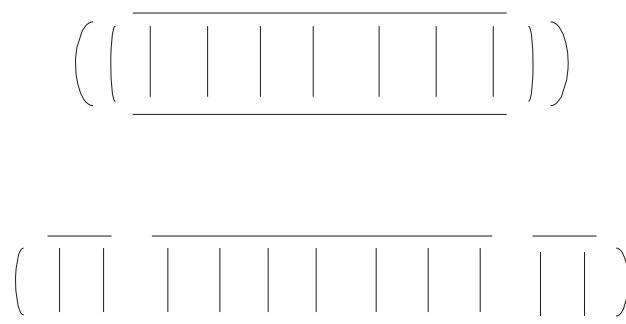


Figure 2.1 **Displacement of fringing with guard ring**

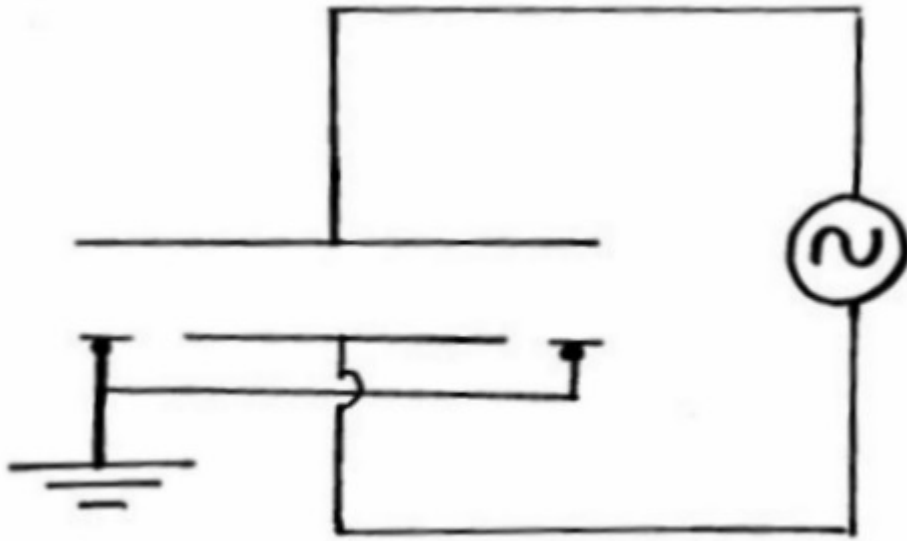


Figure 2.2 Test cell side view

The internal surfaces are coated with an alignment layer (often polyamide) which is rubbed parallel along the preferred director alignment direction, for one cell wall and anti parallel to the preferred director alignment for the other cell wall. When cooled from the isotropic phase the director tends to align with the rubbing direction. If we were to rub both walls in the parallel direction we remove the possibility of a Fredericksz transition and so be left with a PI cell. Such a cell is particularly vulnerable to backflow when relaxing. A different surface coating or combination of the two may be used to create homeotropic or hybrid cells as required. In the case of hybrid aligned cells one substrate alignment is planar and one homeotropic. All of the cells were supplied by Merck. In the case of the hybrid cells it is possible to determine which side is homeotropic by the application of a small droplet to each of

the glass panes where the electrodes are attached and studying them under a microscope; the droplet on the planar side will exhibit birefringence. The cell is sealed apart from two opposing apertures separated by the long axis of the cell. The liquid crystal medium is heated to above its clearing point (the isotropic/anisotropic boundary) so that the cell is filled in the isotropic state. The liquid crystal medium is then applied to one of the apertures and the cell filled by capillary forces. Wires are attached to the electrodes on the sides of the cell with ITO solder and sealed with Araldite. On cooling into the nematic phase the director aligns preferentially with the rubbing direction. The capacitance and conductance of the cells is measured statically both before and after filling the cell with an LCZ meter. An Agilent 4284A LCZ meter was used with an accuracy of 0.05% over a range of 5mV -20Vrms.

2.2 The Freedericksz measurement

-

Static measurement of the capacitance of liquid crystals is an established method of finding the Freedericksz transition since above this threshold there is a sharp change in the capacitance of planar cells. Such measurements allow the determination of the average permittivity through the layer to be found for a given applied field. [Heppke, 1974, Meyerhofer, 1975]] One is also able to plot Voltage curves from which one may find the elastic constants for the material and the parallel and perpendicular permittivities. K_{11} (splay) may be approximated from the value of the threshold V_C .

$$V_C = \sqrt{\pi^2 K_{11} / \epsilon_o \Delta \epsilon} \quad (2.1)$$

The ratio of K_{11} / K_{33} (bend) may be approximated from the gradient of the curve immediately post threshold and then fitted to the whole curve. [Stromer, 2006] A field is applied across the short axis of the cell and the capacitance of the cell is measured; provided that the empty cell capacitance and the diameter of the cell are known the mean permittivity ϵ_r may then be found. If a planar cell containing a material with a positive dielectric anisotropy is used we are able to find the perpendicular permittivity ϵ_{\perp} ; using a homeotropic cell we are able to find the parallel permittivity ϵ_{\parallel} . Application of a high field (several times the threshold magnitude) to

a planar cell also allows ϵ_{\parallel} to be approximated since the bulk of the sample adopts the homeotropic alignment. A sample Fredericksz transition for the well known liquid crystal compound E7 is shown in figure 2.3 (reproduced from chapter 3.3). This was found using the standard static capacitance measurements using an LCR bridge and an applied field of 10kHz.

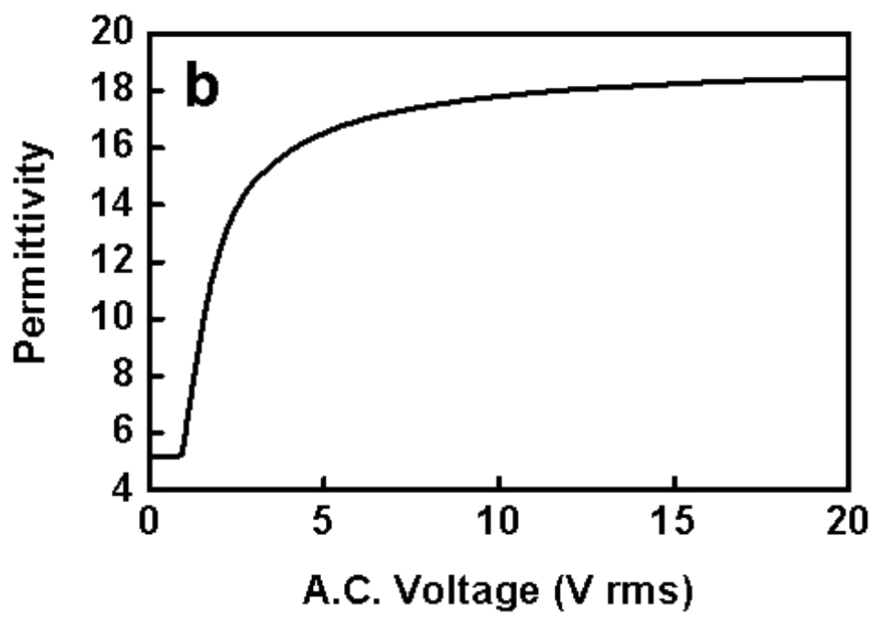


Figure 2.3 Fredericksz curve for E7

2.3 Transient technique and theory

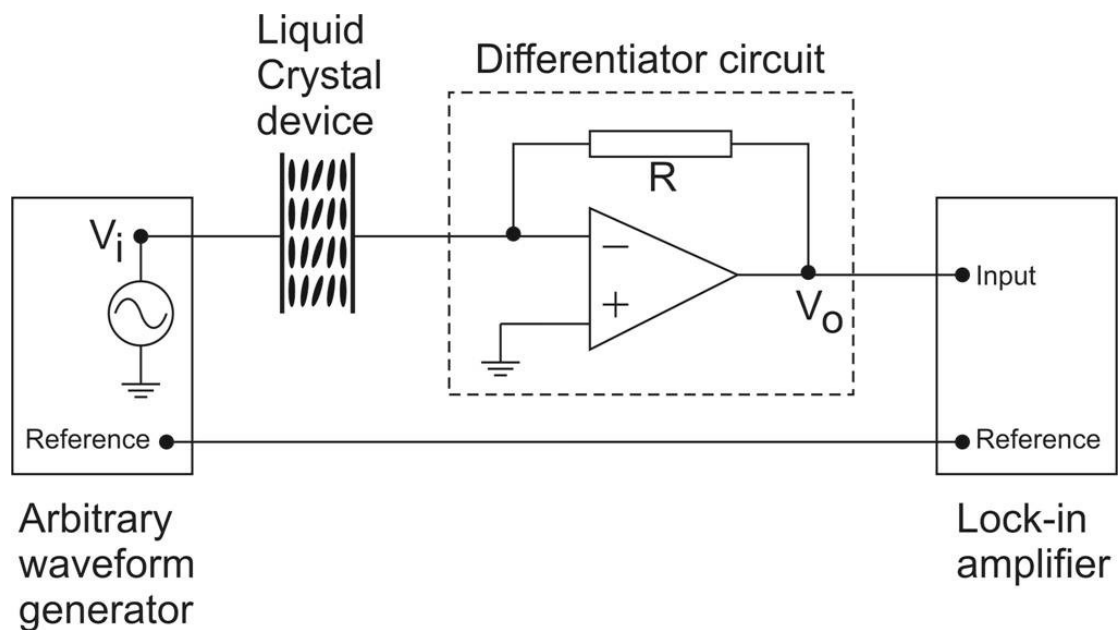


Figure 2.4 Transient technique circuit diagram

The experimental set up for the transient capacitance study is shown in Figure 2.4. In the transient capacitance study the signal applied is an amplitude-modulated sine wave composed of two parts; one sub threshold (typically 100mV) and one above threshold; with an overall period of around 1.0-2.5 seconds. When applied to a planar cell the high amplitude part causes the cell to switch towards a homeotropic alignment and the low amplitude part allows it to relax back into the planar geometry. The

signal was created by modulating the internal channels of a Thurlby Thandahar TTI Arbitrary waveform generator (TGA1412). The finite resistivity of the ITO electrodes was approximately 70Ω which gave an upper frequency limit of around 500 kHz before the electrodes started to act as serial resistors in the circuit.

In passage through the liquid crystal cell the capacitive part of the current is shifted in phase relative to the original signal by -90° . This part of the signal will vary in amplitude according to the amount of capacitance exhibited by the cell and is detected via a lock in amplifier (DSP 7265) which uses a synchronised signal from the waveform generator as a reference signal. The relationship between the voltage $V_o(t)$ and $V_I(t)$ is given by equation 2.2.

$$V_o(t) = -R \frac{d}{dt} (C(t)V_I(t)) \quad (2.2)$$

where $C(t) = \varepsilon(t)C_0$. Now consider an input voltage $V_I = V_{Ipk} \cos(\omega t)$. This is the carrier wave of the a.c. modulated waveform that is applied to the liquid crystal cell. Substituting for the capacitance of the cell and the input voltage in equation 2.2 yields equation 2.3 :

$$V_o(t) = -RC_oV_{Ipk} \left(\cos(\omega t) \frac{d\varepsilon(t)}{dt} - \omega \varepsilon(t) \sin(\omega t) \right) \quad (2.3)$$

The output voltage therefore consists of 2 components. The first term describes a component that is in phase with the input carrier wave and is proportional to the time differential of the permittivity of the liquid crystal layer. The second term in equation 2 describes a component that is 90° out-of-phase, or in quadrature, with the input carrier wave. This latter term is directly proportional to the time dependent dielectric permittivity of the liquid crystal layer.

A decade 8000 variable resistor bank is included as the resistor (Figure 2.1) to allow the magnitude of the signal's voltage to be staged down to a level acceptable to the input limits of the amplifier without affecting the phase of the signal. The output of the lock in amplifier is displayed on a digital oscilloscope (Agilent 54622A) from which the data may be saved to disc. Since the output of the oscilloscope contains 1000 data points per channel on each screenshot of a certain length of time, the change in permittivity may be found millisecond by millisecond, allowing the switching and relaxation processes to be studied in detail. The most detailed data is obtained by setting the resistance to the maximum possible without reaching the full scale deflection of the lock in amplifier's sensitivity setting. Separate readings may be taken for the switching and relaxing parts, doubling the number of data points obtained. The sensitivity of the lock in is set to 20mV for studying the relaxing part and 100mV for the switching part since the larger input voltage gives a correspondingly large output voltage. The resistance is then increased to maximise the signal while avoiding clipping of the signal at high fields. The mean permittivity of the sample may then be found through the relation:

$$\epsilon_r = \frac{V_o}{V_i \cdot \omega \cdot R \cdot C_0} \quad (2.4)$$

Using $\left| \frac{V_o}{V_i} \right| = \left| \frac{Z_o}{Z_i} \right| = R\omega C$ and $C = C_0\epsilon$

where C_0 is the empty cell capacitance of the cell found by applying a static field from an LCZ bridge (Agilent 4284A) before the cell is filled, and V_o is adjusted according to the sensitivity scale of the Lock in amplifier. The temperature in the laboratory was set at 22C by the air conditioning; this is well within the nematic –

isotropic range for all of the materials used measurements of the capacitance of the cells at 22C and 24C showed an increase in parallel and perpendicular permittivities of around 1.9% across that range. The AWG (arbitrary waveform generator) has an output amplitude accuracy of $2\% \pm 1\text{mV}$ so all input voltages were measured via the digital oscilloscope which has a vertical accuracy of $\pm(3\% \times \text{reading} \times 0.1\text{div} + 1\text{mV})$. With typical values of a 2V reading and 50mV divisions this gave an accuracy of around $\pm 0.03\%$. The phase error in the Lock in amplifier was < 0.0001 degrees; much less than the deviation from 90degrees caused by the imperfect nature of the samples as capacitors. Typically the lock in was reading at 90degrees $\pm 5\%$.

An example would be a waveform of 10 kHz frequency with a switching amplitude of 2.523V rms and a relaxing amplitude of 0.2051V rms applied to a cell with an empty cell capacitance of 46.06pF. Setting the sensitivities of the lock in amplifier to 100mV and 20mV for the switching and relaxing parts respectively we maximise the signal by setting the resistance to 3.6 k Ω and 7.0 k Ω for the switching and relaxing parts. The mean permittivities in this case are then found to be:

$$\epsilon_{switch} = \frac{V_o}{2.6286}$$

$$\epsilon_{relax} = \frac{V_o}{2.0775}$$

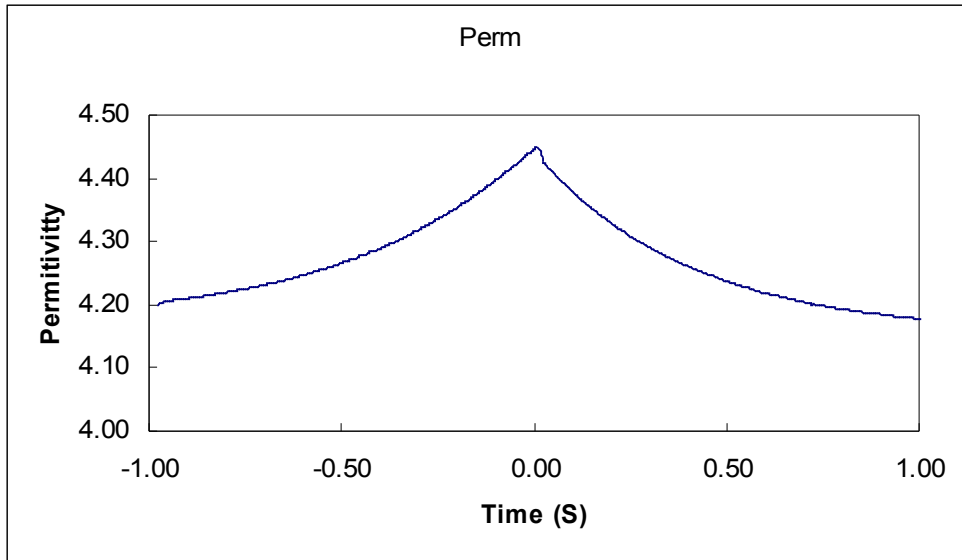


Figure 2.5 Sample procedure results for a planar cell

Figure 2.5 shows the results obtainable utilising the above technique. A slight anomaly may be seen immediately after $t = 0$; this is due to the lock in struggling to cope with the sudden change in magnitude of the signal. The effect is minimal, lasts just a few microseconds and is usually removable by smoothing at the oscilloscope.

Once the data is collected it is compared with theory via a numerical modelling program created by Dr Andrew Smith. The program utilises liquid crystal continuum theory to solve equation 2.5 throughout the cell giving average cell permittivities at time intervals comparable to those found experimentally. These values are graphed and overlaid with the experimental results for comparison.

$$-\eta \frac{d\theta}{dt} = \frac{\partial \omega}{\partial \theta} - \frac{d}{dz} \left(\frac{\partial \omega}{\partial \frac{\partial \theta}{\partial z}} \right) \quad (2.5)$$

This approach allows us to simulate the behaviour of the cell under certain field strengths. We predict the applied torque caused by the field at certain points throughout the layer. Consideration of viscosity and the elastic constants of the material permits us to determine the deviation from the undisturbed director profile at time intervals of our choosing. The program runs on Comsol, formerly Femlab, within Matlab.

2.4 Waveforms used

Variations of the amplitude modulated waveform were also applied to liquid crystal cells and the resultant permittivity profiles studied.

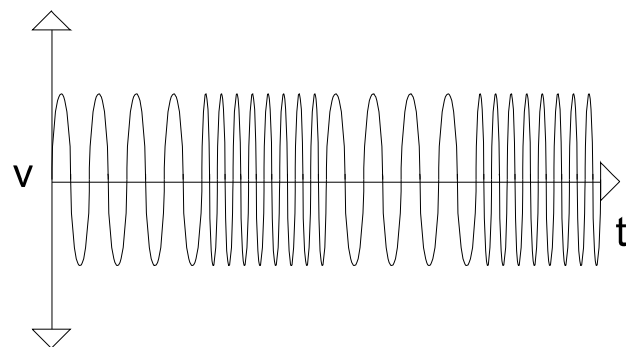
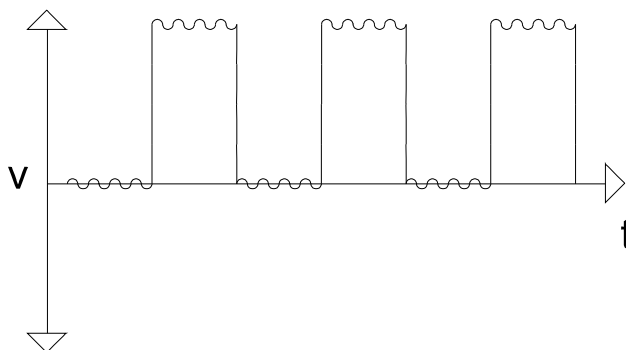
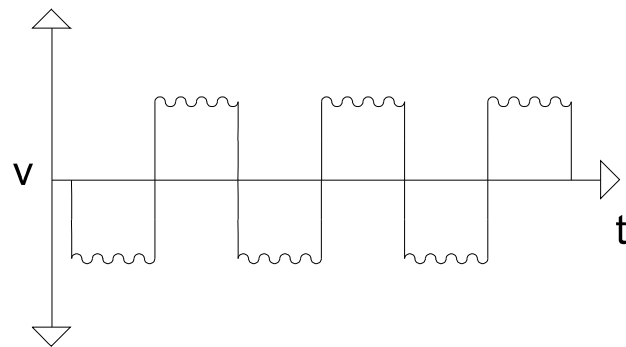
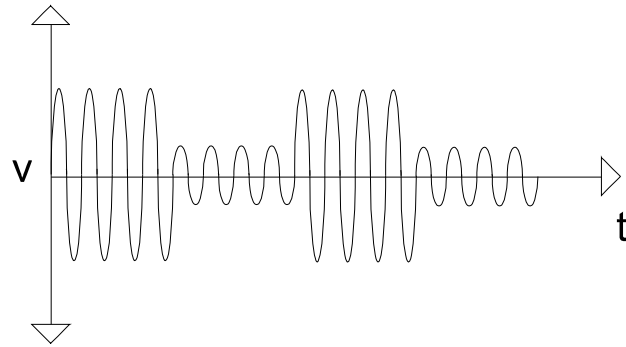


Figure 2.6 Transient technique – modulated waveforms

Figure 2.6 depicts the principal waveforms used. These are largely amplitude modulation based but the technique is extended to frequency modulation (the last part of Figure 2.6) in chapter 4. Two D.C. waveforms are explored, a square wave and an offset square wave. The pulse train waveform is composed of two D.C. pulses of opposing sign (to avoid exposing the cell to too much D.C. bias).

The frequency modulated waveform is composed of two sine waves of common amplitude, one of high frequency and one low (typically 100kHz/1kHz). In all of these variant waveforms a low amplitude tracer (sub threshold) sine wave is summed with the waveform to allow the amplifier to lock in to a single frequency. This wave plays no part in the switching of the liquid crystal cell.

The sudden change in amplitude of the D.C. and pulse train waveforms causes a small spike in the output as the Lock in amplifier struggles to find the signal. This spike has a width of around 2-10 milliseconds and is removed from the data in processing. The notation used varies with the waveform used: V_1 refers to the amplitude of the ‘switching’ part of the waveform and V_2 the ‘relaxing’ part; when applied to the amplitude modulated sine wave. In other Cases (where a tracer wave is used) V_1 refers to the amplitude of the whole waveform and V_2 to the amplitude of the tracer wave. T_1 Refers to the period of application of one part of the waveform such as ‘switching’ or ‘relaxing’, T_2 refers to the period of the entire waveform.

Where frequency modulation is used; F_1 and F_2 refers to the high and low frequencies respectively.

2.5 Validity of technique

The accuracy of the experimental set up was tested by applying a single amplitude wave (varied from 0.25 to 3.5V) to one of the cells. Its response was measured dynamically and the mean permittivity derived. This was then repeated statically with the L.C.Z. meter, the results are in good agreement with a gradient of 0.9901 and an intercept of 0.1294, shown in figure 2.7

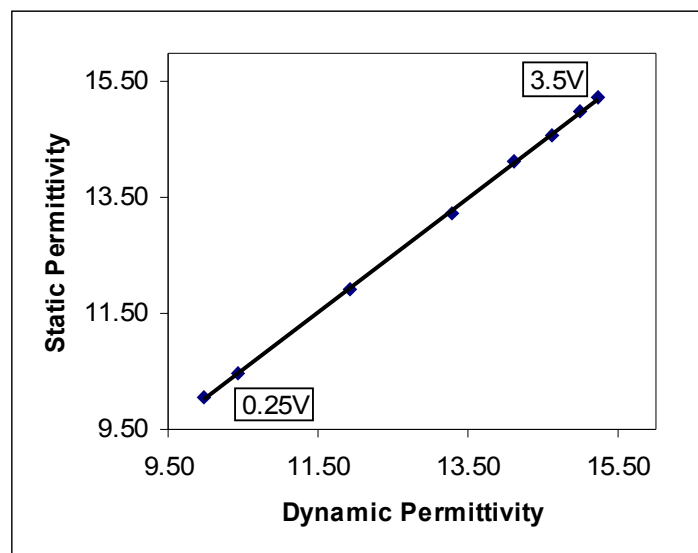


Figure 2.7 **Static vs Dynamic Permittivities**

Figure 2.8 shows the capacitance of the E7 cell varying linearly with the reciprocal of the applied voltage as expected. The table in Figure 2.9 shows the material, alignment, width, empty cell capacitance and relevant permittivities (found statically) of the cells used at time of manufacture.

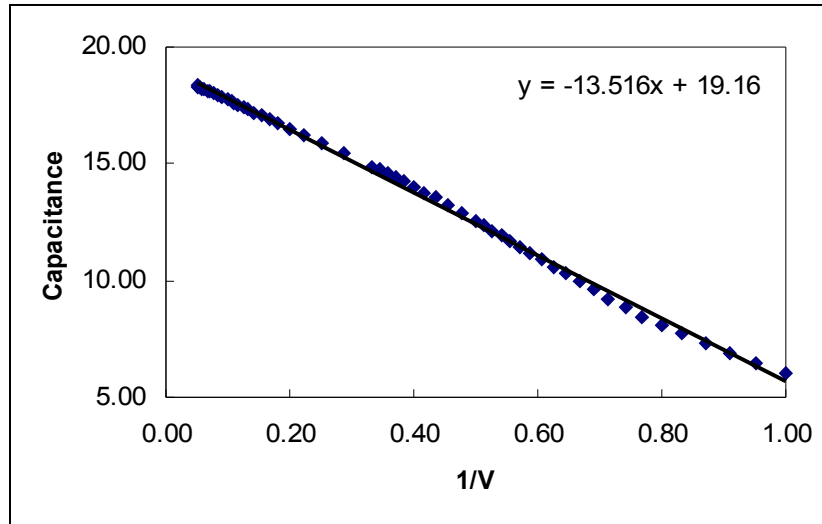


Figure 2.8 Capacitance vs 1/V for E7

Cell name	Alignment	Guard ring?	Co (pF)	G (μ S)	E perp	Epara
CKAPR0401	homeotropic	y	45.5	0.032		19.14
CKAPR0402	homeotropic	y	45.6	0.297		18.84
CKAPR0403	planar	y	46.4	1.925	5.22	
CKAPR0404	planar	y	45.5	2.47	8.33	
CVB0501-1	planar	y	45.32	1.0004	4.63	
CVB0501-2	homeotropic	y	45.35	0.033		16.27
CVBJUN0501	planar	y	43.79	0.01	10.33	
CVBJUN0502	homeotropic	y	44.48	0.17		2.15
CVBJUN0503	han	n	188.1	0.148	9.87	16.56
CVB0601A	planar	y	187.4			
CVB0601B	homeotropic	y	46.06			
CVB0601C	planar	n	212.2			
CVB0601D	han	n	187			
JMH310506-01	planar	n	208	0.0059		
JMH310506-02	han	n	200.7	0.0549		
JMH666A	planar	n	204.68	0.19		
JMH666B	planar	n	204.3	0.023		
CLT0606B	planar	y	45.1	0		

Cell name	Material	Batch	Width	Fill Date
-----------	----------	-------	-------	-----------

			(μm)	
CKAPR0401	E7	MF060303	22	04/05/2004
CKAPR0402	MDA-02-24 19	MF070215	22	30/04/2004
CKAPR0403	E7	MF060303	22	04/04/2004
CKAPR0404	MDA-02-24 19	MF070215	22	04/04/2004
CVB0501-1	MDA-01-20 12	MF050401	22	28/01/2005
CVB0501-2	MDA-01-20 12	MF050401	22	28/01/2005
CVBJUN0501	MLC-2048	CT02062	22	20/06/2005
CVBJUN0502	MLC-2048	CT02062	22	20/06/2005
CVBJUN0503	E7	MF060303	5	01/06/2005
CVB0601A	TL216	641879599	22	01/06/2006
CVB0601B	TL216	641879599	22	01/06/2006
CVB0601C	TL216	641879599	5	01/06/2006
CVB0601D	TL216	641879599	5	01/06/2006
JMH310506-01	TL216 + E7		5	31/05/2006
JMH310506-02	TL216 + E7		5	31/05/2006
JMH666A	E7	MF060303	5	06/06/2006
JMH666B	2F		5	06/06/2006
CLT0606B	E7	MF060303	22	06/06/2006

Figure 2.9 Project Cell details

Chapter 3: Transient Capacitance Study

3.1 Introduction

In this chapter a diagnostic technique for the parameterisation of physical properties of liquid crystals is presented. The method allows the study of the dynamic changes experienced by a liquid crystal cell when exposed to a static or continuously varying field. Particular reference is paid to the Freedericksz transition and subsequent relaxation. Several materials are subjected to the technique and the results presented. The method is shown both to have advantages over current techniques and to produce results which are in line with known values for the materials used.

3.2 Theory

There have been a large number of studies into the time evolution of the reorientation of the optical axis in nematic liquid crystal displays and other optical devices. Well-established methods for probing the time-dependent reorientation of the n-director measure the change in the birefringence of the device using conoscopy, ellipsometry or by measuring the transmission between crossed polarisers [Brochard, 1972], [Blinov, 1983], [Clark, 1986]. These methods give results that depend on some average of the n-director orientation across the whole device thickness. Guided mode and optical waveguide methods are sensitive to differences in the orientation of the local optical axis that might occur through the thickness of the device. These techniques allow the variation in the n-director orientation as a function of both time and position within the device to be measured [Mitsuishi 1996], [Smith 2000].

There has only been limited investigation of the time-evolution of the capacitance of nematic liquid crystal devices when time-varying electric fields are applied to the device and then removed. In reference [Huang, 1995] the change in the capacitance of a surface stabilised cholesteric texture device was studied by monitoring the division of a constant applied voltage between the liquid crystal device and a series fixed capacitor. In practice this measurement is made more complicated because the inevitable presence of ionic contamination in the liquid crystal means that a resistor effectively appears in the circuit. The change in capacitance of a nematic Freedericksz cell after the removal of an applied voltage just above the Freedericksz threshold was studied in reference [Chattopadhyay, 1993] using a commercial capacitance bridge. This allowed voltage on and voltage off time constants to be measured but there was no comparison with the predictions of continuum theory. A quasi-periodic oscillatory

decay in the capacitance was observed after a voltage of 1.0 V r.m.s. was abruptly switched off for a cell containing the material 7CB.

In this study a flexible technique was used to study the transient capacitance of liquid crystal devices that are subjected to continuous amplitude modulated a.c. electric fields. The Freederizksz cell device geometry was used to investigate three nematic materials. It will be shown for two of these materials with low applied voltages that the results can be accurately fitted using nematic continuum theory with a single viscosity. For the third material, unusual relaxation curves were observed suggestive of damage to the cell or degradation of the material, though despite this a broad fit with theory was achieved.

3.3 Static permittivity measurements

Three commercial nematic liquid crystal materials were used in the study; MDA02-2419, E7 and MDA01-2012 (supplied by Merck). The materials were capillary filled into capacitance test cells in the isotropic phase. On each substrate rubbed polyimide surface alignment was used, which gives a low surface pretilt of below 0.5° .

The capacitance was measured as a function of applied voltage using an Agilent 4284A capacitance bridge. Figure 3.1 a, b shows the average permittivity as a function of a.c. voltage at 1 kHz for E7 (a) and MDA01-2012 (b) and at a temperature of 24°C . These are cells 1 and 3 respectively, cell 2 (material: MDA02-2419) will be discussed in the results section. Each of the curves shows a sharp threshold above which the permittivity increases rapidly – the Freedericksz threshold voltage $V = V_C$ [Freedericksz, 1933]. At voltages just above the threshold critical slowing down occurs and so, as is standard practice, small voltage increments and large wait times between increments were used [Raynes, 1981].

All of the materials used in the study exhibit positive dielectric anisotropy, $\Delta\varepsilon = \varepsilon_{\parallel} - \varepsilon_{\perp} > 0$, where ε_{\parallel} is the permittivity measured parallel to the n-director and ε_{\perp} is the permittivity measured perpendicular to the n-director. The permittivity measured below the threshold is therefore the permittivity measure across a planar aligned layer, ε_{\perp} . Above the threshold the field acts to reorient the n-director towards homeotropic alignment so that the largest component of the permittivity is aligned

with the field across the cell. However, if the n-director is anchored parallel to the surfaces then an elastic coupling between the n-director in the bulk of the cell and the n-director at the surface acts against the electric reorientation torque. At higher applied voltages, $V \gg V_C$, a large proportion of the bulk of the cell has reoriented towards homeotropic and the measured permittivity value asymptotes towards ϵ_{\parallel} .

The shape of the permittivity versus a.c. voltage curve is very accurately described using the Frank-Oseen nematic continuum theory [Frank 1958], [Oseen 1933]. In this theory the magnitude of the splay, bend elastic distortions in a nematic liquid crystal director field are parameterized by the K_{11} and K_{33} elastic constants, respectively.

The theory predicts that the Fredericksz threshold voltage is given by

$$V_C = \sqrt{\pi^2 K_{11} / \epsilon_o \Delta \epsilon} .$$

Above the Fredericksz transition the shape of the curve is controlled by the ratio of two elastic constants; K_{33} / K_{11} . The elastic constants and the permittivity values that have been obtained by fitting the static continuum theory to the curves shown in figures (1a) and (1b) are given in table 3.1: Static permittivity as a function of applied a.c. voltage at 10 kHz for (a) MDA01-2012 and (b) E7 measured in the planar Fredericksz geometry.

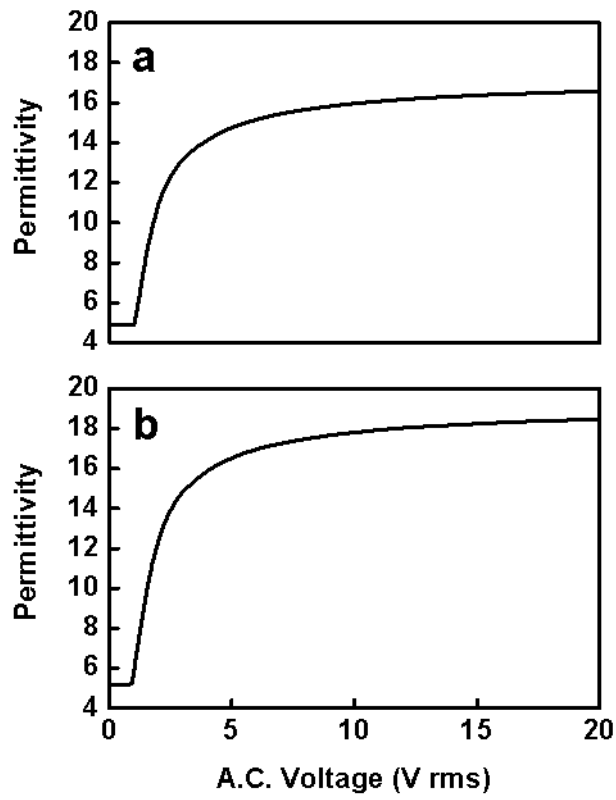


Figure 3.1 Static permittivity for cells 1 (a) and 3 (b)

	E7		MDA01-2012		MDA02-2419	
	(cell 1)		(cell 3)		(cell 2)	
	Static	Dynamic	Static	Dynamic	Static	Dynamic
ϵ_{\parallel}	19.1	19	17.2	17	48.2	36.6
ϵ_{\perp}	5.21	5.35	4.91	4.82	8.25	10.53
K_{11}	10.8	10.5	11.9	12.7	7.3	-
(pN) K_{33}	14.7	15.2	12.1	10.3	15.1	-
(pN) $\gamma_1 \mu \sigma$	-	0.18	-	0.18	-	-
$N^{(2-)}$						

Figure 3.2 table of results

Values obtained in Figure 3.2 for the dielectric and elastic parameters of E7 and MDA01-2012 are from fitting the static and dynamic permittivity data in figures 3.1 and 3.3 through to 3.8 with nematic continuum theory. The value obtained for the Leslie rotational viscosity γ_1 was obtained from the dynamic data. The values shown for cell 2 vary greatly from those found at the time of the cells construction (see figure 2.9). That this disparity is evident in both the static and dynamic measurements is strongly suggestive of damage and/or contamination to the cell and is discussed further in section 3.5.

3.4 Transient permittivity technique

Equipment used:

Resistor:	Decade 8000
Arbitrary waveform generator:	TTi (TGA1242)
Oscilloscope:	Agilent 54622A
Lock in amplifier:	DSP 7265
Differentiator:	741S

The parallel and perpendicular components of permittivity for the chosen material may be found utilising the static A.C. technique espoused by [Stromer et al , 2003] and are shown for the materials in question in table 1.

An arbitrary wave generator was used to create an amplitude modified sinusoidal A.C. field. This signal is applied to a planar aligned, $22 \mu m$ thick nematic liquid crystal cell which is treated as a capacitor. The cell utilises a circular indium tin oxide electrode with an earthed guard ring to minimise fringing of the electric field at the cell edges. Fields exceeding the Freedericksz threshold for the cell cause realignment of the mesogens towards the heterogeneous state. Below this threshold thermal vibrations and internal elastic forces quench the realignment. The uniaxial anisotropy in electric permittivity gives rise to a capacitance which varies with the alignment of the cells director profile relative to the field. The waveform consists of two distinct sections; a high amplitude (switching) section and a low amplitude, sub-Freedericksz (relaxing) section. Both sections utilise a common frequency; chosen, in this case, to be 10 kHz in order to outpace ionic motion and avoid screening of the field. With lower frequencies ion motion occurs, generating a secondary field of opposite polarity to the applied field which partially screens the sample from the applied field.

A differentiator circuit is utilised to reduce the output of the liquid crystal capacitor to an amplitude which is acceptable to the input limits of the lock-in amplifier. The amplifier is locked to the capacitive component of the current; that is, the part of the current which is -90° out of phase with the input signal. This is determined using a synchronised reference signal from the arbitrary wave generator. The output is compared with the original input signal via a digital oscilloscope.

Comparison of the magnitudes of the input and output signal permit determination of the capacitance of the cell using the simple relation:

$$\left(\frac{V_{in}}{V_{out}} \right) = - R \omega C \quad (3.1)$$

where R is the resistance utilised in the differentiator, ω the angular frequency of the wave and C the capacitance of the liquid crystal cell. The mean permittivity of the cell is then obtainable providing that the empty cell capacitance is known. This in turn allows the average director alignment across the cell to be determined from knowledge of the parallel and perpendicular permittivities.

3.5 Transient permittivity results

Planar aligned cells containing three materials (E7, and MDA-01-2012) were studied during switching and relaxation at four different field strengths ranging from very close to the Freedericksz threshold to several multiples of the threshold value. The experiment was performed at two values of T2 (see section 2.4). Despite operating at field strengths close to the Freedericksz transition no oscillation was observed in the cell relaxation profile [Chattopadhyay, 1993]. All three cells show a broadly exponential reduction in permittivity during relaxation which is largely independent of the applied voltage (Though there is some deviation in cell two). The gradient of the switching profile is affected by the input voltage as expected; with higher fields switching the mesogen faster and more completely towards the heterogeneous state. Reduction of the sequence period reduces the time available for relaxation of the sample. In some cases this may decrease the time required for switching as the cell is unable to return completely to a planar alignment before the switching section of the waveform is applied.

Permittivity

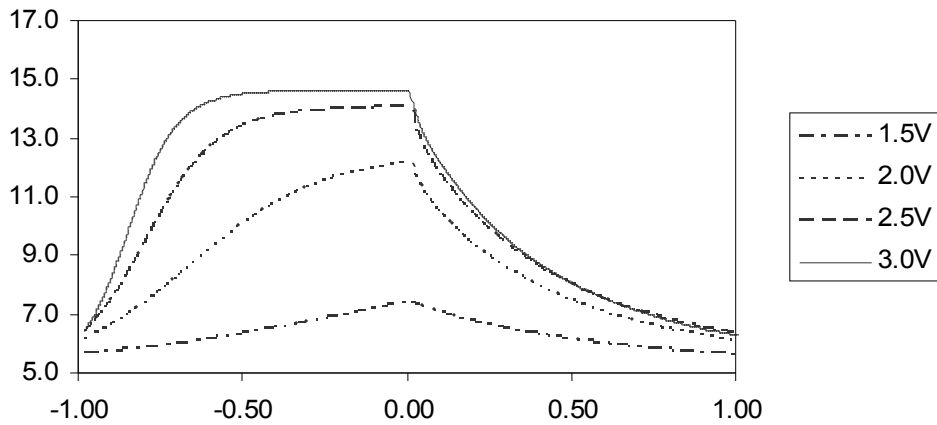


Figure 3.3 cell one fast A.C. modulated results

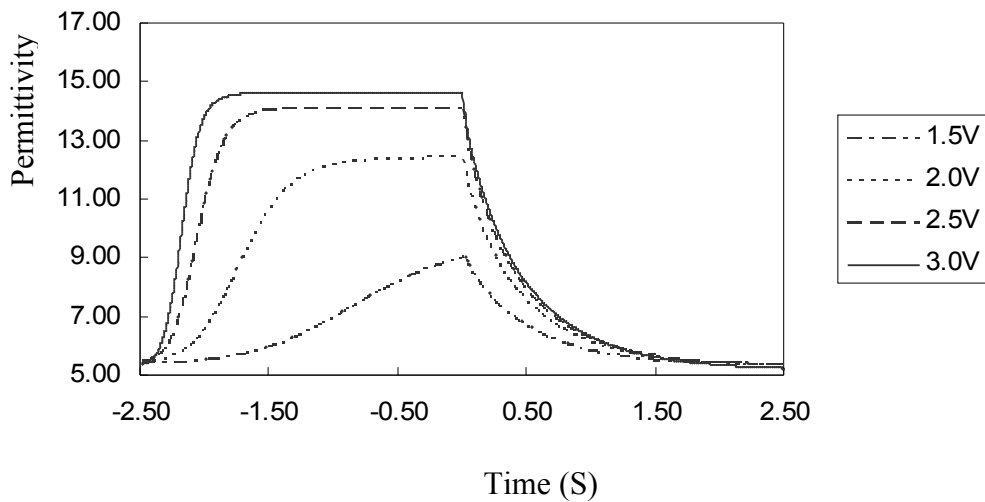


Figure 3.4 cell one slow A.C. modulated results

The experimental results for E7 (cell 1, Figures 3.3, 3.4) show good agreement with liquid crystal continuum theory both in the development of a saturation value for the permittivity at a given applied field strength which is dependant on the magnitude of the field and in the exponential nature of the relaxation curve. The applied post

Freedericksz field strength is listed for the individual curves to the right of each figure. Two overall periods were used; 2.0 seconds and 5.0 seconds. Increased field strength corresponds to fuller and faster switching. Relaxation is seen to be exponential in character and in the longer period study full relaxation is observed for all field strengths. The lower permittivities are in line with static measurements and the higher permittivities are within the bounds of full expression of a homeotropic alignment. The overall permittivity attained upon full switching matches that suggested by the static curves shown in Figure 3.1.

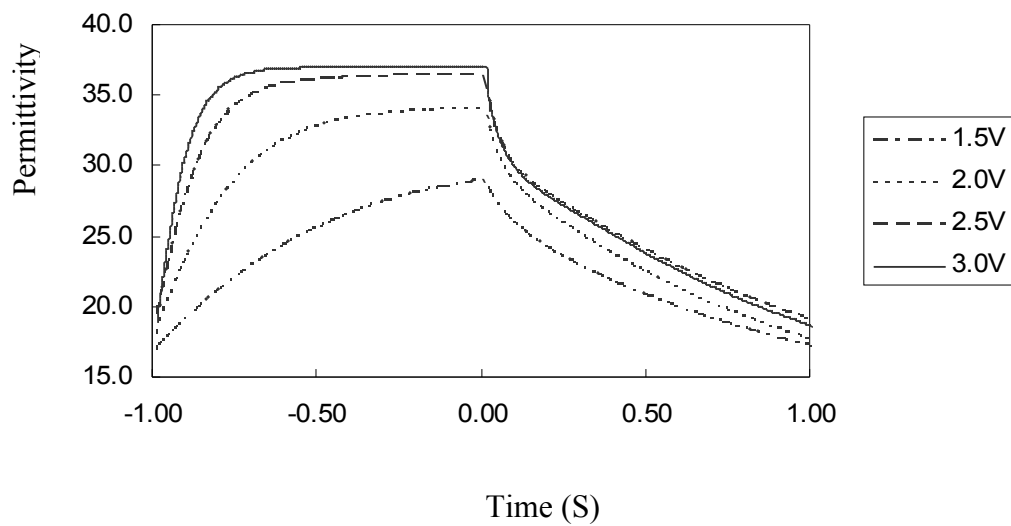


Figure 3.5 cell two fast A.C. modulated results

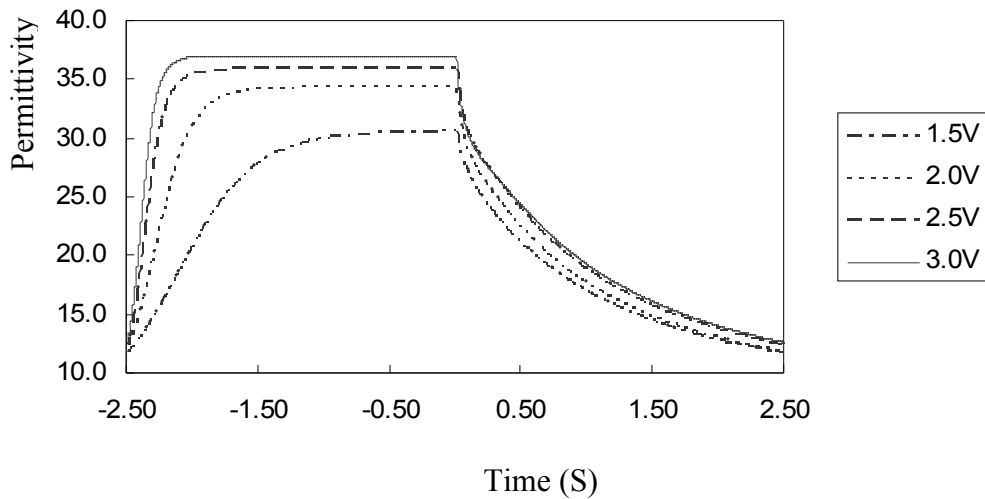


Figure 3.6 cell two slow A.C. modulated results

The results for mda-02-2419 (cell 2, Figures 3.5, 3.6) are initially in line with expectations; higher fields allow for faster and more complete switching. The field strengths quoted are rms values. In the case of an overall period of 2.0 seconds there appears to be a difference in the minimum permittivity levels reached; this is seen not to be the case when the longer 5.0 second period case is considered. Now we are able to see that this is an artefact of the degree of switching evinced being too great to allow full relaxation in the time available. The results for this material proved more resistant to fitting to theory than the other materials studied. The relaxation curves in particular seem to show a deviation from the expected exponential character. As a result only fitted graphs for cells 1 and 3 are included. This could be explained by an unusually high k_{33} value combined with a low k_{11} to prevent too much change to the overall permittivity in the switched state. This effect may also arise from the fact that this cell is older than those of the other materials, and may have suffered more ionisation. If ions are present in significant amounts they would partially shield the cell from the full field strength. Since ionic contamination is ignored in the fitting

program theory would suggest a higher switching level than was observed in the experiments. This would tally with a slightly higher k_{33} value and help explain the unusual relaxation. In addition to the field shielding of an ionically contaminated cell the translational motion of ions under a field (as opposed to the rotational motion of the mesogens) can exacerbate flow effects (which are also omitted from the fitting program). It is known that in materials with a large dielectric biaxiality the field can no longer be assumed to be uniform across the sample. This may have contributed to the inability of the program to fit the experimental data.

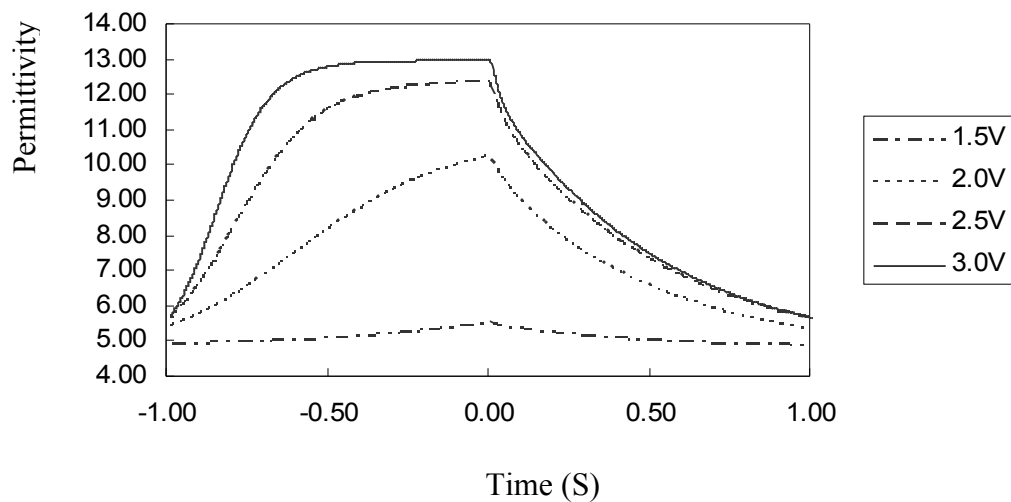


Figure 3.7 cell three fast A.C. modulated results

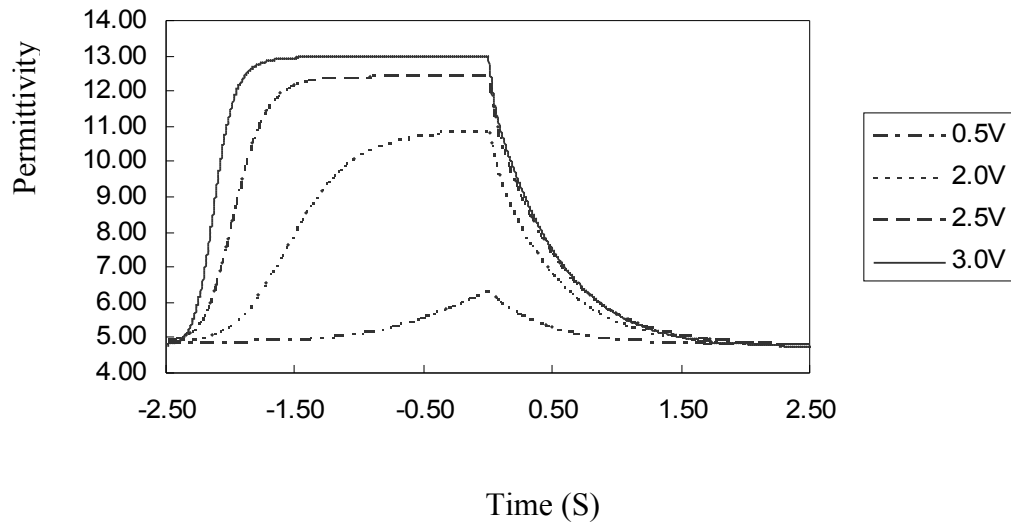


Figure 3.8 cell three slow A.C. modulated results

The results for MDA01-2012 (cell 3, Figures 3.7, 3.8) are similar in character to those for E7 and again tally well with static measurements and the predictions of theory.

The data was fitted with a theoretical model (discussed in section 2.3) which utilised liquid crystal continuum theory to predict the minimum energy configuration of the mesogens using the small angle ($\theta \approx 0$) surface anchoring as the boundary conditions. The model then calculates the expected director profile deviation from the minimum energy configuration for an applied field. The alignment of the mesogens relative to the field vector was then used to determine the average permittivity experienced by the field. A single viscosity was used and this, along with the elastic constants k_{11} and k_{33} were varied to achieve a fit with the predictions of continuum theory.

Variation of the viscosity was found to change the speed of switching and of relaxing in line with what one would expect; a higher viscosity slowing the deformation and relaxation of the director profile. No effect was observed on the maximum or

minimum average permittivity levels. This is displayed in figure 3.9; the dotted line indicating a low viscosity, the solid line a medium viscosity and the dashed line a high viscosity. The viscosity was varied from 0.15 to 0.35 Ns/m.

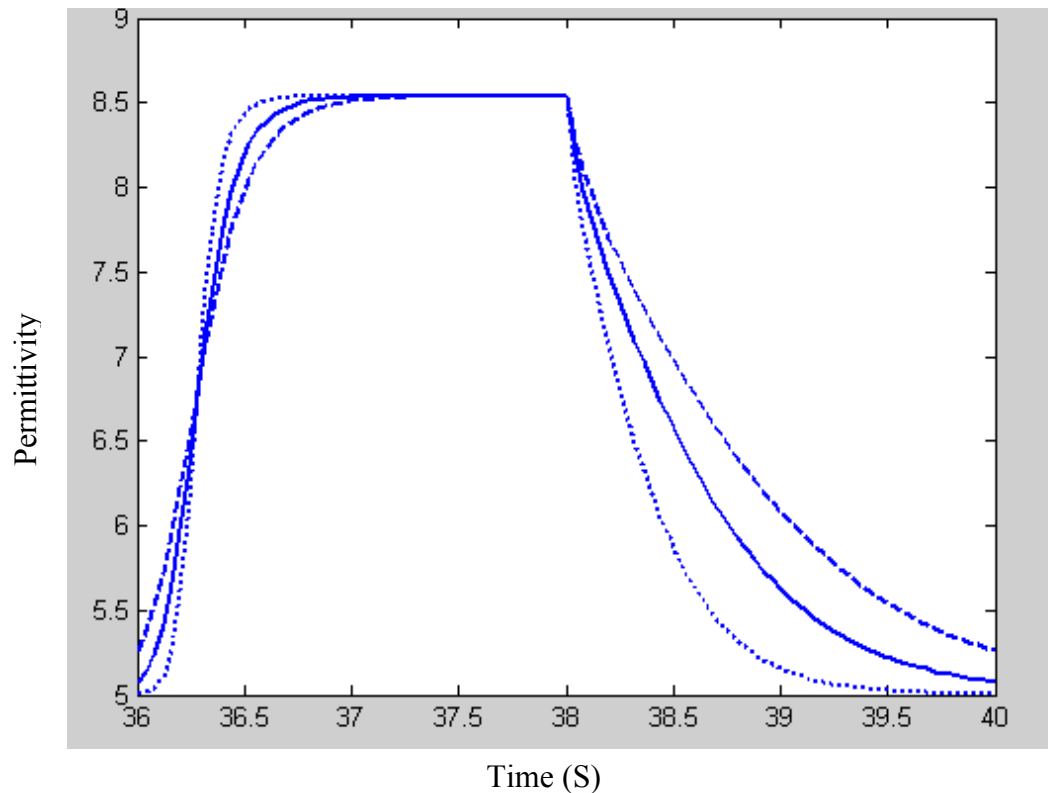


Figure 3.9 Variation in viscosity

In the case of the elastic constants k_{11} and k_{33} we see that they affect both the speed of switching and relaxation and also the maximum permittivity reached. This is shown in figures 3.10 and 3.11 respectively; in each case we move from low values (dotted line) through medium values (solid line) to high values (dashed line). There appears to be little effect on the minimum permittivity level except where the maximum is raised to the point where it is no longer possible for full relaxation to occur prior to the reapplication of the high field component of the waveform. The

effects of variation are qualitatively similar for both of the elastic constants considered. They differ quantitatively in that k_{33} shows a greater degree of variation in the resultant transient permittivity curves when varied over the same range. The elastic permittivities were varied from 5E-12 to 25E-12. the high field used was 5V rms and the low field used was 0.5V rms. A nominal Pretilt of 0.0016 radians was used.

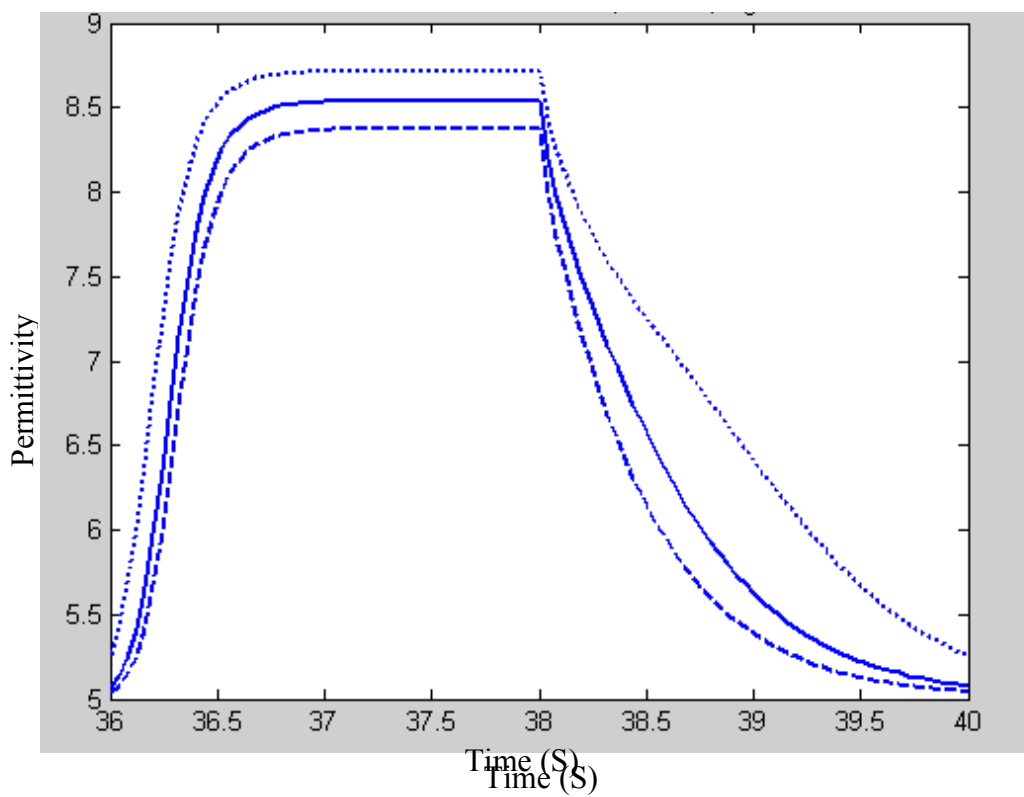


Figure 3.10 Variation in k_{11}

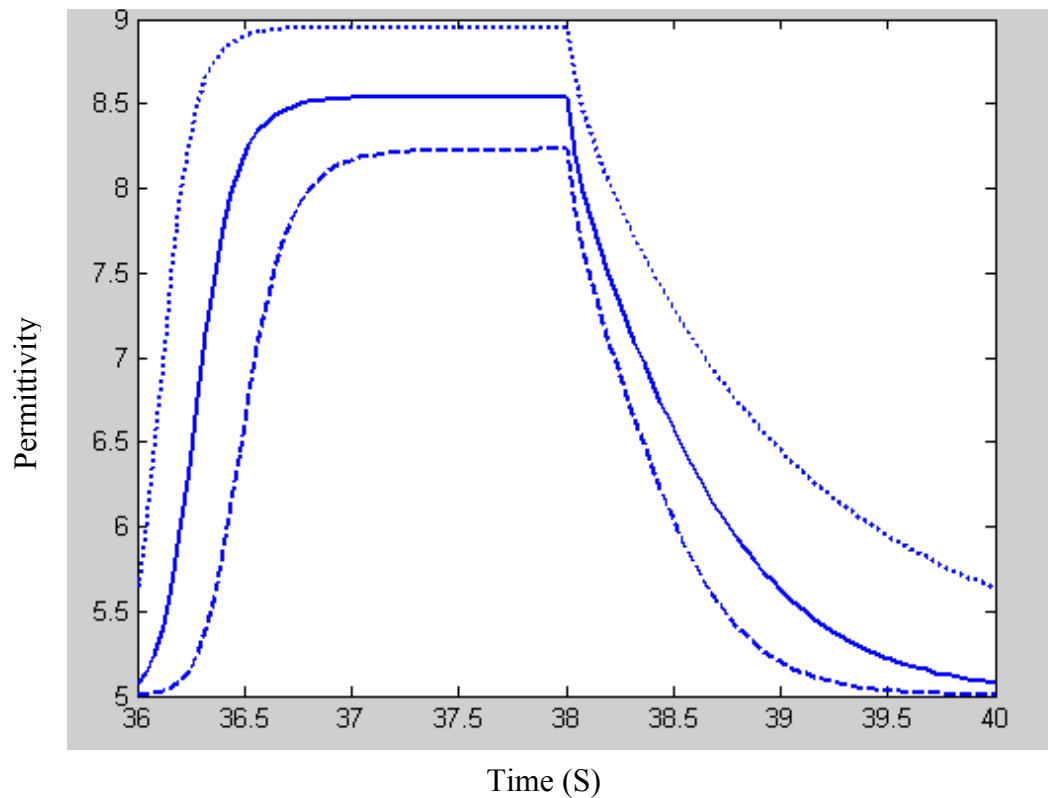


Figure 3.11 Variation in k_{33}

The experimental data shows similar relaxation curves for cell one and cell three without recourse to flow effects. This is likely due to the low field strength causing slow realignment of the mesogens and so minimising flow. This view is supported by the reduction in accuracy of the fit to theory with increased field strengths. The model also omits flexoelectric terms; that the models still fit well to theory suggests that for the samples and voltages used the flexoelectric effect is small and may be neglected. The unusual relaxation curve of cell two proved resistant to the fitting process used, possibly for reasons discussed above. The results for cells one and three are shown in figures 3.12 and 3.13 respectively, as are the predictions of the modelling program.

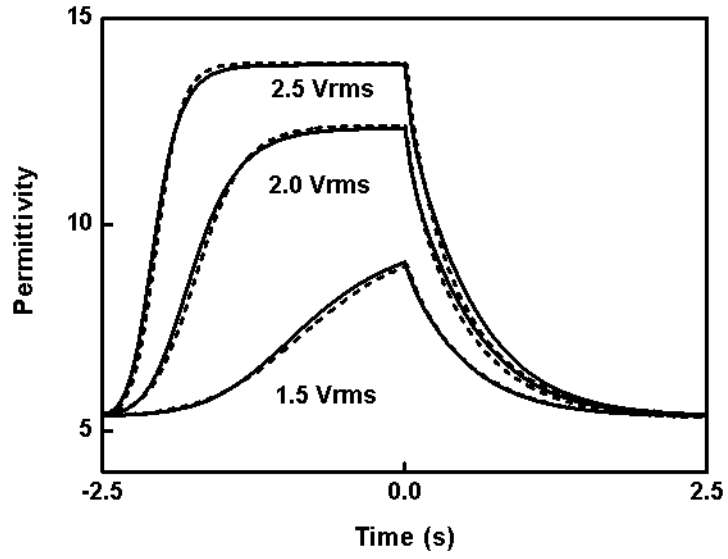


Figure 3.12 Fitted results for cell 1

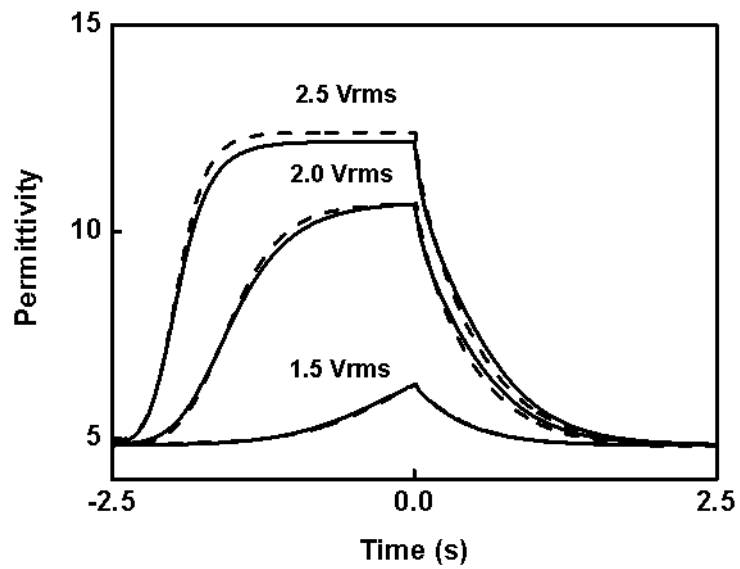


Figure 3.13 Fitted results for cell 2

3.6 Conclusions

The method described is a useful explorative tool for dynamically analyzing director profile deviation in response to an applied field. It permits the parallel and perpendicular components of the electric permittivity to be found and may be used to determine the Fredericksz transition point of a sample. The fit with theory demonstrates that for low fields flow and flexoelectric effects may be neglected. The method is adaptable to D.C. applications with the alteration of the waveform used to a square wave of comparable magnitude to V_1 , summed with a sine wave of sub-Fredericksz magnitude. The method may also be applicable to any dielectric medium in which the permittivities are expected to vary on short time scales.

Chapter 4: Transitive Capacitance Study of Dual Frequency Liquid

Crystals

4.1 Introduction

In this chapter the transient capacitance technique is adapted to frequency rather than amplitude modulation. The technique is applied in both forms to dual frequency liquid crystals and the results compared with theoretical predictions. Recent work on the pulsed addressing of dual frequency HAN cells is explored and attempts are made to manifest some of the theoretical predictions of this work experimentally.

4.2 Theory

Dual frequency liquid crystals, as all polar liquid crystals, manifest different electromagnetic properties when exposed to fields of low and high frequencies. In the case of dual frequency materials there is a Debye type relaxation of the dielectric permittivity along the long and short axes at different frequencies [Brimicombe, 2005]. This is due to the molecular anisotropy of the mesogens; rotation about the long axis takes less time than about the short axis leading to this contribution to the polarisation being removed from the overall dielectric the along the long axis before the short axis when frequencies are raised. [Debye, 1929] Although this does of course happen with any anisotropic liquid crystal molecules, in the case of the materials studied this relaxation reduces the parallel component of permittivity to less than the magnitude of the perpendicular permittivity at frequencies easily achievable experimentally. Furthermore, the difference between the two permittivities δ is of comparable magnitude (though opposite in sign) at very high and very low frequencies. This may be seen by sequentially exposing planar and homeotropic cells to low magnitude fields of increasing frequency (the resultant average permittivity then being measured using an LCR bridge) as is shown in figure 4.1

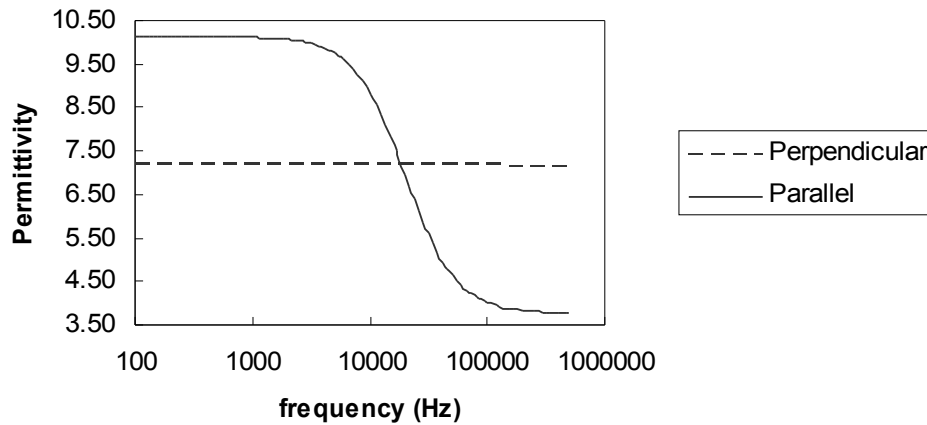


Figure 4.1 High frequency dielectric relaxation

In materials where the relaxation of this component of the parallel permittivity leads to a value lower than that of the perpendicular permittivity the same material changes from a positive to a negative dielectric anisotropy [Raynes, 1974]. The frequency at which this occurs is termed the crossover frequency. At or around this frequency application of an external field is unable to couple to the polarisation to exert torque on the mesogens and so switch them from one state to another. This is due to the effective isotropy of the mesogens when exposed to a field of that frequency.

One such material is TL216 developed by Merck. This material was characterised by [Mottram, 2006]. Static capacitance tests included in that paper are displayed below in figure 4.2. Comparison with the empty cell capacitance then allows calculation of the effective average permittivity from which the average angle made by the director with the field may be inferred. Sub Freedericksz fields leave the director profile largely undisturbed in the planar geometry and allows determination of the perpendicular permittivity component; similarly the homeotropic alignment may be used to find the parallel component.

Application of the amplitude modulated waveform (of low frequency to the planar cell and high frequency to the homeotropic cell) produced results consistent with the established permittivities, and showed relaxation which was exponential in character as expected.

The results are as we would expect when applying an amplitude modulated sine wave of a single frequency to a planar nematic cell and are shown in figure 4.2. In this case the susceptibility is shown:

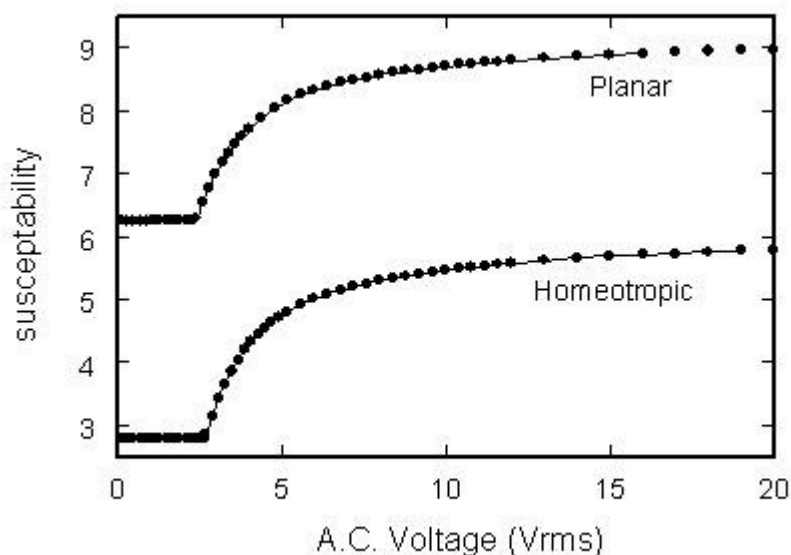


Figure 4.2 static capacitance results

[In any application of this technique we need to be aware of the possible effects of dielectric heating. Dielectric heating occurs from the loss induced by the Debye type relaxations of one or more contributions to the effective dielectric constant \$\epsilon_{eff}\$. The degree of heating \(\$\Delta T\$ \) is in linear proportion to the material width \(d\) and the](#)

effective dielectric anisotropy; considered to be the difference between low and high frequency values ($\Delta \varepsilon_{para}$), and is proportional to the square of the applied voltage [Maddock 1946]. Although M. Schadt (1980) found that significant temperature increases (several Kelvin) could be achieved experimentally, certain factors suggest that this will be of minimal importance in this case. Firstly, $\Delta \varepsilon_{para}$ for the material TL216 is around a fifth of the value of the material studied by Schadt, though the cell sizes are of comparable order of magnitude. Secondly the temperature rises discussed by Schadt are considered only statically; that is as t tends to ∞ . The time dependence of this effect cannot be ignored in a dynamic study. With a similar cell to those used in this chapter it was found that around 100 seconds was required to achieve 90% of the expected temperature increase. Since significant fields were applied for just a few seconds at most, and generally at lower field strengths than those in the paper this effect may be largely ignored. Lastly, in the case of the pulsed addressing section, where higher voltages were applied, the duration of application was reduced to less than a millisecond. The equation derived by Schadt for this purpose is as follows.

$$\Delta T = \left[\frac{V^2 A \varepsilon_0 (\Delta \varepsilon_{para})}{d(C + q_1 t)} \right] \times \left[\frac{\tau_n \omega^2 t}{(1 + \omega^2 \tau_n^2)} \right] \quad (1)$$

where V is the applied voltage, A the electrode area, d the nematic layer thickness, t the time available for heating, τ_n the relaxation time, ω the applied frequency, ε_0 the permittivity of free space and C the mean heat capacity for the cell (including substrate)

4.3 Amplitude modulation

Fields of 5-7V RMS were applied to a planar aligned dual frequency cell for a period of 2 seconds followed by a sub Freedericksz threshold field (approx 0.2V) for a further 2 seconds. Gradual alignment of the director with the field is observed in the first section, an exponential decay is then seen in the relaxation period. These results have been fitted to theory using a simple modelling program which utilises a single rotational viscosity and neglects both flow effects and flexoelectricity. The experimental results are shown below; alone (figure 4.3) and with fits (figure 4.4).

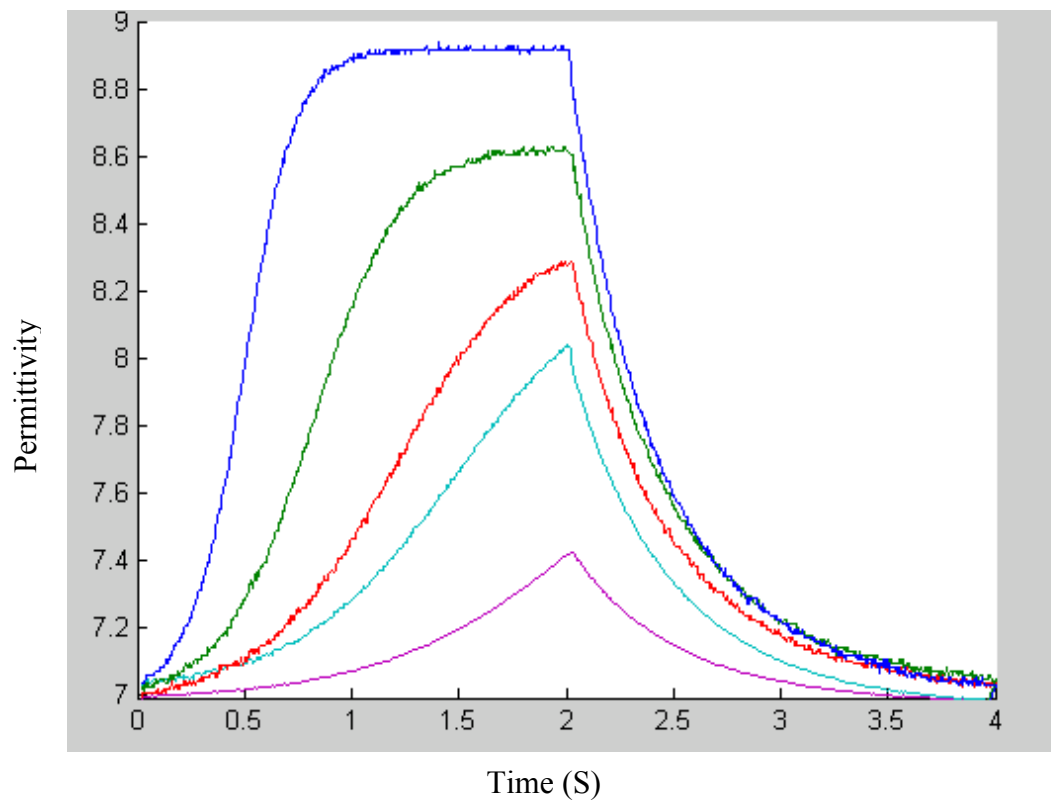


Figure 4.3

Amplitude modulated planar results

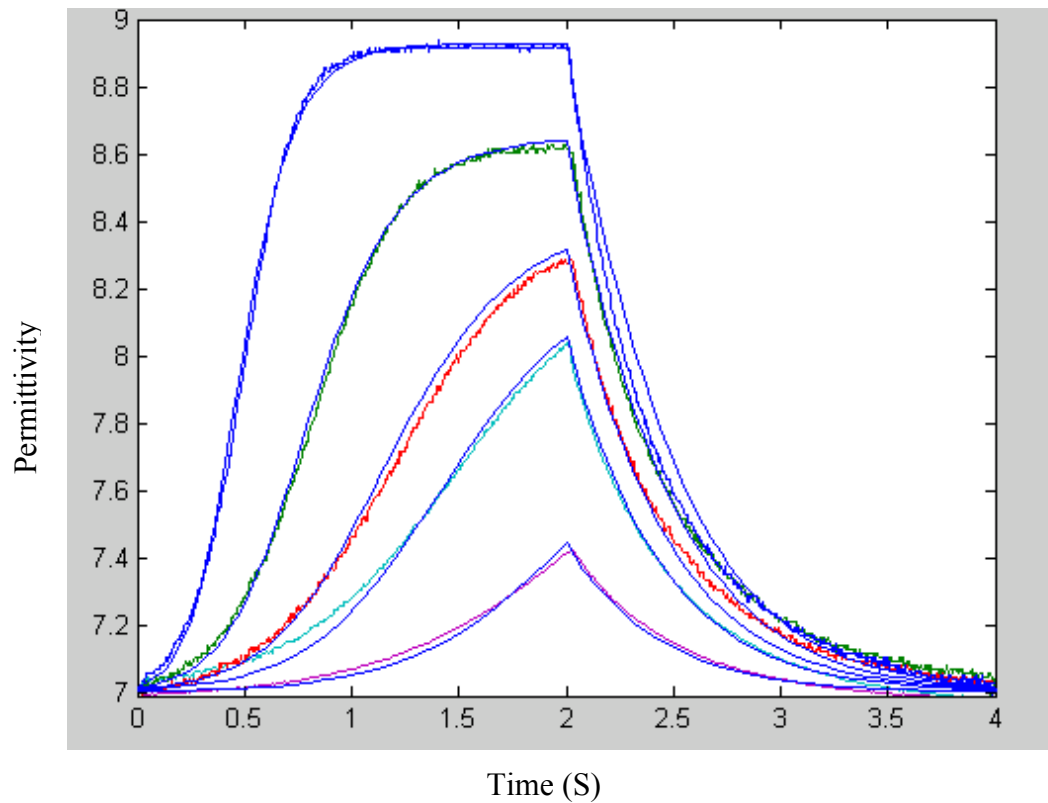


Figure 4.4 Planar amplitude results with fits

These fits were achieved using values for the elastic constants k_{11} , k_{33} of 15.8 and 23.2 respectively. The rotational viscosity chosen was 0.25 and the Pretilt was 0.00158° . From these graphs we may see that although there is some small difference in the shape of the curves, the permittivity measured when switched and unswitched generally fits well to theory without recourse to either flow effects or flexoelectricity. As the results are in line with the expected values we may conclude that ionic contamination, if present, has little impact on switching behaviour at the frequency used (1kHz). Had such been present in significant quantities we would have expected some shielding of the field to occur.

4.4 Frequency modulation

In addition to the amplitude modulated wave form previously discussed, switching between states may be achieved using a constant amplitude (RMS) signal which varies in frequency. This has the advantage of allowing one to use the field to forcefully return the cell to its planar state without relying solely on the visco-elastic forces otherwise driving the relaxation process. The high frame rate of video displays requires liquid crystal materials which switch rapidly between the on and off states; in such a field the ability to control the relaxation time is highly desirable. [Jewell, (2005)] In Figures 4.6, 4.7 it is clear that, although dependant on applied voltage, the time taken to drive the cell into a switched state is considerably shorter than the time required for it to relax back into the unswitched state. As the dielectric anisotropy is broadly similar in magnitude (though opposite in sign) at low and high frequencies we may expect that the forced relaxation of the cell will be faster even than the switching of the cell. This is since in the case of relaxation the director will experience both the visco-elastic forces usually in play and the torque from the interaction between the polar molecules and the applied field which will be of similar magnitude to the original switching force.

A frequency modulated waveform of amplitude above the Freedericksz threshold was combined with a probe sine wave of a single frequency (49kHz) and of amplitude below the threshold. This waveform was applied to the material in both the planar and homeotropic geometries. In the planar case the low frequency component of the wave acted to align the director in the bulk of the cell with the applied field, overcoming the visco-elastic forces and causing switching. The high frequency component was

greater than the crossover frequency and so the material had an effectively negative dielectric anisotropy. This acted to align the short axis of the mesogens with the field and so pushed the director back into the planar position.

As the planar alignment had been distorted from its low energy configuration by the switching part of the waveform, the visco-elastic forces act in concert with the applied field and the cell is switched back to the planar alignment in roughly 1/3 of the time taken to deform it into the homeotropic state. In the Homeotropic cell this process is reversed with the high frequency component switching the cell into the planar alignment and the low frequency component acting to restore the homeotropic alignment at a much faster rate.

Note that the permittivity as observed from the comparison of input and output voltages is in either case that determined by the frequency of the probe wave rather than that of the high or low components of the waveform. In order to find the actual average permittivity of the cell it is necessary to first interpret this permittivity as an average deviation of the director alignment and then apply that average alignment to a set of permittivities consistent with those experienced at the frequency of the driving wave being applied.

The results are shown for a planar cell using field strengths of 5, 6 and 7V rms in figure 4.5. The results for the analogous homeotropic case are shown in figure 4.6.

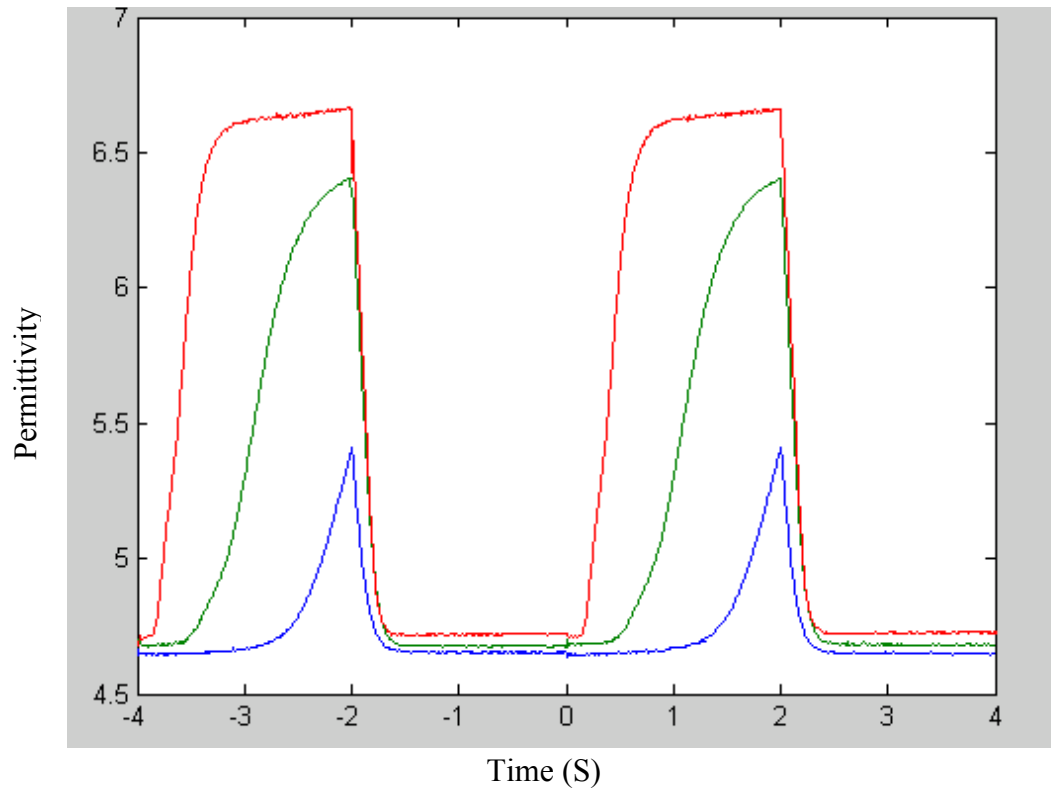


Figure 4.5 Frequency modulated planar results for 5, 6 and 7V

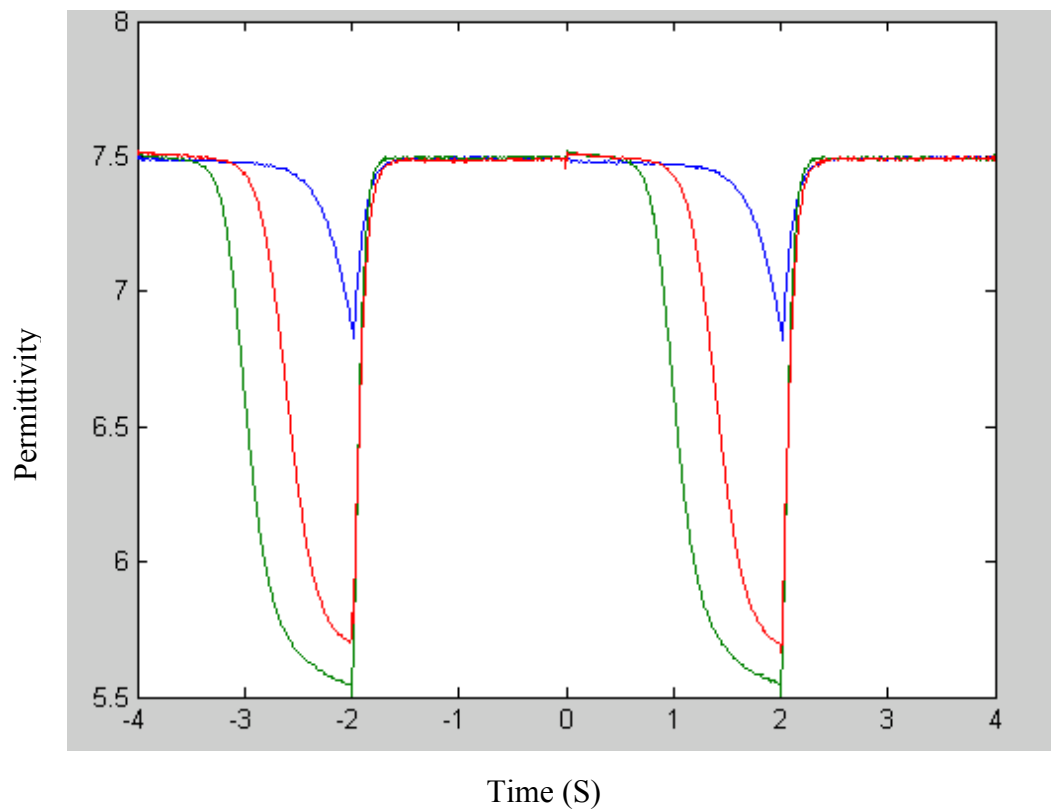


Figure 4.6 Frequency modulated homeotropic results for 5, 6 and 7V

The comparison with theoretical expectations (dashed lines) shown in figure 4.7 was found utilising the same fitting program as previously described though with a lower rotational viscosity and till angle (0.2 and 0.008 respectively).

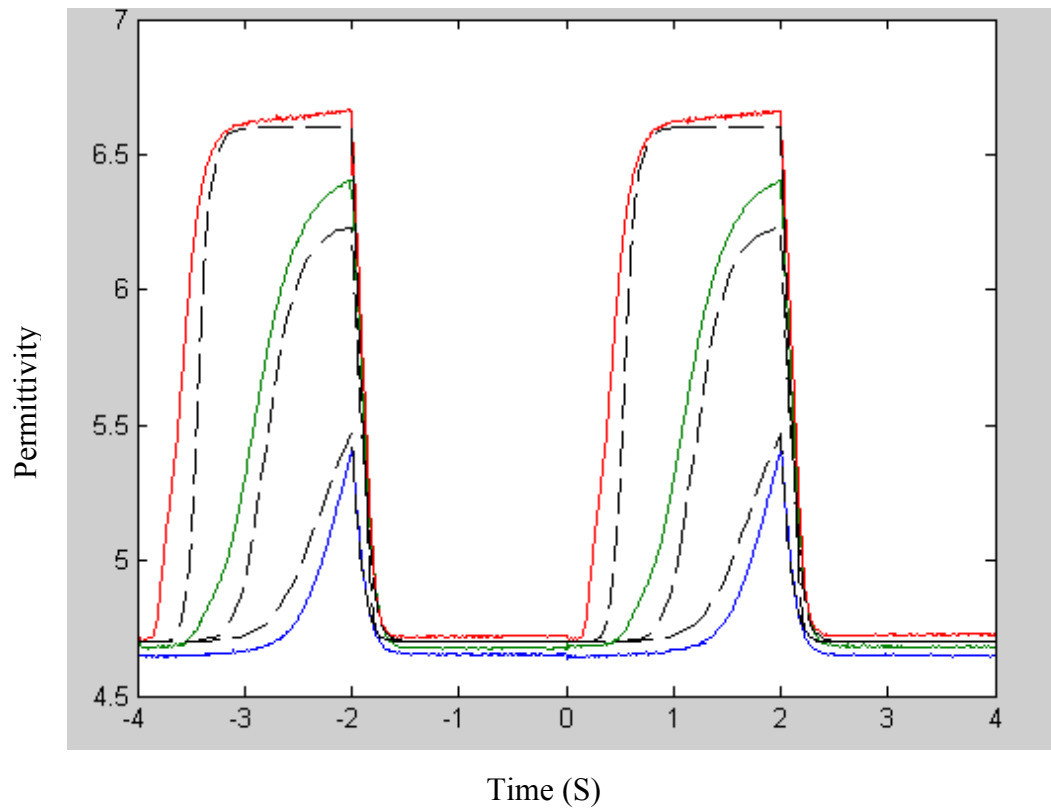


Figure 4.7 planar frequency results with fits

4.5 Homeotropic defects

The corresponding fits for the homeotropic case are harder to find. In the planar case uniaxial anisotropy allows for a degeneracy in the alignment adopted in response to the applied field. That is, in attempting to adopt an energetically favourable orientation with respect to the field (in this case normal to the cell substrate) the individual mesogens are equally likely to move through $+90^\circ$ as -90° relative to the long axis of the substrate. It should be noted that this in no way affects the director orientation provided that there is no permanent dipole attached to the long axis.

In the homeotropic case it is the low frequency part of the signal which effects forced relaxation in that the positive dielectric anisotropy of the mesogens reinforces the tendency of the director towards lying normal to the substrate and parallel to the field. When the high frequency component of the sequence is applied the material adopts a negative dielectric anisotropy and so is driven towards the planar alignment (in this case in opposition to the inherent visco-elastic forces). As in the planar case, in this system the mesogens are driven through 90° relative to the cell substrate if a sufficiently large field is applied. Unlike the planar case the homeotropic mesogens experience a range of possible degeneracies relative to the long axis of the cell substrate. While, as in the planar case, this makes no difference to bulk properties such as the director, the relative lack of orientational homogeneity leads to an increased manifestation of defect textures. This makes it effectively impossible to obtain fits for the planar and homeotropic cases from identical physical parameterisation.

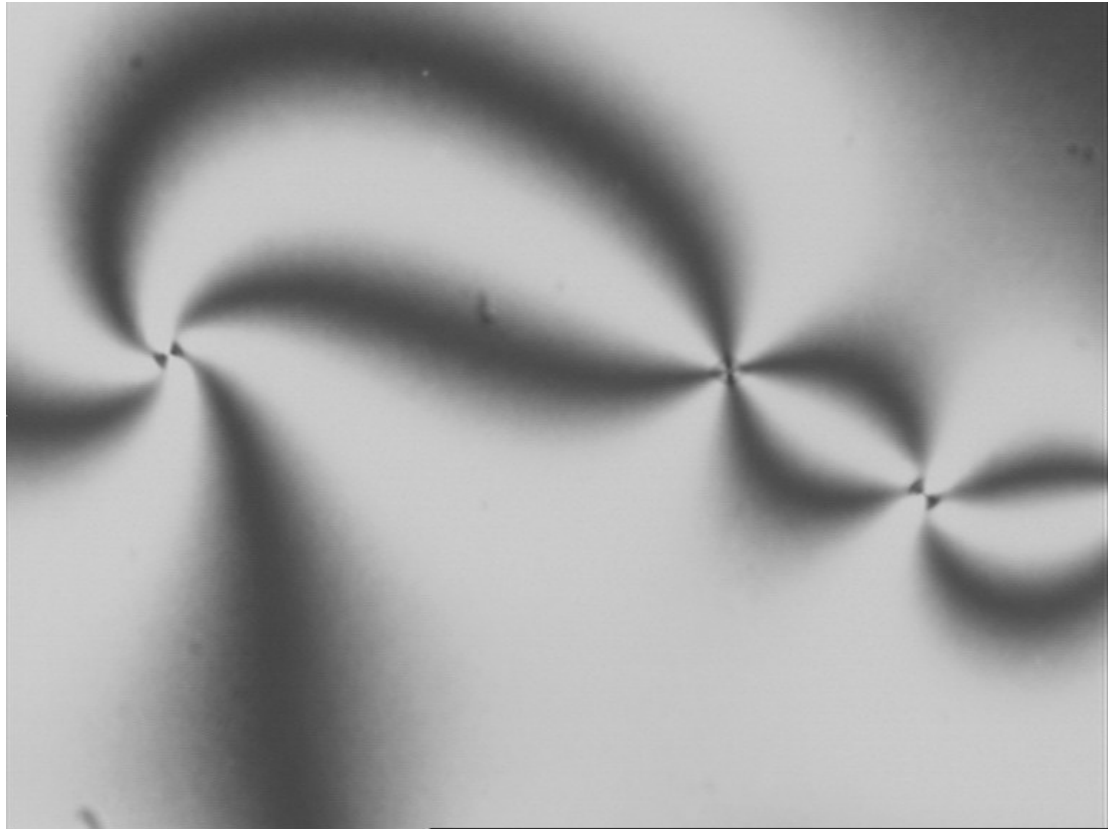


figure 4.8 homeotropic defect structure

This defect structure can be seen in figure 4.8; a micrograph at 400x magnification of a dual frequency homeotropic cell under a field of 6Vrms at a frequency of 100kHz. The cell is viewed between crossed polarisers and clearly displays Schlieren texture. [Nehring, 1972] The dark area represent regions where the director is perpendicular to the plane of the cell, where the dark areas meet are disclinations (line defects).



figure 4.9 planar defect structure

By contrast the view of a planar cell under a 6 V rms field of 1kHz shows a striated texture largely devoid of significant defects (figure 4.9).

4.6 Pulsed addressing

Additionally; given the work of Mottram and Brown the pulse width response was investigated. In this paper they discussed the theoretical application of step pulses to the dual frequency material studied in this chapter. Using hybrid aligned nematic cells allows the switching between two stable states; HAN and vertical. In this case the method of driving between the two states was the application of brief D.C. step functions. The application of a short D.C. pulse allows the reaction of the material to the high frequency components of the leading edge of the pulse. This, as previously discussed, causes the material to experience a negative dielectric anisotropy. This, in turn, causes the director to align perpendicular to the field. In the case of broader pulses this effect is soon overridden by the return to positive dielectric anisotropy (this component being excited by the D.C. field) and the director aligns parallel to the field.

With these findings in mind a pulse train waveform was applied to a dual frequency H.A.N. cell. The pulse train was composed of two D.C. pulses of opposing sign (to avoid too long an exposure to continued D.C. bias; continued exposure of nematics to high voltage dc fields risks dielectric breakdown) [Dierking, 2001] separated by 400ms. The height of the pulses was varied and the response monitored in order to find the amplitude required to cause half switching (defined as a mean permittivity equal to the average of ϵ_{\perp} and ϵ_{\parallel} at the peak of the response). Half, rather than full switching was chosen as the fields required to cause full switching tested the limits of the capabilities of the equipment used. The pulse widths chosen (0.5ms and 50ms) were considerably larger than those shown in the paper (0.2ms and 0.025ms); because

of the high voltages required to cause switching in such a short time. Since the theoretical predictions of Mottram and Brown suggest that the case of both long and short pulses there will be an initial dipping in the value of ϵ_{para} , but that the implications of this will be minimised for the longer pulse it was hoped to see a difference in response between the two pulses. For short pulse widths the response was expected to differ in that the pulse would engender the high frequency permittivities; reducing $\Delta\epsilon$ and so requiring disproportionate amplitude to achieve the required level of switching [Mottram, 2006]. In the case of the longer pulse the material was expected to exhibit a higher ϵ_{para} for a greater proportion of the pulse, thus requiring proportionately less voltage to cause the same level of switching. As the voltages needed to achieve this in the time available are considerable an amplifier was employed to raise the output of the signal generator prior to application to the cell. The speed at which the switching occurred tested the capabilities of the lock in amplifier. The results of broad and short pulses can be seen below for a wide variety of field strengths (figures 4.10 and 4.11)

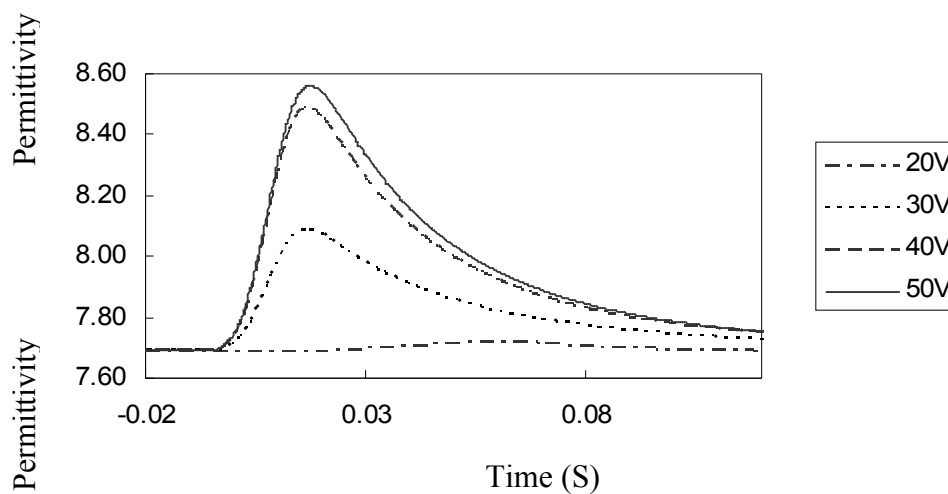


Figure 4.10 Short frequency pulse height variation

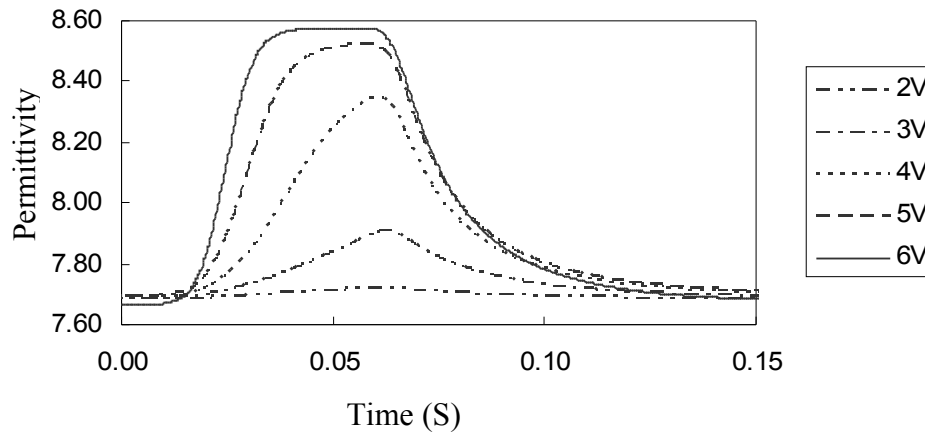


Figure 4.11 Long frequency pulse height variation

As expected there is indeed more than a tenfold increase in the field strength required to achieve half switching in the case of the short pulse. A systematic investigation was undertaken to map the different pulse height permittivity responses, the results are clearly exponential in character and are displayed in figure 4.12

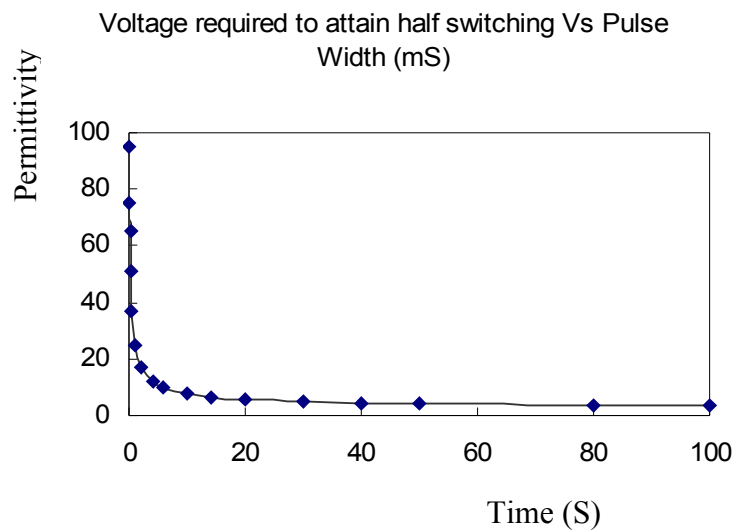


Figure 4.12 Voltage required for half switching

4.7 Discussion

It has been demonstrated that dual frequency materials respond in the same manner as other liquid crystals tested when exposed to the amplitude modulated transient capacitance technique. It has further been shown that this method may be adapted to frequency rather than amplitude modulation. This opens up the possibility of devices driven with a constant amplitude applied ac field; the switching being achieved through the variation of frequency. Indeed there is also the opportunity to choose ones switching and relaxation times (within limits) simply by selecting a frequency close to the crossover frequency. In this way the effective $\partial \epsilon$ of the material may be changed from moment to moment within a device. This allows for flexible device structures that may be 'tuned' as desired once manufactured. Use of the modified technique has been shown to be valid in the cases studied; in as much as the results are broadly similar to those predicted by numerical simulation. The concept of pulsed addressing of dual frequency liquid crystals has been experimentally attempted and the results are found to be consistent with theoretical predictions. For a more accurate picture of the pulsed addressing results it would be advantageous to repeat the procedure with more robust equipment.

Chapter 5: Transient capacitance of flexoelectric and ionic liquid crystals

5.1 Introduction

It is the aim of this chapter to investigate the flexoelectric effect in E7 and TL216 (a low ionic conductivity material) by comparing the transient capacitance response of different alignment geometries and cell thicknesses. By adapting the transient technique to utilise D.C. waveforms it is hoped that the effects of ionic contamination may be decoupled from the flexoelectric effect. The ionic response will be assessed by comparing the amplitude modulated A.C. and D.C. responses in planar geometry. The flexoelectric response will then be assessed via a comparison of the A.C. and D.C. responses in the HAN geometry.

5.2 Theory

In determining the permittivity of a liquid crystal cell we must also consider the possible effect of ions. Ionic impurities may cause increased defects in the internal structure of a liquid crystal cell and may interfere with the electromagnetic properties of the sample. [Blinov, 1983] There are several causes for the presence of ions in a sample; in manufacturing liquid crystal materials it is very hard to avoid the inclusion of ions. They may also be introduced at the filling stage and, in addition, may be created in a cell due to electrochemical breakdown from exposure to light or strong (particularly D.C.) fields [Collings 1990]. The presence of ions hinders attempts to use electric fields to measure and manipulate liquid crystal cells as the ions affect the fields and are also affected by the fields. As the field is applied the ions react to the field gradient and migrate to the cell walls. This creates an internal field opposite in polarity to the original and so shielding the sample from the full effect of the field. Without knowing how many ions are present it is therefore impossible to know exactly what field strength the sample is experiencing. In addition, the mass motion of ions may exacerbate flow effects in the sample as shown in Figure 5.1

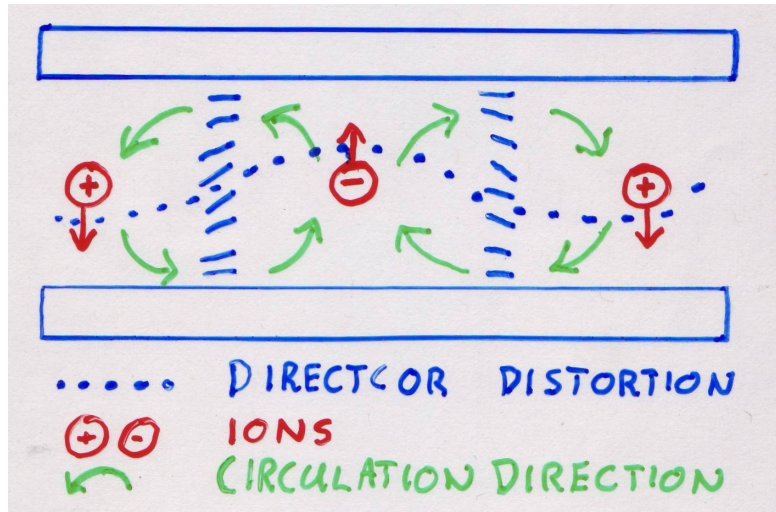


Figure 5.1 Flow effects arising from ionic contamination

The flexoelectric effect is the liquid crystal analogue of piezoelectric effect. In the piezoelectric effect the lattice structure of a crystal is exposed to mechanical stress (e.g. by bending). This causes an alteration in the interstitial distances along one axis, as a result of this there is an imbalance in charge along the axis of distortion. This imbalance creates an electromagnetic field. The process may be reversed in as much as an applied field will cause concomitant spatial distortion within the lattice. Liquid crystals with mesogens possessed of an internal dipole and one of a set of shape anisotropies may experience a similar effect. It has been shown that for molecular shapes which may be termed pear or banana, elastic deformations can cause the mesogens to adopt a packing structure which causes a similar spatial imbalance of charge. [Meyer, 1969]. The flexoelectric effect generates an internal field in response to a splay or bend distortion, usually orthogonal to the applied field creating the distortion. As with the piezoelectric effect this is reversible in that an applied field may cause splay and/or bend distortions.

These two considerations (ionic contamination and flexoelectric effect) present hazards for measuring techniques involving applied fields. Furthermore it can be

difficult to isolate one effect from the other and so to ascertain the influence of either. In addition there is a degeneracy between the flexoelectric response and the effect of varying the elastic constants. [Smith 2007] Both have the effect of shifting the slope of the Fredericksz curve. In order to counter this problem several ‘low ionic’ liquid crystals have been developed. One such material (TL216) has been developed by MERK and is examined here. It is the intention in this chapter to explore the differences between this material (TL216) and more conventional liquid crystal materials and, in doing so, to seek to expand the transient capacitance technique as a diagnostic tool.

When a D.C. field is applied to an ionically contaminated cell the ions migrate to the electrodes and reduce the field strength; when a high frequency A.C. field ($>kHz$) is applied the ions are unable to move fast enough to respond; nonetheless they are able to disrupt the flexoelectric field while dispersed in the liquid crystal medium. Models based on liquid crystal continuum theory are able to predict an expected value for the flexoelectric effect in certain geometries. [Smith 2007] As the ionic effect cannot be properly quantified individually it is hard to decouple these two processes.

5.3 Experimental

Cell	Material	Thickness(μm)	Alignment
1	TL216	5	planar
2	TL216	5	HAN
3	TL216 +2% E7	5	planar
4	E7	5	planar
5	E7	22	planar
6	E7	5	HAN

Figure 5.2 Table of materials and cells used

A.C. fields of frequencies greater than 1 kHz oscillate too quickly for significant ion motion to occur while prolonged D.C. fields allow for the ions to plate out at the electrodes. Using the transient capacitance technique as detailed in the experimental methods chapter comparisons were made between A.C. rms voltages and equivalent D.C. fields for both TL216, E7 and a mix of the two materials (TL216 +2% by weight of E7). The alignments sizes and materials used are detailed in Figure 5.2, the results are shown below for a variety of voltages and applied waveforms.

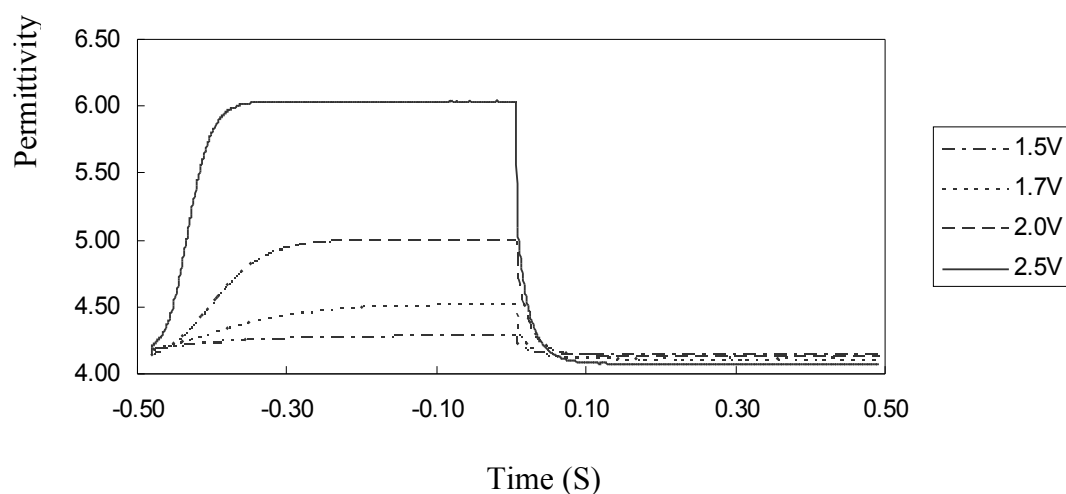


Figure 5.3 application of A.C. fields to Cell 1 (TL216 $5\ \mu m$ planar cell)

An amplitude modulated sine wave (consisting of a high amplitude ‘switching’ component of 0.5S duration followed by a low amplitude ‘relaxing’ component of equal length) was applied to the low ionic material in a 5 micron width planar cell. The results, in terms of the time evolution of average permittivity, are shown in Figure 5.3 and were in good agreement with the static permittivity measurements.

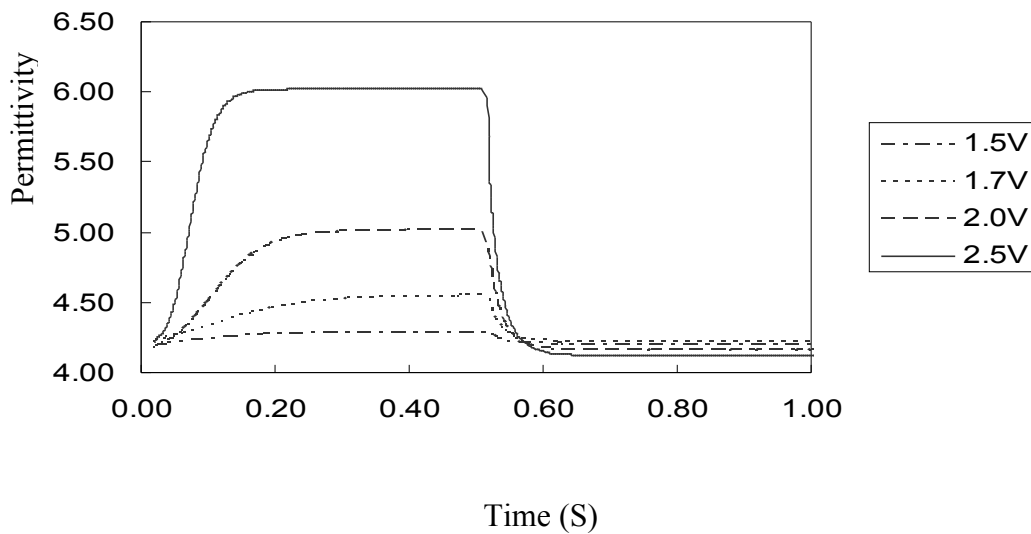


Figure 5.4 application of D.C. fields to a low ionic $5\ \mu m$ planar cell

The same cell was then exposed to a D.C. step function equal in amplitude to the RMS amplitude of the switching part of the aforementioned waveform (shown in figure 5.4)

The results were compared for evidence of ionic response in figure 5.5, should there be significant ionic contamination the D.C. results should show significantly lower permittivities when switched. When overlaid the A.C. and D.C. responses show good agreement. This is strongly supportive of the TL216 material being free of ionic

Permittivity

contamination as the presence of ions would lead one to expect a lower effective field strength to be manifest in the D.C. trials.

**A.C. (solid) vs D.C. (dash) for low ionic material
1.5/1.7/2.0/2.5V**

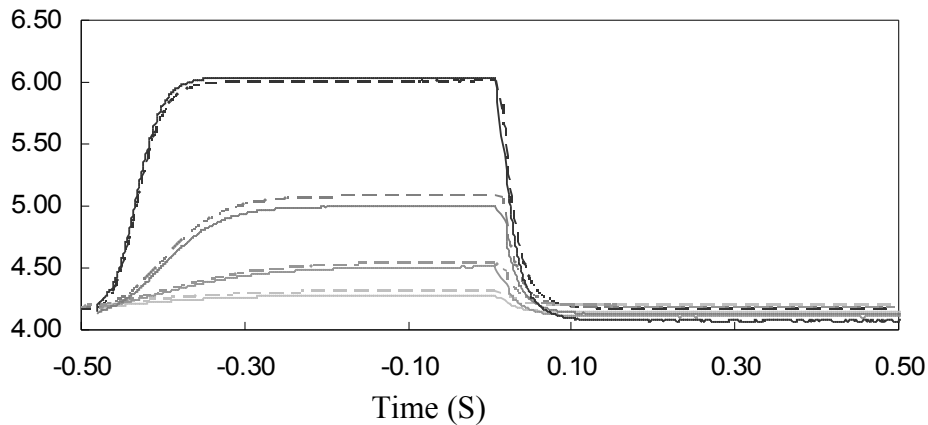


Figure 5.5 A.C. (dashed) and D.C. fields applied to a low ionic $5\ \mu m$ planar cell

In addition to the application of the technique to a planar cell the trials were extended to Hybrid Aligned Nematic (HAN) cells; possessed of both planar and homeotropic alignment layers. The change between the two alignment layers constitutes a splay deformation and therefore may be expected to generate a flexoelectric field. The same studies were carried out on the HAN cells and the results in terms of A.C. fields, D.C. fields are shown in figures 5.6 and 5.7 respectively.

Permittivity

A.C. modulation for 5 micron HAN cell TL216

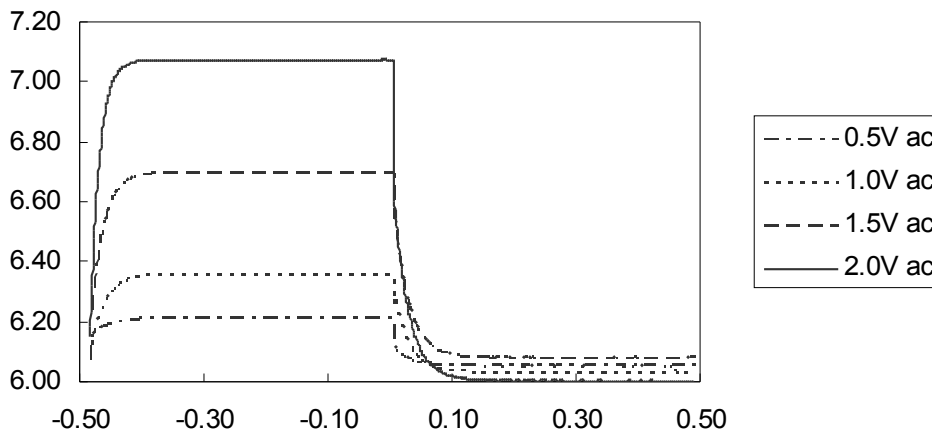


Figure 5.6 A.C. fields applied to a low ionic $5\ \mu m$ HAN cell

Figure 5.6 shows that while the results conform qualitatively to the expected changes in permittivity there is a discrepancy of around 0.1 in the base line permittivities.

This discrepancy is less in evidence in the D.C. trials, shown in figure 5.7

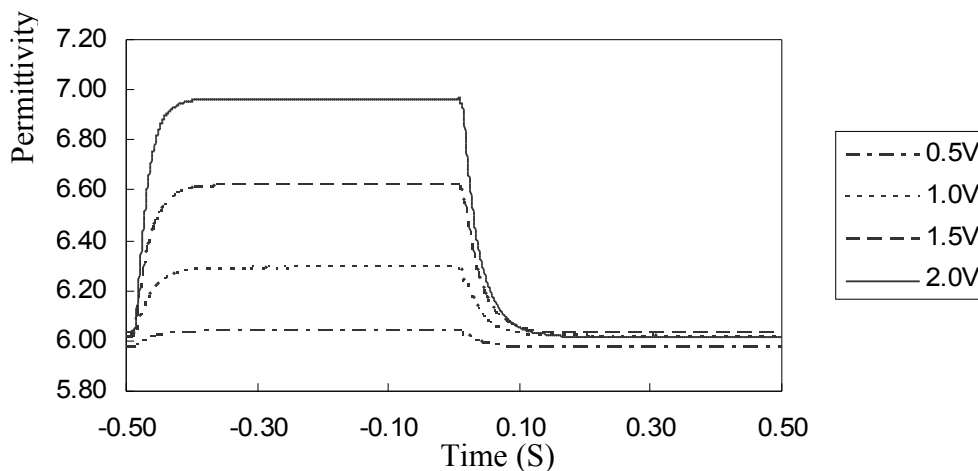


Figure 5.7 D.C. fields applied to a low ionic $5\ \mu m$ HAN cell

Permittivity
Permittivity

A.C. Vs D.C. for 5 micron HAN cell TL216

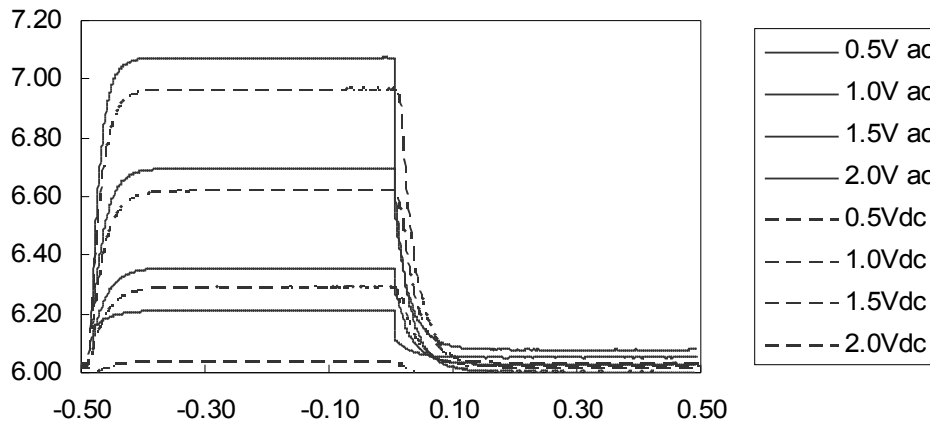


Figure 5.8 A.C. and D.C. fields applied to a low ionic $5\ \mu m$ HAN cell

When the two sets of measurements are overlaid (figure 5.8) one may see that there is indeed a difference between the A.C. and D.C. responses. This is not as great as it may appear at first sight; around 0.1 in terms permittivity for most field strengths (around 1.5% difference from the A.C. values). In light of the earlier results for planar cells this may be due to increased conductivity from the homeotropic substrate of the hybrid geometry.

The application of a D.C. step wave to a low ionic H.A.N. cell shows a variation in the mean permittivity of several percent; the effect is shown to be consistent over a range of voltages. Since we may discount the effect of ions in this sample we may conclude that this is the effect of flexoelectricity. The flexoelectric field generated by the splay distortion of the director profile makes an angle φ between the plane of the cell and the applied field. In the case of a positive step this opposes the applied field; in the case of a negative step it reinforces the applied field. This seems to account for

the discrepancy between the planar and hybrid results and is shown in figures 5.9 and 5.10 below.

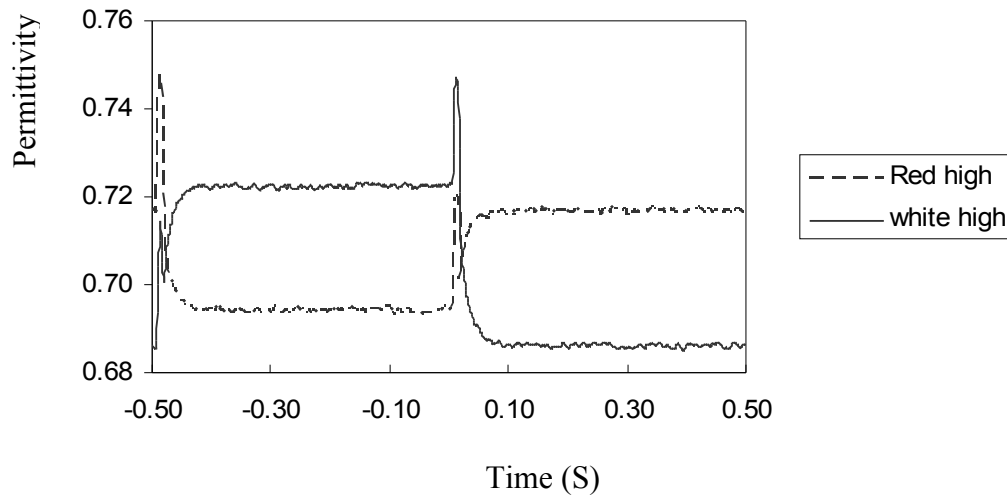


Figure 5.9 A.C. and D.C. fields applied to a low ionic $5\mu m$ HAN cell

The cells were constructed with a red sheathed wire connected to the homeotropic substrate and white to the planar substrate. Swapping the leads of a H.A.N. cell under an applied D.C. field shows the expected offset in the capacitance. There is no evidence that the homeotropic alignment layer is significantly conductive.

Offsets for 5 micron han low ionic d.c. +/- V = 0.5 - 5.0

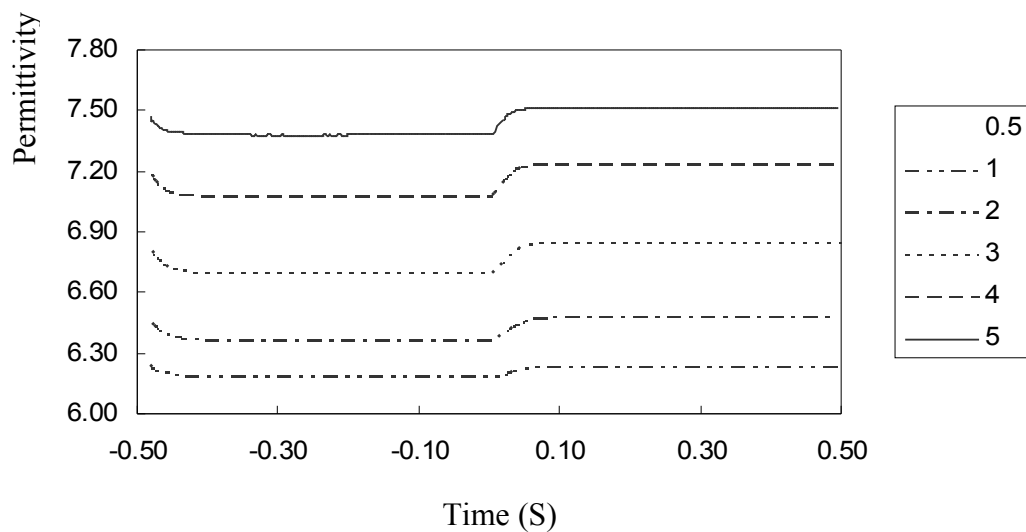


Figure 5.10 D.C. offsets from lead reversal in low ionic $5\mu m$ HAN cell for 0.5– 5V

In figure 5.10 we can see what appears to be a field dependence of the offset. This is explored in figure 5.11 and found to be the case over the range studied.

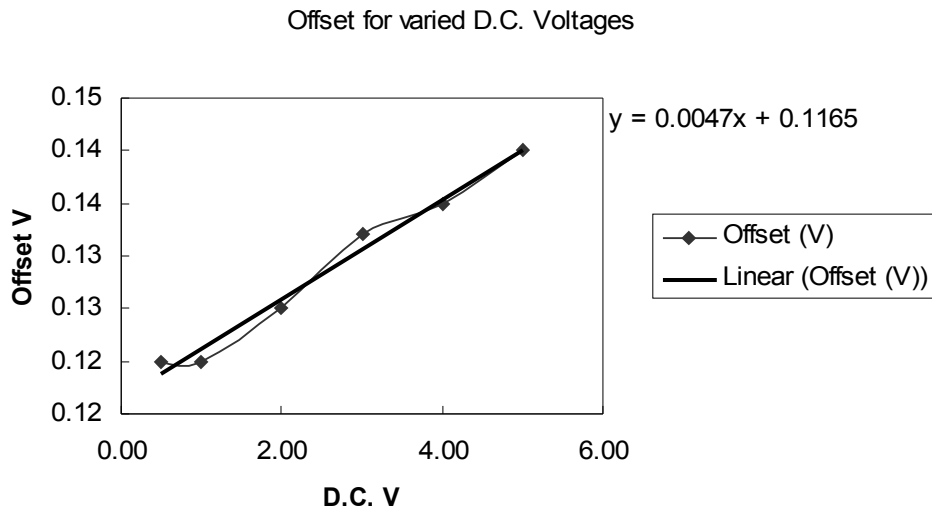


Figure 5.11 Linearity of D.C. offset in a low ionic $5 \mu m$ HAN cell

The higher the field the more of the bulk liquid crystal is forced into the planar alignment and the closer ϕ comes to 90° ; that is it approaches the layer normal along which the field is applied. This increases its effect upon the field strength. The linearity of this effect over the range of interest is shown in figure 5.11

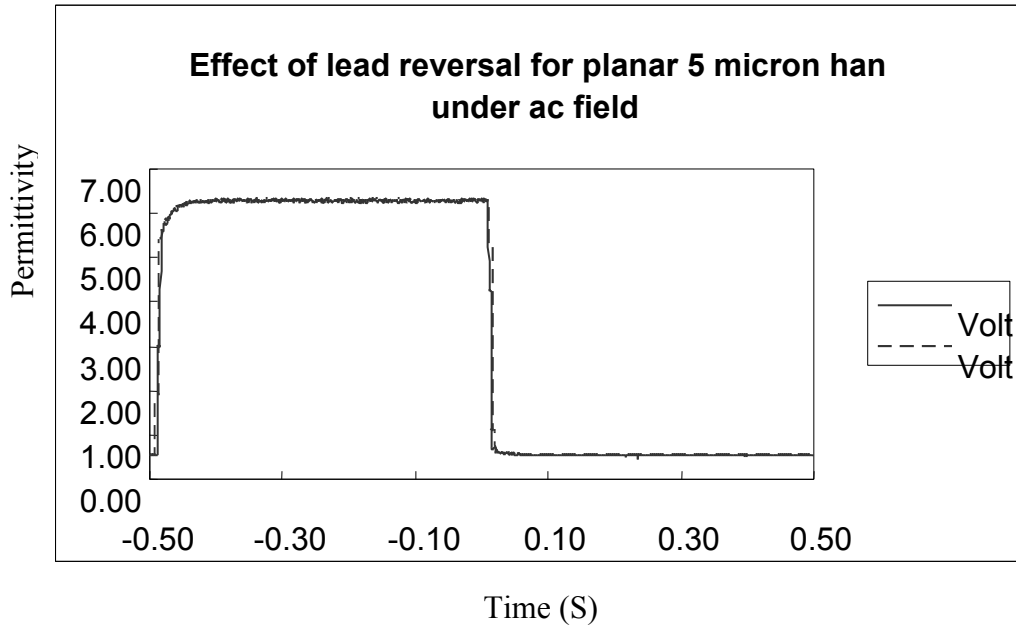


Figure 5.12 Negation of offset in a low ionic $5 \mu m$ Planar cell

As the planar cell is symmetric we would expect no difference between which lead was connected to the high and low fields; none was in evidence (figure 5.12).

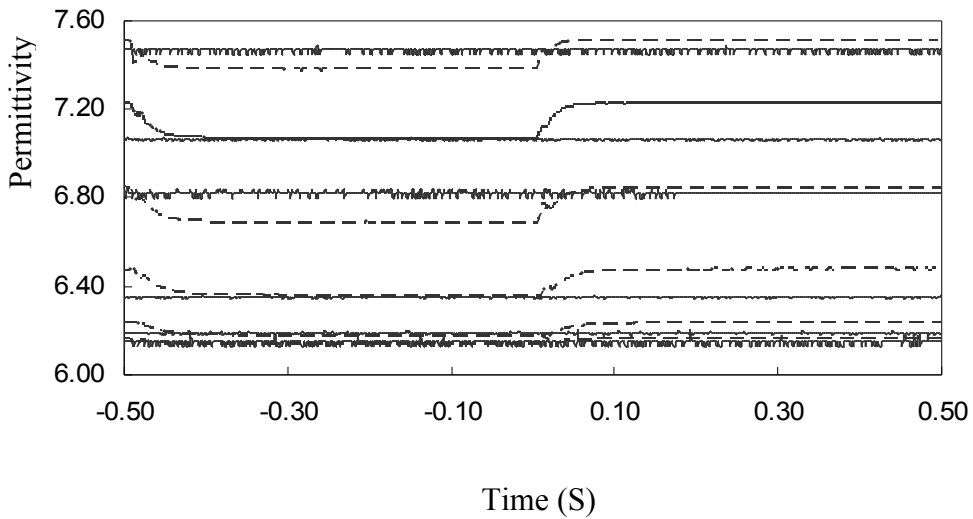


Figure 5.13 Comparison of D.C. offset with A.C. rms equivalent

A sine wave of constant amplitude and frequency (static test) was applied to the H.A.N. cell at a variety of amplitudes matching those of the +/- D.C. step wave (5.13). The results in all cases lay between the observed offsets.

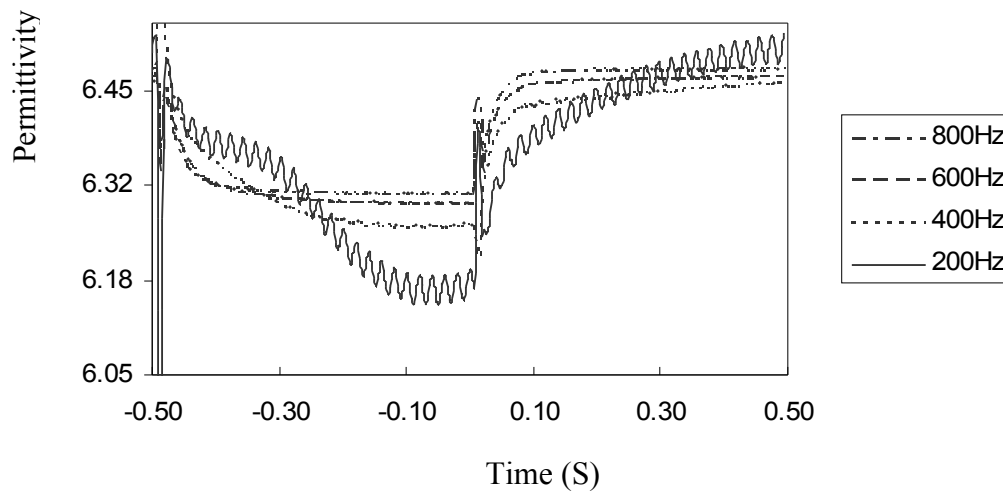


Figure 5.14 Normalised frequency variation in a low ionic $5\mu m$ HAN cell

The frequency of the field has some small effect on the measured mean permittivity of the sample below 800Hz; above this value it converges on the expected theoretical values (figure 5.14). Should the sample be ionic in character we would have expected a much greater effect when lowering the frequency to a level where ions might respond. [Costa 2001].

In order to test this as strictly as possible; some of the TL216 was mixed with 2% by weight E7, a liquid crystal mixture known to be fairly ionic in nature. Cells created with this mixture are prefixed JMH. Such a small amount should have little effect on the observed permittivities when measured statically or transiently. The introduction of the associated ions should be visible in the A.C./D.C. planar comparisons as an increased discrepancy between the two. The same experiments were performed but

with little measurable difference in the results. We may conclude that the mixture was not significantly ionic in nature at this concentration for the results to exceed the experimental error. The results are shown below.

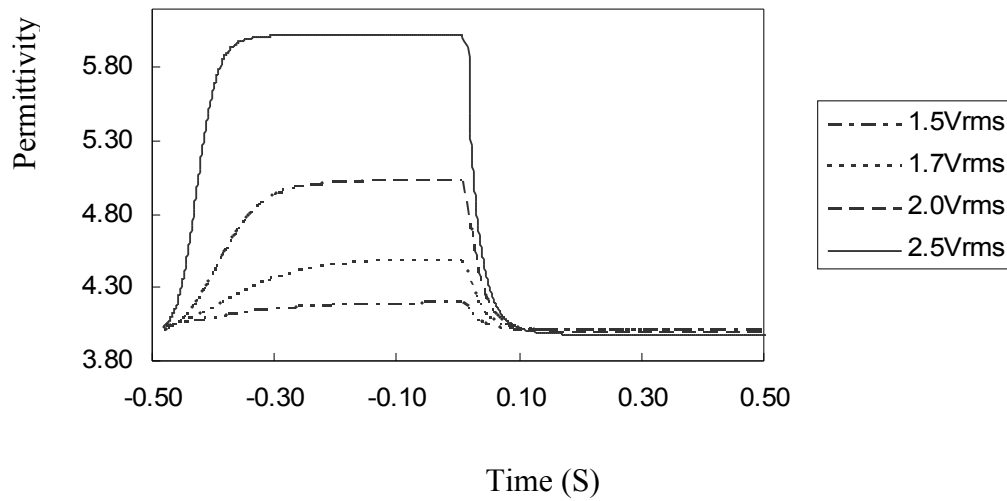


Figure 5.15 Application of A.C. fields to JMH $5\ \mu m$ Planar cell

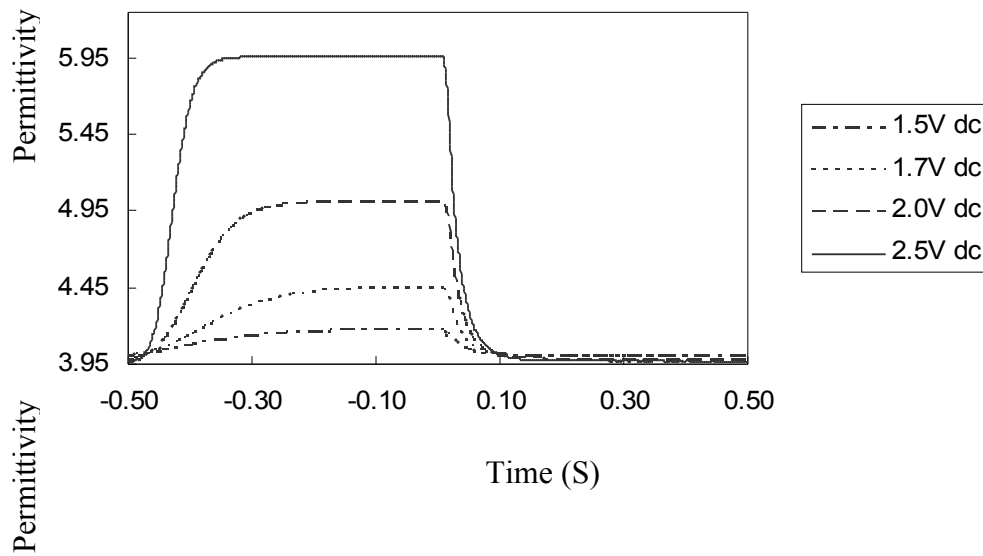


Figure 5.16 application of D.C. fields to a JMH $5\ \mu m$ planar cell

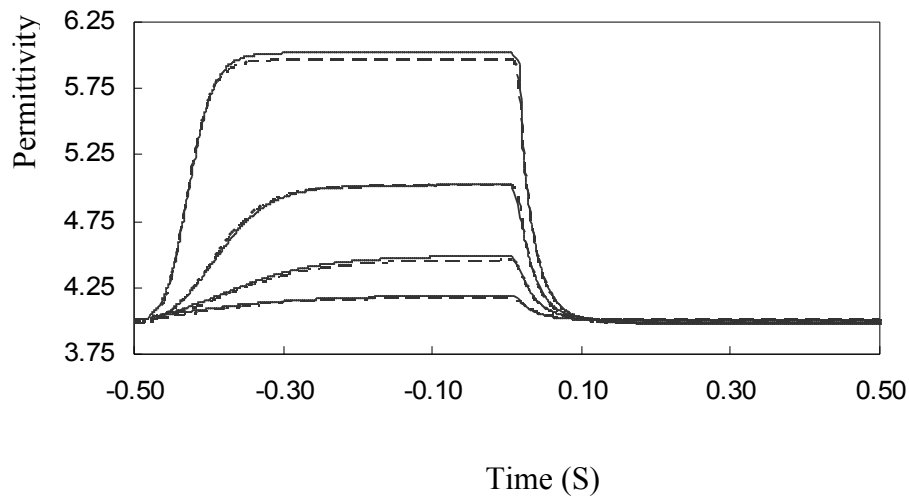


Figure 5.17 Overlay of A.C. and D.C. fields to a JMH $5\ \mu m$ planar cell

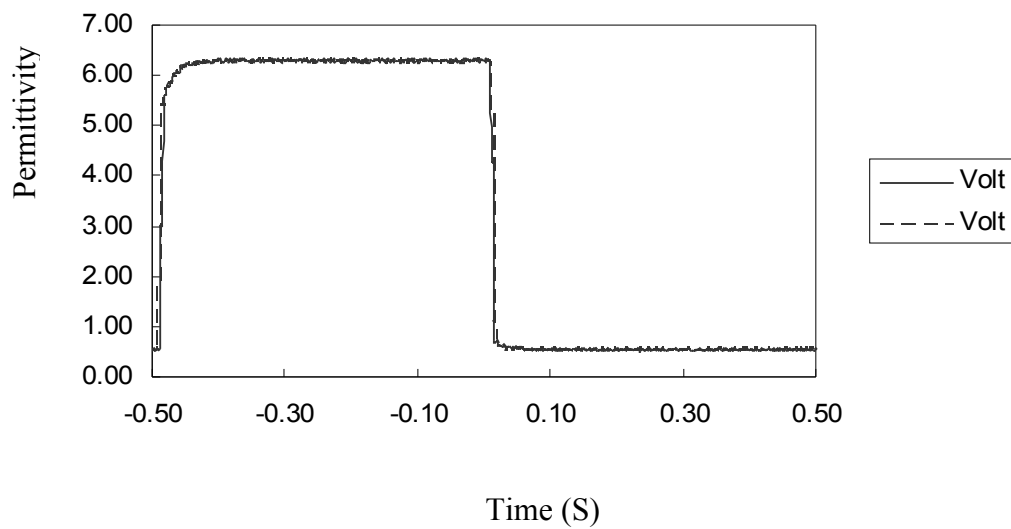


Figure 5.18 D.C. lead reversal for a JMH $5\ \mu m$ planar cell

There was no difference in reversing the leads of a TL216 + E7 (JMH) Han Cell.

It is possible that the TL216 mixture may be made more ionic by long exposure to ultraviolet light and/or strong D.C. fields. In this manner electrochemical breakdown may be induced without adulterating the mixture unduly. It is unknown how long this process may take however, and for both the sake of expediency and lack of excess of the material it was not attempted. Instead the same experiments were conducted with identical cells prepared with pure E7. While this can give us no quantitative information due to the inherent differences in the two materials it should allow the qualitative nature of the tests to be assessed.

As before a planar cell was exposed to A.C. modulated waves and then D.C. step waves of equal magnitude. The results for E7 are displayed in figures 5.19 -5.21:

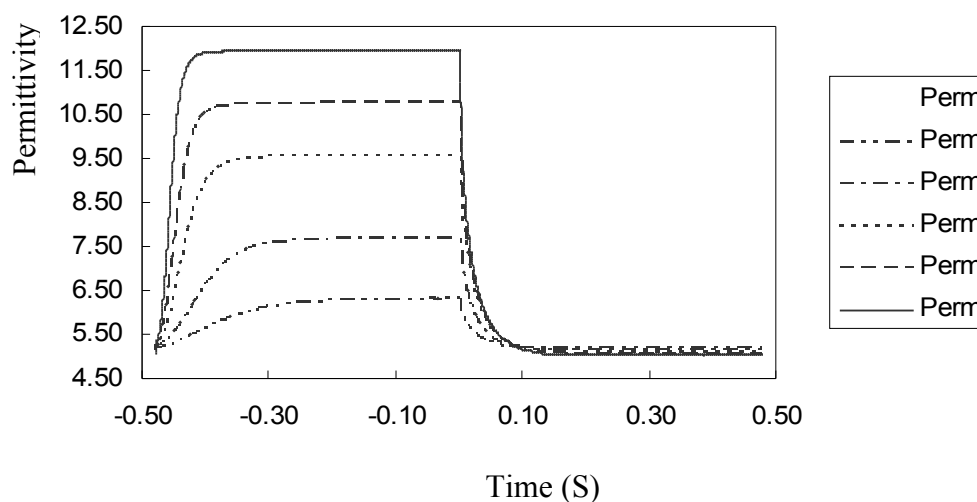


Figure 5.19 application of A.C. fields to an E7 $5\mu m$ planar cell

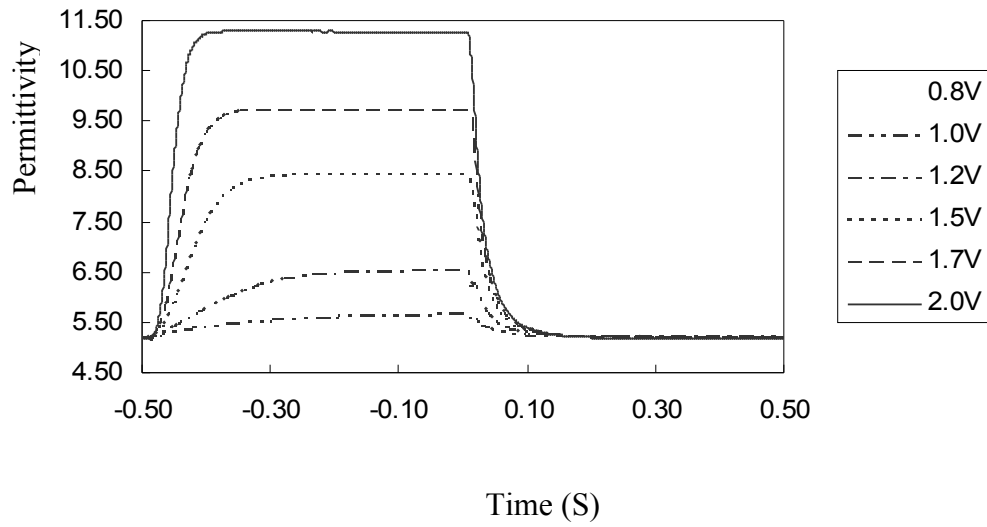


Figure 5.20 application of D.C. fields to an E7 $5\mu m$ planar cell

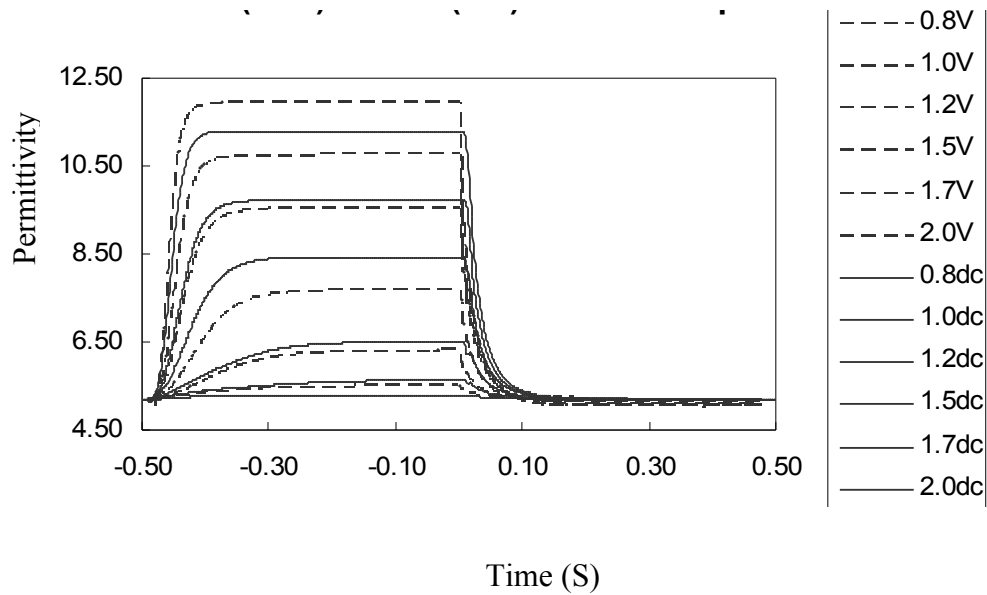


Figure 5.21 Overlay of A.C. and D.C. fields to an E7 $5\mu m$ planar cell

Although both the A.C. and D.C. responses look appropriate when the data is overlaid we see that there is great discrepancy (around 15%) between the two sets.

The D.C. mean permittivity is consistently below the value measured for the A.C. field at each high amplitude part of the waveform studied. The two agree only for the low amplitude part of the waveform where the ions diffuse into the mixture and play no part in shielding the field. This is consistent with the presence of ions in the sample which are drawn to the electrodes under a high D.C. field and plate out the applied field, generating a lower amount of distortion in the director profile for a given field strength. The same may be seen in experiments conducted on 22 micron cells (figures 5.22 – 5.24). Note that the thicker cells require longer waveform sections for significant switching to occur but show the same reduced permittivity effect when D.C. fields are applied.

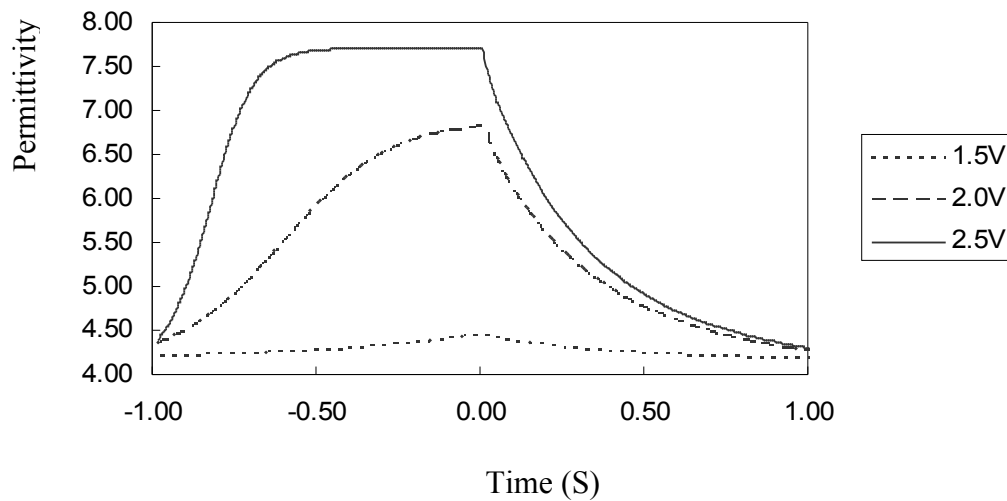


Figure 5.22 application of A.C. fields to an E7 $5\mu m$ planar cell

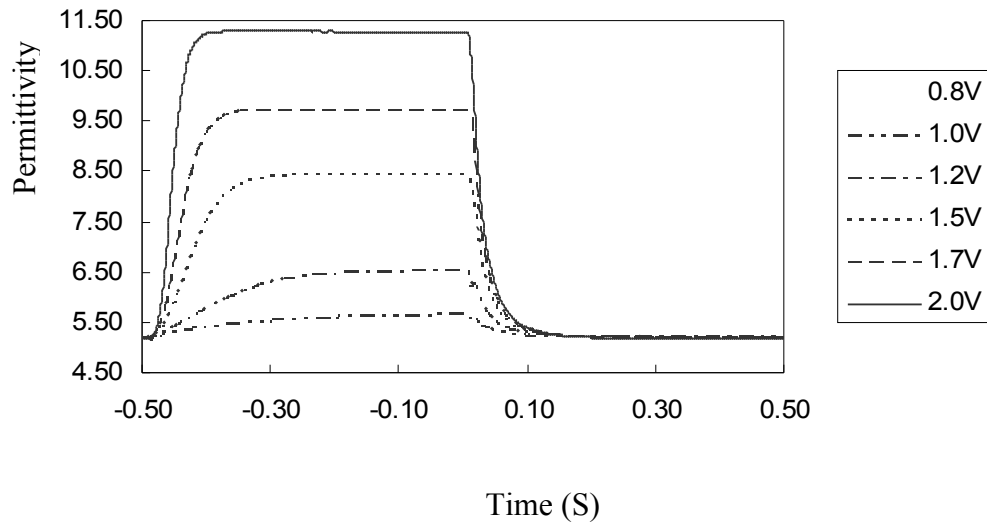


Figure 5.23 Application of D.C. fields to an E7 22 μm planar cell

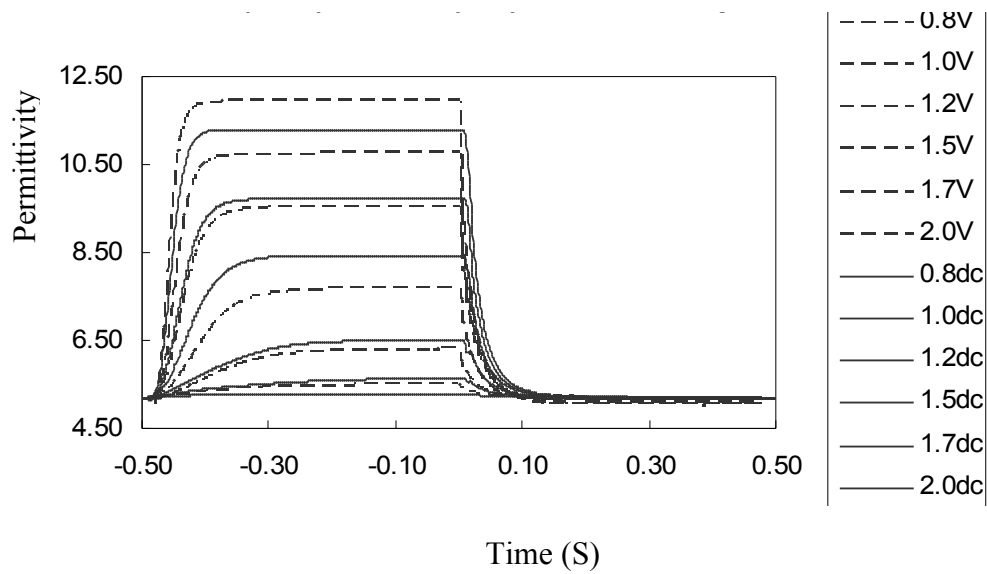


Figure 5.24 Overlay of D.C. and A.C. fields to an E7 22 μm planar cell

5.4 Behaviour of ions

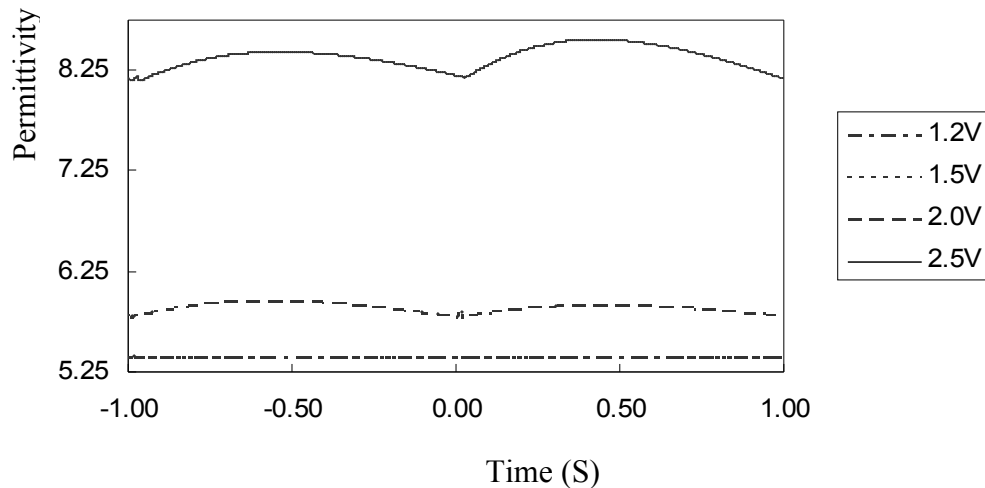


Figure 5.25 Application of D.C. +/- fields to an E7 22 μm planar cell

In looking at the response of the H.A.N. cell we see that the offset of the TL216 cell is hidden by ion spikes. As the field is applied the cell initially responds with an increased capacitance due to realignment of the director. The ions migrate to the electrodes and begin to reduce the field noticeably from around 40 milliseconds; reducing the measured capacitance. On the change in sign of the applied field the field created by the ions initially reinforces the field strength causing fast realignment of the director profile; the ions quickly disperse within the sample reducing the effective field before plating out the opposite electrodes and reducing the field still further. In the second part of the graph there exists a second maximum; it may be that this is related to the flexoelectric field since this is an asymmetric effect, however it may also be due to an imbalance in the electric sign of the ions. This may also account for the different height of the ion peaks.

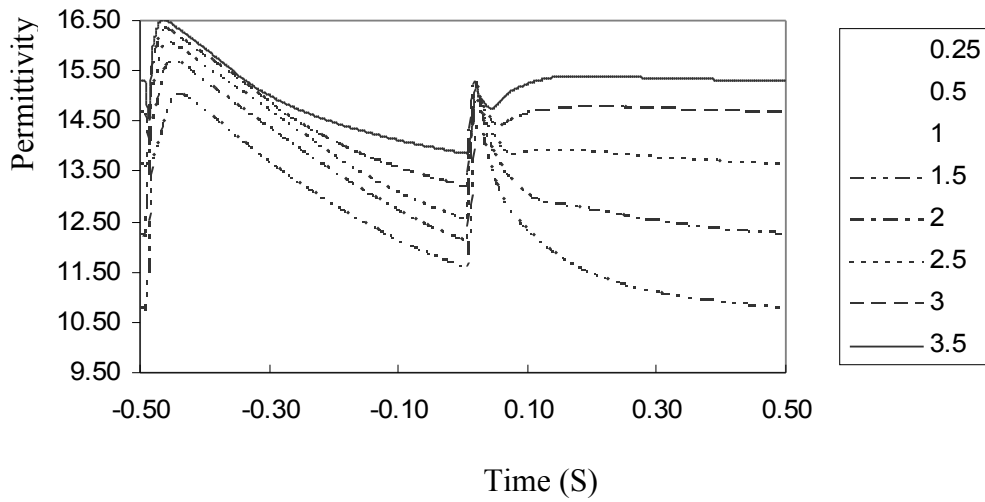


Figure 5.26 Ion spikes in an E7 $5\mu m$ HAN cell

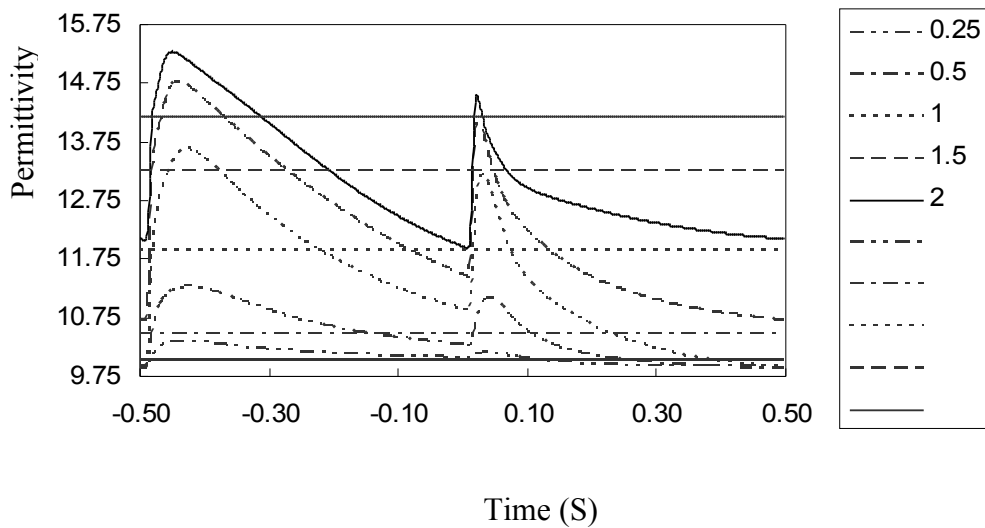


Figure 5.27 Ion spikes and A.C. overlay in an E7 $5\mu m$ HAN cell

Comparison of this data with single amplitude A.C. fields shows that the permittivities measured with the D.C. step waves vary around the true values. In each case the sudden reversal of the fields to coincide with the ionic field leads to a greater than expected permittivity as the director over rotates. The ions then shield the applied field, reducing the permittivities.

5.5 Discussion

A low ionic material (TL216) was tested using the transient capacitance technique in the planar geometry. This was undertaken both with a fast A.C. amplitude modulated waveform of the type previously described and a D.C. step function analogous to the A.C. waveform. No significant differences were found and the material was deemed to be effectively free of ionic contamination. Similar tests were performed on the same material in the HAN geometry and a consistent, field dependant offset was found. In the apparent absence of ions this offset was attributed to flexoelectricity. The flexoelectric effect was considered to arise from the splay deformation arising from the HAN geometry. The material was adulterated with a small amount of another known to contain significant amounts of ions (E7). This admixture was similarly tested but found to be largely identical to TL216. The high ionic material (E7) was tested in a pure form and found to show evidence of significant ionic contamination. The high ionic material was also studied in the HAN geometry.

CHAPTER 6 DOUBLE MINIMA IN THE SURFACE

STABILISED FERROELECTRIC

LIQUID CRYSTAL SWITCHING RESPONSE

6.1 Introduction

A double minimum has recently been observed in the time – voltage switching response for a smectic C* liquid crystal layer in the surface stabilised geometry [Lymer, 1999]. Liquid crystal continuum theory is used to demonstrate that this unusual switching behaviour arises if the equilibrium orientation of the molecular director rotates around the smectic cone as a function of distance through one half of the layer only. The double minimum is shown to evolve for large differences between the ϵ_2 and ϵ_1 components of the smectic C biaxial permittivity tensor. The fast, bistable, electro-optical switching response of Surface Stabilised Ferroelectric Liquid Crystal (SSFLC) devices [Clark, 1980] has been exploited for applications including miniature displays for camera viewfinders [Clark, 2000] and in high resolution, polarisation insensitive, diffractive optical elements [Warr, 199; Brown, 2003].

6.2 Theory

The SSFLC exploits the strong coupling between an applied electric field E and the spontaneous polarisation P_S of the smectic C* material. The chiral pitch of the material is unwound, provided the layer thickness is much less than the pitch, due to the strong alignment interaction with the uni-directionally rubbed polymer surfaces that coat the confining plates.

An internal layer structure that can result from this type of confinement is depicted in figure (6.1). The thick lines in the side view (a) show the molecular director, i.e. the local optical axis, which lies on the smectic cone of half angle θ . The smectic layers form a chevroned structure with layer tilt angles of $\pm\delta$. The equilibrium orientation of the director can vary through the thickness of the cell in several ways, and some possible director profiles are depicted by the positions of the filled circles in figures (1b) to (1e). The director orientation at a given position z in the layer is described by the azimuthal angle $\phi(z)$. The direction of the P_S vector along the C_2 symmetry axis and at the tangent to the smectic cone is illustrated at one director position.

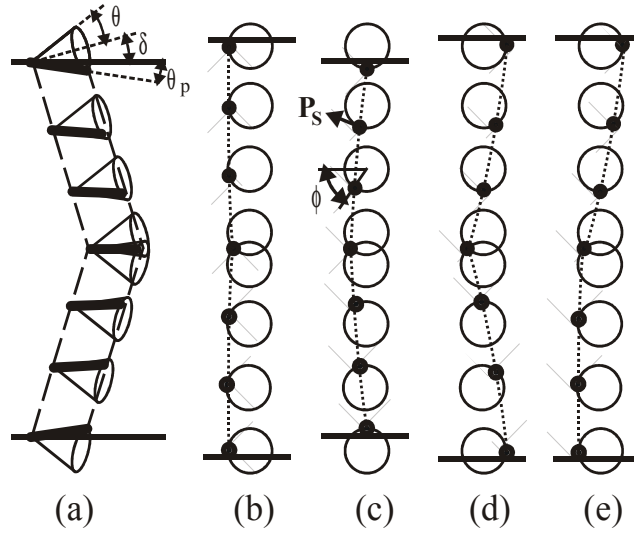


Figure 6.1 Illustration of the surface stabilised ferroelectric liquid crystal layer geometry. The chevron structure, layer tilt angle δ and smectic cone angle θ are depicted in the side view (a). End views are shown for the for cases where the azimuthal angle at the surfaces, ϕ_{SU} / ϕ_{SL} , were as follows : (b) $0^\circ / 0^\circ$, (c) $90^\circ / -90^\circ$, (d) $180^\circ / -180^\circ$, and (e) $180^\circ / 0^\circ$.

Smectic C materials are inherently biaxial, with large differences measured between the 3 principle permittivities, Figure (6.2) : ϵ_3 along the liquid crystal molecular director which is typically the long axis, ϵ_2 parallel to the C_2 symmetry axis, and ϵ_1 which is mutually perpendicular to ϵ_2 and ϵ_3 [Elston, 1990; Jones 1991; Brown 1999]. In materials where the dielectric biaxiality $\partial\epsilon = \epsilon_2 - \epsilon_1$ is high, typically $\partial\epsilon > 0.5$, the electro-optical switching response of an SSFLC layer can show a minimum [8]. This occurs due to the competition between the coupling of the applied electric field to the spontaneous polarisation P_S and to the biaxial dielectric permittivity. The P_S coupling promotes switching, and this dominates at low field, whereas the dielectric coupling usually impedes switching, and this dominates at high voltages.

A theoretical model based on liquid crystal continuum theory has been used to generate time – voltage switching curves for pulsed voltages applied across the SSFLC layer in the geometries shown in figure (6.1). The time evolution of the liquid crystal director, $\phi(z, t)$, has been calculated by solving the discretised form of equation (6.1) on a linear array of points using a numerical relaxation technique [Carlsson, 1992].

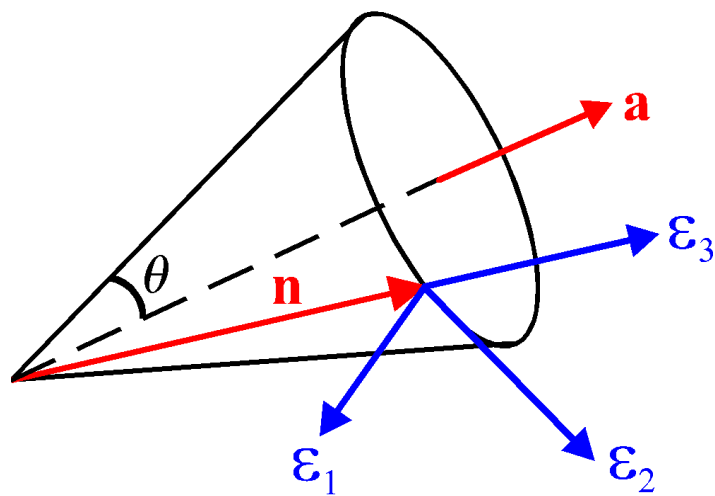


Figure 6.2 Diagram of the smectic cone geometry displaying the three principle permittivities.

Letting \underline{a} describe the layer normal, \underline{b} the c2 axis and \underline{c} the vector from the centre of the cone face to the director, shown in figure (6.2), we have that:

$$\eta \frac{\partial \phi}{\partial t} = B \left(\frac{\partial^2 \phi}{\partial z^2} \right) + P_S E \cos \delta \sin \phi - \frac{1}{2} \varepsilon_o E^2 \partial \varepsilon \sin 2\phi \cos^2 \delta - \frac{1}{2} \varepsilon_o E^2 (\varepsilon_3 - \varepsilon_1) \cos \phi \left(\frac{1}{4} \sin 2\theta \sin 2\delta - \sin \phi \cos^2 \delta \sin^2 \theta \right) \quad (6.1)$$

where B is an isotropic elastic constant and η is the viscosity for rotation around the smectic cone. The electric field profile, $E(z)$, was obtained at each time step by integration of the Maxwell equation, $\nabla \cdot \mathbf{D} = 0$. With variations in the z-direction only the displacement field is given by $D_z = \varepsilon_o \varepsilon_{zz}(z)E(z) + P_z(z)$ where $\varepsilon_{zz}(z)$ and $P_z(z)$ are the z-components of the dielectric permittivity tensor and the polarisation vector respectively. The equation was generated in the following manner:

Letting \underline{a} describe the layer normal, \underline{b} the c2 axis and \underline{c} the vector from the centre of the cone face to the director, shown in figure (6.2), we have that:

$$\underline{a} = \begin{pmatrix} \cos \delta \\ 0 \\ \sin \delta \end{pmatrix} \quad \underline{b} = \begin{pmatrix} -\sin \delta \cos \phi \\ \sin \phi \\ \cos \delta \cos \phi \end{pmatrix} \quad \underline{c} = \begin{pmatrix} \sin \delta \sin \phi \\ \cos \phi \\ -\cos \delta \sin \phi \end{pmatrix} \quad (6.2)$$

$$\underline{n} = \underline{a} \cos \theta + \underline{c} \sin \theta = \begin{pmatrix} \cos \theta \cos \delta + \sin \theta \sin \delta \sin \phi \\ \sin \theta \cos \phi \\ \cos \theta \sin \delta - \cos \delta \sin \phi \sin \theta \end{pmatrix} \quad (6.3)$$

$$\underline{k} = \underline{n} \times \underline{b} = \begin{pmatrix} \sin \theta \cos \delta - \sin \delta \sin \phi \cos \theta \\ -\cos \theta \cos \phi \\ \sin \delta \sin \theta + \cos \delta \sin \phi \cos \theta \end{pmatrix} \quad (6.4)$$

The free energy may be described by:

$$\omega = \omega_B - \frac{1}{2}\epsilon E^2 - PE \quad (6.5)$$

Where:

$$2\omega_B = \left[(B_1 \sin^2 \phi + B_2 \cos^2 \phi) \cos^2 \delta + B_3 \sin^2 \delta - B_{13} \sin 2\delta \sin \phi \right] \left(\frac{\partial \phi}{\partial z} \right)^2 \quad (6.6)$$

We are then required to solve the Euler-Lagrange equation:

$$\eta \frac{d\phi}{dt} = \frac{\partial \omega}{\partial \phi} - \frac{d}{dz} \left(\frac{\partial \omega}{\partial \left(\frac{\partial \phi}{\partial z} \right)} \right) \quad (6.7)$$

6.3 Method

The director was fixed at the surfaces, $\phi(z=0) = \phi_{SU}$ and $\phi(z=d) = \phi_{SL}$. The azimuthal angle ϕ of the director at $z = d/2$ was calculated by assuming that the free energy at the chevron interface, W_{ch} , is given by equation (2). Similar phenomenological expressions have successfully been used in the literature to model the SSFLC time response and to reproduce single minimum SSFLC time – voltage curves [MacLennan, 1990; Said, 2001].

$$W_{ch} = W_o \left(\left[\frac{\phi - \pi/2}{\phi_{ch}} \right]^2 - 1 \right)^2 \quad (8)$$

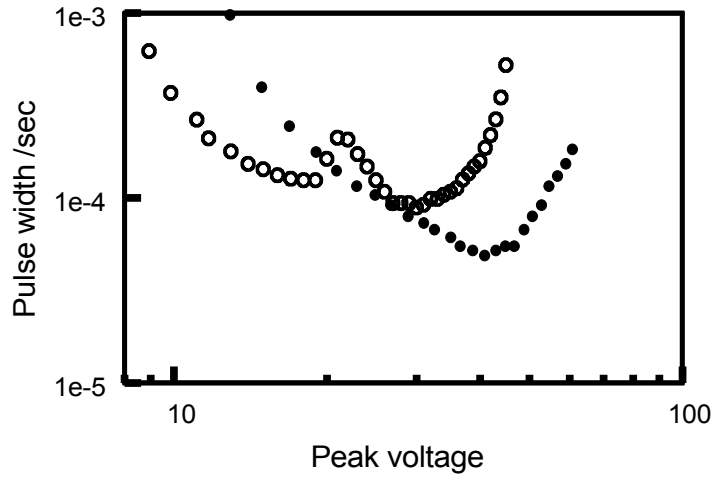


Figure 6.3 Curve (a) shows a single minimum and corresponds to a rubbed nylon alignment layer. Curve (b) shows two minima with a sharp cusp between them. This was observed for the same material but with a polyimide alignment layer.

Figure (6.3) shows time – voltage switching curves from reference [Lymer, 1999] for a high biaxiality smectic C* material in the SSFLC geometry. Curve (a) shows a single minimum and this was observed for Nylon 6, 6 surface alignment layers. In curve (b) however, there is a double minimum where the voltage minima are separated by a sharp peak. This unusual switching curve resulted from using thin polyimide (probimide 32) alignment layers. The dramatic differences between the two types of switching behaviour that are observed for the same smectic C* material can be explained in terms of differences in the through-layer equilibrium director profiles caused by the different alignment layers.

Several possible director profiles at equilibrium, i.e. with no applied voltage, are illustrated in figures (6.1b) to (6.1e). In each case the lower of the two possible bistable positions of the director at the chevron cusp, $\phi(z = d/2) = (\pi/2) \pm \phi_{ch}$, is shown where $\phi_{ch} = \arcsin(\tan \delta / \tan \theta)$. The differences between the director profiles arise due to the differences in the positions of the director at the upper surface, ϕ_{SU} , and at the lower surface, ϕ_{SL} . Figures (6.1b), (6.1c) and (6.1d) show the cases of $\phi_{SU} / \phi_{SL} = 0^\circ / 0^\circ$, $90^\circ / -90^\circ$ and $180^\circ / -180^\circ$ respectively. For typical values of δ and θ [Brown, 1999] the director profile is the most uniform in (6.1b) and the least uniform, with a large in-plane twist from the surface to the chevron cusp, in (6.1d). Figure (6.1e) shows the case where $\phi_{SU} / \phi_{SL} = 180^\circ / 0^\circ$. This is distinct in that the director profile is uniform in the upper half of the layer, but twisted, or “half-splayed” in the lower half. In a real device the different profiles in figure (6.1) can arise depending on whether the layer tilt δ has the same sign as the tilt of the director at the surface, θ_p , as

with the C1 geometries (6.1b), (6.1d) and (6.1e), or it has the opposite sign, as with the C2 geometry in (6.1c) [Jones, 1993].

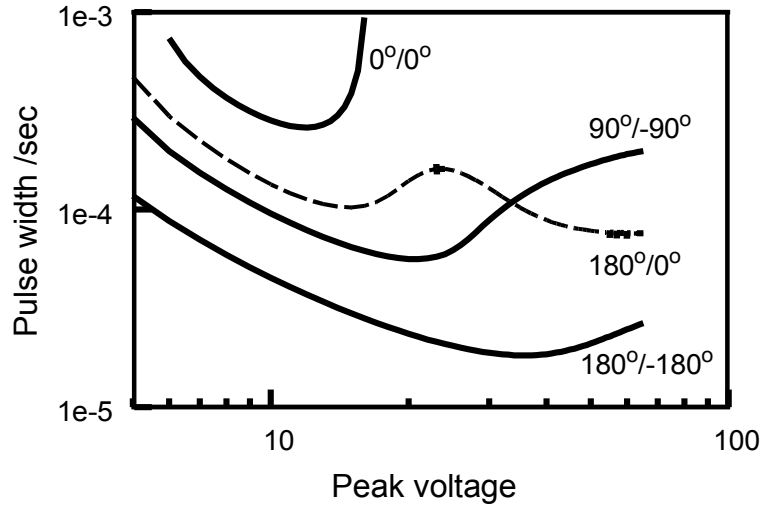


Figure 6.4 Time – voltage switching curves generated by the continuum simulation with the parameters from table I for the geometries shown in figure (1). Values for ϕ_{SU} / ϕ_{SL} are shown next to the appropriate curve.

Figure (6.4) shows time – voltage switching curves that have been generated by the numerical solution of equations (1) and (2) as a function of time using the parameters shown in table I. The equilibrium profiles in figures (6.1b) to (6.1e) were each used as the starting point for the simulation at time $t \leq 0$. A voltage was applied at time $t = 0$ with a polarity that acts to increase the azimuthal angle ϕ by coupling to the spontaneous polarisation. A significant increase in ϕ across the bulk region between the chevron and the surface - in either half of the layer - causes a switching torque to be exerted at the chevron interface. A torque of sufficient magnitude causes the director to switch across to the higher of the two possible bistable positions, $\phi(z = d/2) = (\pi/2) + \phi_{ch}$, at the chevron cusp. The pulse width is defined here as the

time taken for the director at the chevron interface to switch to the halfway point,

$\phi(z = d/2) = \pi/2$, at each voltage.

Symbol	Value	Name
ϵ_1	5.0	permittivity
$\partial\epsilon$	1.15	dielectric anisotropy
$\Delta\epsilon$	-2.0	dielectric biaxiality
P_s	$6.6 \times 10^{-5} \text{ C m}^{-2}$	spontaneous polarisation
δ	21.0°	layer tilt angle
θ	25.0°	smectic C cone angle
B	$1.0 \times 10^{-11} \text{ N}$	elastic constant
W_o	$2.0 \times 10^{-4} \text{ N m}^{-1}$	chevron energy
d	$1.5 \times 10^{-6} \text{ m}$	layer thickness

Figure 6.5 Values used for the dielectric, elastic and physical parameters of the smectic C* liquid crystal in the numerical simulations.

6.4 Conclusion

The curves for which the initial director profile is symmetrical about the chevron interface, i.e. when $\phi_{SU} / \phi_{SL} = 0^\circ / 0^\circ$, $90^\circ / -90^\circ$ and $180^\circ / -180^\circ$, all show a similar shape with a single minimum. However, the position of that minimum moves to a higher voltage and a lower pulse width time as $|\phi_{SU}|$ (which equals $|\phi_{SL}|$) is increased. Although the time evolution of the director profile within the layer in each case is complicated, this dependence can be explained by the nature of the coupling between the applied field and the dielectric permittivity. This coupling acts to maximise the component of the permittivity that is aligned with the field. The two values of ϕ for which this maximisation would occur are $\phi = (\pi / 2) \pm \phi_{AC}$, where ϕ_{AC} is readily derived by allowing the value of E to tend to infinity in equation (1). If the initial director angle in the bulk of the layer lies in the range $\phi < \pi / 2$ then the dielectric coupling acts to stabilise the director angle towards $\phi = (\pi / 2) - \phi_{AC}$, whereas if bulk director angle is predominantly in the range $\phi > \pi / 2$ then this stabilisation is towards the higher angle, $\phi = (\pi / 2) + \phi_{AC}$. The former case obtains for the $|\phi_{SU}| = 0^\circ$ profile in figure (6.1b) for which the dielectric coupling impedes switching and increases the switching time. The opposite effect occurs in the latter case, exemplified by $|\phi_{SU}| = 180^\circ$, where switching to higher values of ϕ is favoured, which reduces the switching time.

The curve for $\phi_{SU} / \phi_{SL} = 180^\circ / 0^\circ$ in figure (6.4) shows a double minimum. The equilibrium initial director profile from which this was calculated is depicted in figure (6.1e). The lower half of the profile is the same as the nearly uniform $0^\circ / 0^\circ$ case in (1b), and the upper half of the profile is the same as the twisted $180^\circ / -180^\circ$ profile in (6.1d). The position of the maximum of the $180^\circ / 0^\circ$ switching curve lies at a time

and voltage that is between the positions of the minima for the $0^\circ / 0^\circ$ and $180^\circ / -180^\circ$ curves. When a voltage is applied both sides of the layer exert a torque at the chevron interface. At lower voltages there are contributions from the fast director re-orientation from the upper half of the layer and the slower director re-orientation in the lower half of the layer. At higher voltages the lower half of the layer does not switch at all and the $180^\circ / 0^\circ$ curves tends towards the $180^\circ / -180^\circ$ curve. The extra maximum in the $180^\circ / 0^\circ$ curve arises at intermediate voltages when the switching torque from the lower half of the layer is tending to zero, but before the reorientation in the upper half dominates.

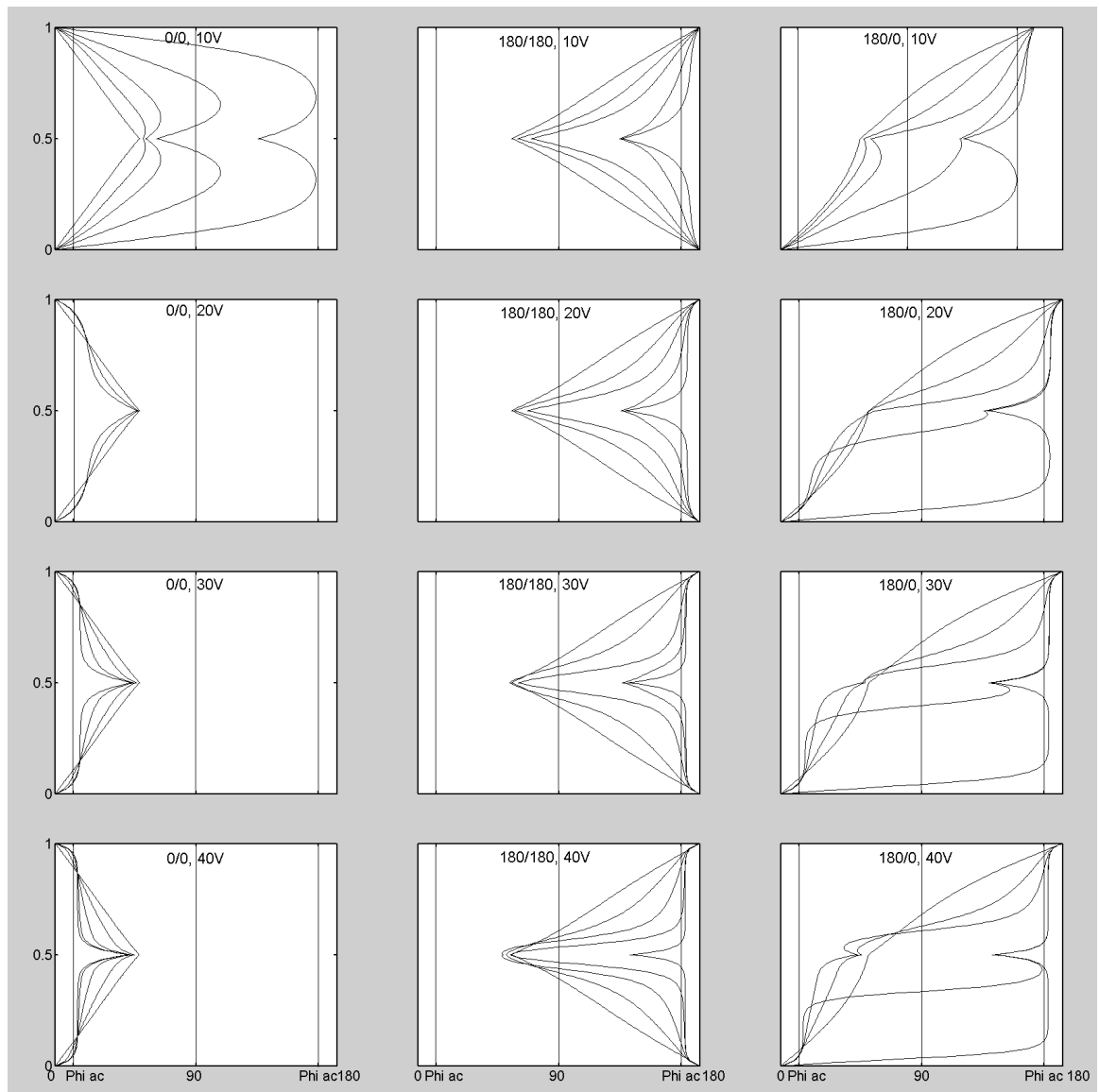


Figure 6.6 The time evolution of director profiles across the layer for the $0^\circ / 0^\circ$, $180^\circ / 180^\circ$ and $180^\circ / 0^\circ$ geometries at field strengths of 10, 20, 30 and 40V.

In Figure (6.6) we see a set of graphs displaying the evolution of the director profile for the 0/0, 180/180 and 0/180 geometries at various field strengths. Considering the first column of graphs with 0/0 anchoring we can see that the 10V field couples with the dielectric polarisation of the mesogens causing a distortion in the director profile. With time the torque generated by this overwhelms the elastic forces at the centre of the chevron and causes switching from one bistable position to the other. At higher field strengths this process is halted by the A.C. stabilisation. Since $\phi < \pi / 2$; as the field approaches infinity the director aligns with the lower A.C. stabilisation line at $\phi = (\pi / 2) - \phi_{AC}$ making switching impossible.

Looking now at the second set of graphs; with 180/180 anchoring we see that the spontaneous polarisation coupling acts to switch the chevron centre to its second stable position at all field strengths. The coupling to the dielectric initially acts to align the director with the upper A.C. stabilisation line in the region near the edge of the chevron where $\phi > \pi / 2$. In the central region however $\phi < \pi / 2$ and so the director attempts to align with the lower A.C. stabilisation line. This retards switching at higher fields.

In the case of a profile anchored at 0/180, as is shown in the third set of graphs, some elements of both of the above cases are evident. At low fields the spontaneous polarisation term dominates and switching times decrease with increased voltage. At medium fields the spontaneous polarisation coupling of the lower arm outweighs that of the upper arm since its spread of angular values is wholly within the lower band of $0 < \phi < \pi / 2$; whereas the angular spread of the upper arm is not contained within the band $\pi / 2 < \phi < \pi$. Moreover the ϕ values of the lower arm are closer to the ac stabilisation line than those of the upper arm. This causes switching times to increase with applied field strength. At high fields the upper and lower arms become

A.C. stabilised quite quickly; this largely negates the difference which arose from the proximity of the lower arm to the A.C. stabilisation line. Without this imbalance the upper arm exerts greater torque at the centre of the chevron because its director occupies a wider range of angular values for a given number of mesogens. In this region switching times reduce with increases in the applied field. As the applied field is raised still further the director of the upper arm near to the centre begin to experience A.C. stabilisation forces comparable to the existing elastic forces and switching times begin to increase again. As the applied field approaches infinite strength; the A.C. stabilisation of the upper arm near the centre exceeds these elastic forces and the director reorients towards the lower A.C. stabilisation point making switching impossible.

In order to study the processes influencing the dynamics at the centre of the chevron the modelling program was adjusted to output the torque applied to the director immediately above and below the centre. The evolution of the torque at each of these points is displayed in Figure (6.7).

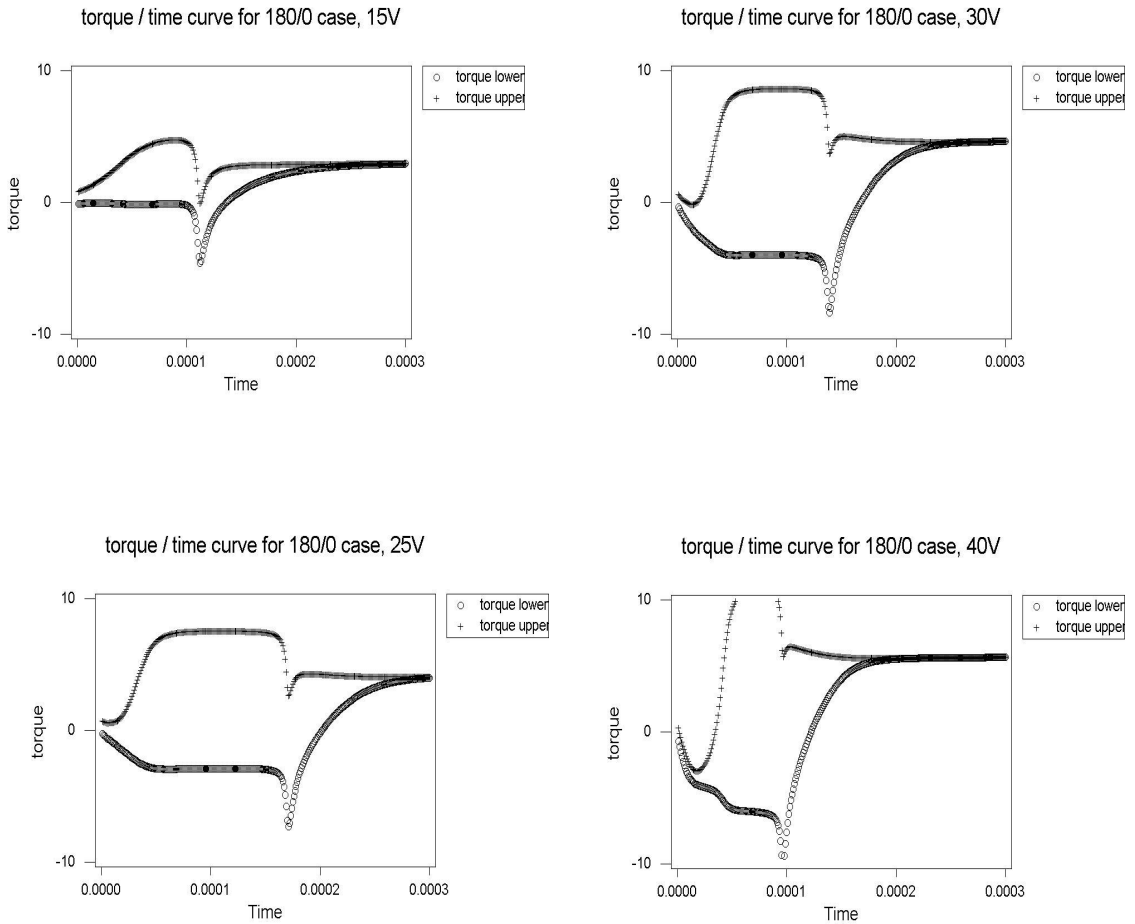


Figure 6.7 The time evolution of torque exerted on the centre of the chevron in the $180^\circ / 0^\circ$ geometry by each arm of the chevron. Torque supporting switching to the second bistable point is depicted as positive.

The point of switching is visible as a sharp peak on each graph. As expected for the half twisted geometry, the upper arm provides greater torque than the lower arm for all voltages. This is due to the director covering a wider range of angular values in the upper arm. It should be noted that by comparison the lower arm exerts almost no torque at all at lower voltages, but that what torque it does exert is negative. The

torque is of course dependant upon $\frac{d\phi}{dz}$ which is why the upper (twisted) arm exerts a much greater amount. Such is not so clearly the case in the high voltage limit when A.C. stabilisation quickly reduces the distance over which the director orientation changes within the lower arm. Consideration was also given to the torque arising from the 0/0 and 180/180 cases in figure (6.8).

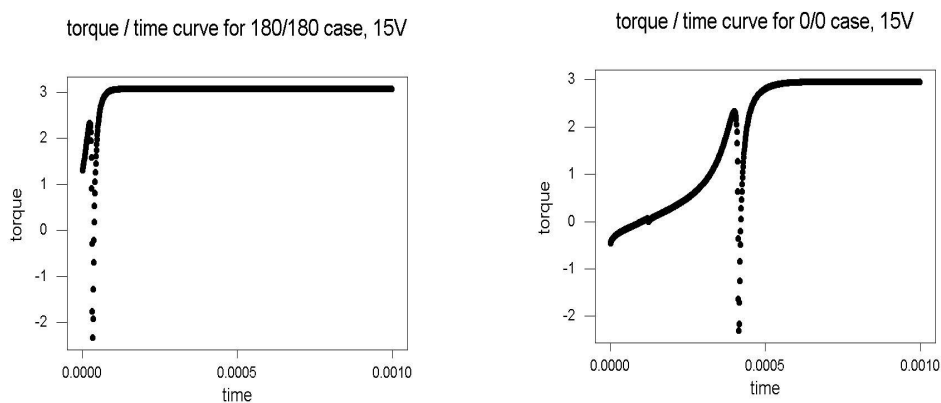


Figure 6.8 The time evolution of torque exerted on the centre of the chevron in the $0^\circ / 0^\circ$ and $180^\circ / 180^\circ$ geometries. Since these cases are symmetrical the torque presented is the sum of both arms.

Since the torque equation assumes that the torque experienced at the centre of the chevron is the average of the upper and lower arms, switching is reached when an average of around 2.5Nm is experienced in the 180/0 case at low V this comes almost completely from the upper arm. As the visco-elastic forces in the 0/0 case oppose the switching from one bistable state to another switching takes around 8 times longer at the same applied field than for the 180/180 case. This can be seen in the curve below in the negative initial torque of the 0/0 geometry. In the 180/180 geometry the visco-

elastic forces support the switching process, allowing it to occur in less than a tenth of a microsecond at 15V.

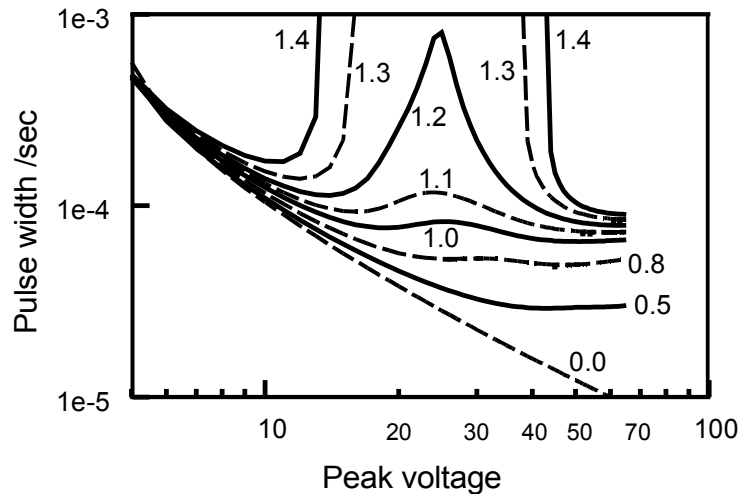


Figure 6.9 Time – voltage switching curves generated by the continuum simulation for the geometries shown in figure (1) with ϕ_{SU} / ϕ_{SL} varied from $90^\circ / 90^\circ$ to $180^\circ / 0^\circ$.

The evolution of the double minimum as a function of the dielectric biaxiality, $\partial\epsilon$, is shown in figure (6.9) for the $180^\circ / 0^\circ$ curve. The dielectric biaxiality was varied between $\partial\epsilon = 0.0$ and $\partial\epsilon = 1.4$. At values up to $\partial\epsilon = 0.5$ only a single minimum is seen in the time – voltage switching curve. At values above this, where $\partial\epsilon > 0.5$, the double minimum shape starts to evolve until a sharp peak is seen between the two minima at $\partial\epsilon = 1.2$. At still higher values the switching curve is actually split into two regions and, remarkably, the pulse width time is infinite between the two regions. This strong dependence on the value of the biaxiality is consistent with the critical influence of the dielectric coupling to the applied field on the switching process. That the double

minima arises from the half twisted geometry may be clearly seen in figure (6.10) by using the model to look at the Tau-V curves for an evolving series of geometries interspaced between the 180/0 case and a symmetrical geometry such as 90/90.

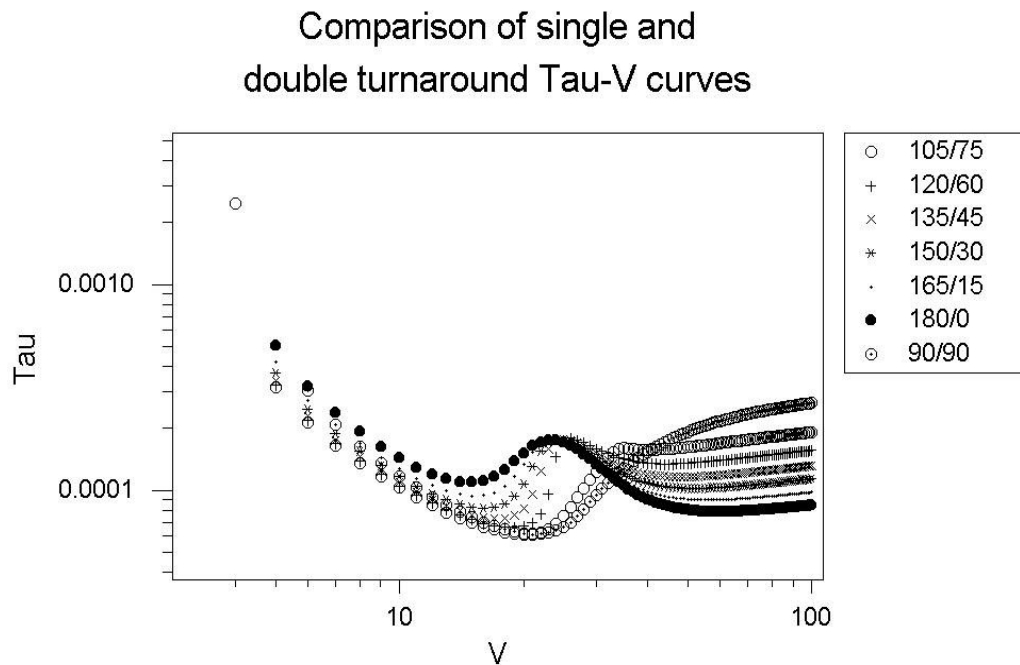


Figure 6.10 Time – voltage switching curves generated by the continuum simulation for the geometries shown in figure (1) with $\phi_{SU} / \phi_{SL} = 180^\circ / 0^\circ$. The parameters from table I were used except for the dielectric biaxiality $\partial\epsilon$ which was varied between $\partial\epsilon = 0.0$ (lower curve) and $\partial\epsilon = 1.4$ (upper curve) as indicated in the figure.

6.5 Summary

The existence of a double minimum in the time - voltage response of an SSFLC has been shown to arise naturally from surface alignment geometries that might be described as 'half splayed'. This is shown to arise from considerations of the torque applied to the director at the chevron interface. The time voltage response is shown to be a continuum of

Conclusions and Further Work

The transient capacitance technique presented herein appears to be a robust and useful tool for analyzing the mechanics of motion within liquid crystal compounds of all kinds. The technique is applicable to samples containing low or high ionic contamination and to samples with a low frequency dielectric orientation relaxation. The waveform may be adapted to be A.C., D.C., amplitude modulated, frequency modulated, or pulsed. The results generally fit well to theory without recourse to flow and flexoelectric effects; though it is recommended that for high fields or high precision studies that some account of backflow be made. The technique is adaptable to any dielectric with anisotropic permittivities. The technique could also be used as a feedback loop in a display device; giving a dynamic account of the degree of switching in a given pixel.

An analysis of the likely causes of a double minimum in the switching response of a SSFLC has produced a geometrical explanation shown to be consistent with current theoretical descriptions of Smectic C* materials. It is hoped that this may (in combination with structure-property relations) lead to the predictive design of more efficient zenithally bistable devices.

References

- Bates M. A, (2005), Testing experimental analysis techniques for liquid crystals using computer simulation, *Liquid Crystals* **32**, 1365
- Billeter J., Pelcovits R., (2000), Orientational order of liquid crystals in electric and magnetic fields. *Liquid Crystals*, **27**, 1151
- Blinov L. M., (1983), Electro-optical and Magneto-optical Properties of Liquid Crystals (J. Wiley, Chichester).
- Bradshaw M.J. and Raynes E.P, (1981), Study of elastic constant ratios in nematic liquid crystals *Liquid Crystals*. **72**, 35
- Brimicombe P. D., Parry-Jones L. A., Elston S. J., and Raynes E. P, (2005), Modeling of dual frequency liquid crystal materials and devices, *Journal of applied Physics* **98**, 104104
- Brimicombe P. D. and Raynes E. P, (2005), The influence of flow on symmetric and asymmetric splay state relaxations, *Liquid Crystals* **32**, 1273
- Brochard F, (1972), Dynamics of the Orientation of a Nematic-Liquid-Crystal Film in a Variable Magnetic Field, *Physical Review Letters* **28**, 1681
- Brown C. V., Mottram N, (2003), Influence of flexoelectricity above the nematic Fredericksz transition, presentation BLCS Conference
- Brown C.V. and Kriezis E.E, (2003), Calculation of the efficiency of polarization insensitive surface-stabilized ferroelectric liquid-crystal diffraction gratings *Applied Optics* **42**, 2257

- Brown C.V. and Jones J.C, (1999), Surface-Stabilized Ferroelectric Liquid-Crystal Diffraction Gratings with Micrometer-Scale Pitches, *Journal of applied Physics* **86**, 3333
- Bryan–Brown G. P., Brown C.V., Jones J. C, Patent GB95521106.6
- Carlsson T., Stewart I.W. and Leslie F.M., (1992), An Elastic Energy for the Ferroelectric Chiral Smectic C* Phase, *Journal of Physics Mathematics and General* **25** (8), 2371
- Chattopadhyay P, (1993), Capacitive Transients During Freedericksz Transition in 7CB and 8CB, *Molecular crystals and Liquid Crystals*. **237**, pp 1-7,
- Clark M. G, (1986), in *non-linear Phenomena and Chaos*, edited by S. Sarkar (Adam Hilger, Bristol)
- Clark N.A., Crandall C., Handschy M.A., Meadows M.R., Malzbender R.M., Park C. , and Xue J.Z. (2000), FLC microdisplays, *Ferroelectrics*. **246**, (1-4), 1003
- Clark N. A. and Lagerwall S. T, (1980), Layer compression in free-standing liquid-crystal films, *Applied Physics Letters*. **36**, 899
- Collings P. J. (1990), “Nature’s delicate phase of matter”, 1st Edition, Institute of physics, Bristol
- Collings P. J., Hird M, (1997) “Introduction to Liquid Crystals Chemistry and Physics”, 1st Edition, Taylor and Francis, Bristol
- Costa M. R. (2001), Ionic impurities in nematic liquid crystal displays, *Liquid Crystals*. **28**, 1779
- Debye P, *Polare Molekeln* (Hirzel Verlag, Leipzig, 1929)
- Derfel G. and Felczak M. (2002), Smectic layer structure of ferroelectric liquid crystal formed between fine polymer fibres, *Liquid Crystals*. **29**, 889

- Derfel G., Buczkowska M., (2005) Flexoelectric deformations of homeotropic nematic layers in the presence of ionic conductivity, *Liquid Crystals*. **32**, 1183
- Dierking I, (2001) Dielectric breakdown in liquid crystals *Journal of Physics D: Applied Physics*. **34**, 806-813
- Dierking I., (2005) Polarization–tilt coupling of a ferroelectric liquid crystal with varying molecular configuration *Journal of Physics: Condensed Matter*. **17**, 4403-4410
- Elston S.J., Sambles J.R. and Clark M.G. The Optics of Ferroelectric Liquid Crystals (1990), *Journal of applied Physics*. **68**, 1242
- Fazio V. S. U. *et al* (1999) Alignment transition in a nematic liquid crystal due to field induced breaking of anchoring *Europhysics Letters*. **46**, 38-42
- Felczak M., and Derfel G. (2003), Threshold flexoelectric deformations in homeotropic nematic layers *Liquid Crystals*. **30**, 739
- Frank F. C., (1958). On the theory of liquid crystals *Disc. Faraday Soc.* **25**, 19
- Fredericksz V. and Zolina V. (1933), New Method for Measuring the Twist Elastic Constant K_{22} / χ_a and the Shear Viscosity γ_1 / χ_a for Nematics *Trans. Faraday Soc.* **29**, 919
- De Gennes P. G. (1968), Recent Advances in Liquid Crystals, *Solid state Communications*. **6**, 919.
- de Gennes P.G. and Prost J. (1993), “The Physics of Liquid Crystals”, 2nd Edition, Clarendon Press, Oxford
- Guan Rong-Hua *et al* First-order Fréedericksz transition at the threshold point for weak anchoring nematic liquid crystal cell under external electric and magnetic fields (2003) *Chinese Physics*. **12**, 1283-1290

- Heppke G. and Schneider F. (1974) Meta stable deformations in nematic liquid crystals *Zeitschrift Naturforsch*, **29a**, 310
- Huang X-Y, Yang D-K. and J.W. Doane, (1995) Transient dielectric study of bistable reflective cholesteric displays and design of rapid drive scheme *Applied Physics Letters*. **67** (9), 1211
- Jadzyn J., Czechowski G., and Dejardin J. (2006), Dielectric and viscous properties of mesogenic *n*-nonylcyanobiphenyl (9CB), *Journal of Physics: Condensed Matter*. **18**, 1839
- Jewell S. A. and Sambles J. R. (2005), Optical characterization of a dual-frequency hybrid aligned nematic liquid crystal cell, *Optical Express*. **13**, 2627
- Jones J. C., Towler M. J. and Hughes J.R. (1993), Fast, high-contrast ferroelectric liquid crystal displays and the role of dielectric biaxiality *Displays*. **14**, 86
- Jones J. C., Towler M.J. and Raynes E.P. (1991). The importance of dielectric biaxiality for ferroelectric liquid crystal devices *Ferroelectrics* **121**, 91
- Jun-ichi Fukuda *et al* (2003) Effect of confining walls on the interaction between particles in a nematic liquid crystal *Journal of Physics: Condensed Matter*. **15**, 3841-3854
- Kashnow R.A. (1973), Characteristics of the amplitude modulation of light as a result of the Freedericksz transition in a liquid-crystal cell with a dichroic dye, *Applied Physics Letters*. **23**, pp 290-2,
- Luckhurst G. R., Sugimura A., Timimi B. A. (2005), Electric-field driven director oscillations in nematic liquid crystals *Liquid Crystals*. **32**,1449
- Lymer K.P. and Jones J.C., UK patent GB2338797, 17th June 1999. Equivalent filings: US6326940 and JP2000035563.

Maclennan J. E., Handschy M. A. and Clark N. A. (1990), Biaxial model of the surface anchoring of bent-core smectic liquid crystals *Liquid Crystals*. **7**, 787

Maddock A J, (1946) Dielectric Heating, *Scientific instruments*, **165**, 23

Maier W. and Saupe A. (1961), A simple molecular-statistical model of nematic liquid crystals *Zeitschrift Naturforsch.* **16**, 262

Meyer R. B. (1968), Effects of electric and magnetic fields on the structure of cholesteric liquid crystals *Applied Physics Letters*. **12**, 281

Meyer R. B. (1969), Piezoelectric Effects in Liquid Crystals, *Physical Review Letters*. **22**, 918

Meyerhoffer D. (1975), Field induced distortions of a liquid crystal with various surface alignments *Physical Letters*. **51A**, 407

Merck, Liquid Crystals Division, Merck KGaA, 64271 Darmstadt, Germany

Mitsuishi M. (1996), Optical switching of a metal-clad waveguide with a ferroelectric liquid crystal *Applied Physics Letters*. **69**, 2199

Mottram N. J. and Brown C. V. (2006) Pulsed addressing of a dual-frequency nematic liquid crystal *Physical Review E*. **74**, 1

Nehring J., Saupe A. On the schlieren texture in nematic and smectic liquid crystals (1972), *Journal of the Chemical Society, Faraday Transcripts 2*, **68**, 1

Oseen C. W., (1933). The theory of liquid crystals, *Transcripts Faraday Society*. **29**, 883

Raynes E. P. and Shanks I. (1974), Fast-switching twisted nematic electro-optical shutter and colour filter, *Electronic Letters*. **10**, 114

Raynes E.P. (1987), Liquid crystal materials and devices *Molecular Crystals and Liquid Crystals*. **4**, 69

- Said S. M. and Elston S. J. (2001), Modelling of switching in surface-stabilized ferroelectric liquid crystal cells using a three-variable model in one dimension, *Liquid Crystals*. **28**, 561
- Schadt M. and Helfrich W. (1971), Voltage-dependent optical activity of a twisted nematic liquid crystal *Applied Physics Letters*. **18**, 127
- Schadt M. (1981), Dielectric heating and relaxations in nematic liquid crystals, *Molecular Crystals and Liquid Crystals*. **66**, 319
- Schadt M., (1982), Low-frequency dielectric relaxation in nematics and dual-frequency addressing of field effects, *Molecular Crystals and Liquid Crystals*. **89**, 77
- Scheffer T.J. and Nehring J. (1984), A new highly multiplexable liquid crystal display, *Applied Physics Letters*. **45**, 1021
- Smith A. A., C.V. Brown and N. J. Mottram, (2007) Theoretical analysis of the magnetic Fréedericksz transition in the presence of flexoelectricity and ionic contamination. *Physical Review E*. **75**, 041704
- Smith N.J. and Sambles JR (2000) “Optically resolving dynamic processes in commercial liquid crystal cells”, *Applied Physics Letters*. **77**, 2632
- Stewart I. W., (2005), Stability of equilibrium states in finite samples of smectic C* liquid crystals *Journal of Physics A – Maths and General*. **38**, 1853
- Stewart I. W. (2004), *The static and dynamic Continuum theory of Liquid Crystals* Taylor and Francis, London,
- Stromer J. F., Raynes E. P. (2006), Study of elastic constant ratios in nematic liquid crystals *Applied Physics Letters*. **88** 051915
- Takeda A. et. al. (1998) *Proceedings of the Society for Information Display conference*, SID Digest, p1077

Towler M. J., Highes J. R, and F. C. Saunders, (1991), Switching behaviour of smectic C* liquid crystals, *Ferroelectrics*. **113**, 453

Warr S. and Mears R. (1995), Polarisation insensitive operation of ferroelectric liquid crystal devices, *Electronics Letters*. **31**, 714

Waters C.M., V. Brimmel and Raynes E.P., (1983) Proceedings of 3rd International Display Research Conference, Kobe, Japan, 396

Waters C.M., Raynes E.P. and Brimmel V. (1985), Design of highly multiplexed liquid-crystal dye displays *Molecular Crystals and Liquid Crystals*. **123**, 303

Publications and Conference Talks

Publications:

“Static and transient dielectric response of a nematic two-frequency material”

C.V. Brown, T. Müller, J.M. Hind and A.A.T. Smith

Submitted to *Journal of Applied Physics*

J.M. Hind, A.A.T. Smith and C.V. Brown, (2006), Transient capacitance study of switching in the nematic Freedericksz geometry, *Journal of Applied Physics* **100** (9), 094109

C.V. Brown, J.M. Hind, K.P. Lymer and J.C. Jones, (2004), Double minimum in the surface stabilised ferroelectric liquid crystal switching response, *Applied Physics Letters* **85** 1763-1765 .

Conferences Attended:

British Liquid Crystal society Annual General Meeting, York, 2006.

Oral presentation "Time resolved capacitance study of Dual Frequency Nematic Liquid Crystals"

British Liquid Crystal society Annual General Meeting, Exeter, 2005.

Oral presentation "Transient Capacitance Studies of nematic liquid crystals"

Rank Prize Conference, Grasmere, June 2005.

Oral presentation "Double minimum in the ferroelectric liquid crystal switching response"

Nottingham Trent University Research School Meeting 2005.

Oral and poster presentations “Ionic and flexoelectric effects in liquid crystals”